Recruitment of reovirus RNAs to viral factories

by

Christopher Harim Lee

B.S., University of Georgia, 2013

Submitted to the Graduate Faculty of the

School of Medicine in partial fulfillment

of the requirements for the degree of

Doctor of Philosophy

University of Pittsburgh

2021

UNIVERSITY OF PITTSBURGH

SCHOOL OF MEDICINE

This dissertation was presented

by

Christopher Harim Lee

It was defended on

September 28, 2021

and approved by

Maninjay Atianand, Ph.D., Assistant Professor, Department of Immunology

Jeff Brodsky, Ph.D., Professor, Department of Biological Sciences

Paul R. Kinchington, Ph.D., Professor and Chair, Department of Molecular Genetics and Biochemistry

Seema Lakdawala, Ph.D., Associate Professor, Department of Microbiology and Molecular Genetics

Dissertation Director: Terence S. Dermody, M.D., Professor, Department of Pediatrics and Microbiology and Molecular Genetics

Recruitment of reovirus RNAs to viral factories

Christopher Harim Lee, Ph.D.

University of Pittsburgh, 2021

Viruses face monumental challenges when colonizing a cell. They are much smaller than the cells they infect, yet they can efficiently replicate in relatively-large complex environments. Viruses thrive in such environments by constructing structures optimized for producing more viruses. These intracellular structures, called viral factories, concentrate viral and host factors that enable efficient viral packaging and replication. The mammalian orthoreovirus (reovirus) is a double stranded RNA virus that builds distinct cytoplasmic factories in infected cells. However, mechanisms underlying the formation of these structures are not well defined. Two reovirus nonstructural proteins, σNS and μNS, are required for viral factory formation, but the function of σNS in this process has been enigmatic. This thesis is focuses on defining the role of σNS in viral factory formation. I determined that σNS is required to recruit viral mRNAs into factory scaffolds. Additionally, I describe how σNS forms a helical oligomer. Lastly, I discovered that σNS is not solely responsible for regulating RNAs recruited to factories. My findings define a function for σNS in factory formation and provide the foundation for additional studies that will enhance our understanding of reovirus factory formation and replication.

Table of Contents

List of Tables

List of Figures

Acknowledgements

I'd like to share my deepest gratitude to all those who have helped me along my journey. The University of Pittsburgh has been a fantastic place to develop my scientific skills, and I'm continually inspired by the awesome research that's conducted here. Hail Pitt!

I am grateful to all my mentors who graciously guided me through my graduate schooling. I was lucky to have a tough choice when choosing between four mentors, following my initial rotations. You all were instrumental in my scientific development, and I appreciate the knowledge you imparted on me. Thank you all for giving me an opportunity to learn in your laboratories, and I enjoyed being a part of each one of your teams. Additionally, I am thankful for my thesis committee continually helping me hone my research skills. Your input was instrumental as I developed my project, and I appreciate all the interactions we've had. Lastly, to my dissertation mentor, Dr. Terry Dermody, thank you for giving me every opportunity to succeed and thrive. You are a kind respectful mentor who leads by setting an amazing example, inspiring others to be better. You've taught me how to be a better storyteller, problem solver, and scientist. I am eternally grateful and proud to be your mentee.

When first entering graduate school, I was advised that I should find a lab where it would feel like I would be going to the beach every day. I am grateful that I found that place. To the Dermody Lab, thank you all for making my time in lab grand. The science was exciting but having great company allowed me to keep pushing through the worst

days. It was an absolute pleasure being a member of the lab, and that's because of the wonderful people it's composed of. I will always cherish the memories I had here.

To all my friends that I've made in grad school, if you know you know. ☺

Finally, to my loving family I'll see you soon! I'm coming home!

1.0 Introduction

1.1 Thesis Overview

Viruses are much smaller than the cells they infect. However, they have evolved to efficiently replicate in immensely complex intracellular environments. Viral proteins transform the cell interior and establish local habitats concentrated with viral and host factors, called viral factories. These structures promote viral replication while shielding against host intrinsic immune defenses. Viral factories are essential for viral replication, but mechanisms used for constructing factories are not well understood for many viruses.

Mammalian orthoreoviruses are double-stranded (ds) RNA viruses that infect most mammalian species predominately through enteric routes and may trigger celiac disease in humans. A key feature of reovirus replication is the formation cytoplasmic viral factories. Mechanisms that underly the formation and function of these structures are not well defined. Two reovirus nonstructural proteins, σNS and μNS, are required for viral factory formation, but the function of σNS in this process has been enigmatic. This thesis is focused on the role of σNS in viral factory formation. Enhancing our understanding of this process could yield insights about key viral replication steps that occur within factories, such as assortment, packaging, and replication of the segmented dsRNA genome. Additionally, findings made from studies of reoviruses could help elucidate conserved replication mechanisms used by other dsRNA viruses.

In Chapter 1, I introduce *Reoviridae* viruses and the types of factories they form and review the current literature about the reovirus nonstructural proteins responsible for factory formation. In Chapter 2, I report how σNS is required to recruit viral mRNAs into factory scaffolds. This work was published in 2021 (1). In Chapter 3, I describe the structure of σNS, which will be submitted for publication in 2022. In Chapter 4, I present how σNS might preferentially recruit viral mRNAs to factories. Finally, in Chapter 5, I summarize my thesis results and discuss avenues for future studies. Collectively, this work defines a function for σNS in reovirus replication.

1.2 Reoviridae family of viruses

The *Reoviridae* family of viruses is the largest and most diverse family of dsRNA viruses. This family is composed of 15 genera of viruses that include more than 75 virus species (2). The family name originated from the first virus isolated from this group, mammalian orthoreovirus, colloquially termed reovirus. Reovirus was first isolated from stool samples of children by Albert Sabin in the 1950's (3). "Reo" is an acronym that stands for respiratory enteric and orphan. The first two words describe typical routes of infection, and orphan was used to designate the absence of a clear disease association in humans (4). However, it was later discovered that reovirus is virulent in young mice (3) and is implicated in the development of celiac disease in humans (5). Additionally, other viruses in this family are pathogenic. Diseases induced by *Reoviridae* viruses include gastroenteritis in animals and humans (rotavirus), neurological disease in humans (Colorado tick fever virus), and hemorrhagic disease in fish (aquareovirus) (2).

Thus, discoveries about *Reoviridae* replication could lead to improvements in human health and agriculture. Despite the diversity of viruses in this family, they all share common features including similar nonenveloped virion structures, viral replication mechanisms, and nonstructural proteins to construct viral factories.

1.2.1 *Reoviridae* virions

Reoviridae viruses can be classified into two groups based on the appearance of the icosahedral capsid (Fig. 1A). All viruses in the family have one to three concentric capsids, and the outer shell is either turreted or nonturreted (Fig. 1B). The presence of multiple outer layers likely evolved to aid in structural stability and enhanced viral tropism, as many of these viruses infect through the enteric route, which exposes viruses to harsh conditions like low pH and proteases (6-8). A turreted capsid has large proteinaceous spikes at the 12 icosahedral vertices and is classified in the subfamily Spinareovirinae (Latin: Spina-, English: thorn). Viruses in this subfamily include Colorado tick fever virus (triple-layer capsid) and reovirus (double-layer capsid). Alternatively, viruses with non-turreted and smooth outer capsids are included in the subfamily Sedoreovirinae (Latin: Sedo, English: smooth). Viruses in this subfamily include rotavirus (triple-layer capsid) and bluetongue virus (triple-layer capsid).

Within the innermost capsids, *Reoviridae* viruses package 9-to-12 segments of distinct dsRNA, depending on the number of viral genes required for replication (2, 9-12). Each dsRNA genome segment usually encodes a single viral protein, but some dsRNAs encode multiple proteins using multiple open reading frames (13). Packaging of *Reoviridae* dsRNAs, also known as assortment, is a specific process, as only one

copy of each gene segment is packaged. Low particle-to-PFU ratios achieved by these viruses would not be feasible for randomly packaging > 9 dsRNA segments (14). Additionally, assortment does not appear to occur in an incomplete manner. When purifying virions from infected cells, only packaged virions with a complete constellation of gene segments or virions without any segments are observed, suggesting that either each unique gene segment is packaged, or none are (14). Speculative mechanisms that dictate this precise process likely depend on intersegmental RNA-RNA interactions (15). This proposed packaging mechanism suggests that dsRNAs are not directly packaged, but instead dsRNA synthesis occurs during or after properly sorted viral mRNAs are packaged (14, 15).

Once the viral gene segments are packaged, the segments are not released unless the structural integrity of the capsid is somehow compromised (16). Sequestering viral dsRNA genomes is a key feature of *Reoviridae* viruses that likely evolved to prevent immunostimulatory dsRNAs from being sensed by the host. Long strands of dsRNA are not native to cells. Thus, if these pathogen-associated molecular patterns (PAMPs) are recognized by host factors like melanoma differentiation-associated protein 5 (MDA5), protein kinase R (PKR), or retinoic acid-inducible gene 1 (RIG-I), an antiviral state is activated that could impede viral replication (17). As such, viral gene expression does not occur by releasing the dsRNA genome. Instead, *Reoviridae* viruses package RNA-dependent-RNA polymerases (RdRp) and other RNA synthesis cofactors, including proteins with guanylyltransferase and methyltransferase activity, within the innermost capsid adjacent to each icosahedral vertex (Fig. 1C) (18, 19). The RdRps use negative-sense strands of packaged dsRNA segments as

templates to transcribe mRNAs (20). Transcription is a regulated process that occurs only when mature virions are activated by removal of the outer capsid or conformational changes (21, 22). In the presence of nucleotides and divalent cations, activated virions become transcriptional machines, and newly synthesized mRNAs are extruded through pores at the icosahedral vertices (Fig. 1C).

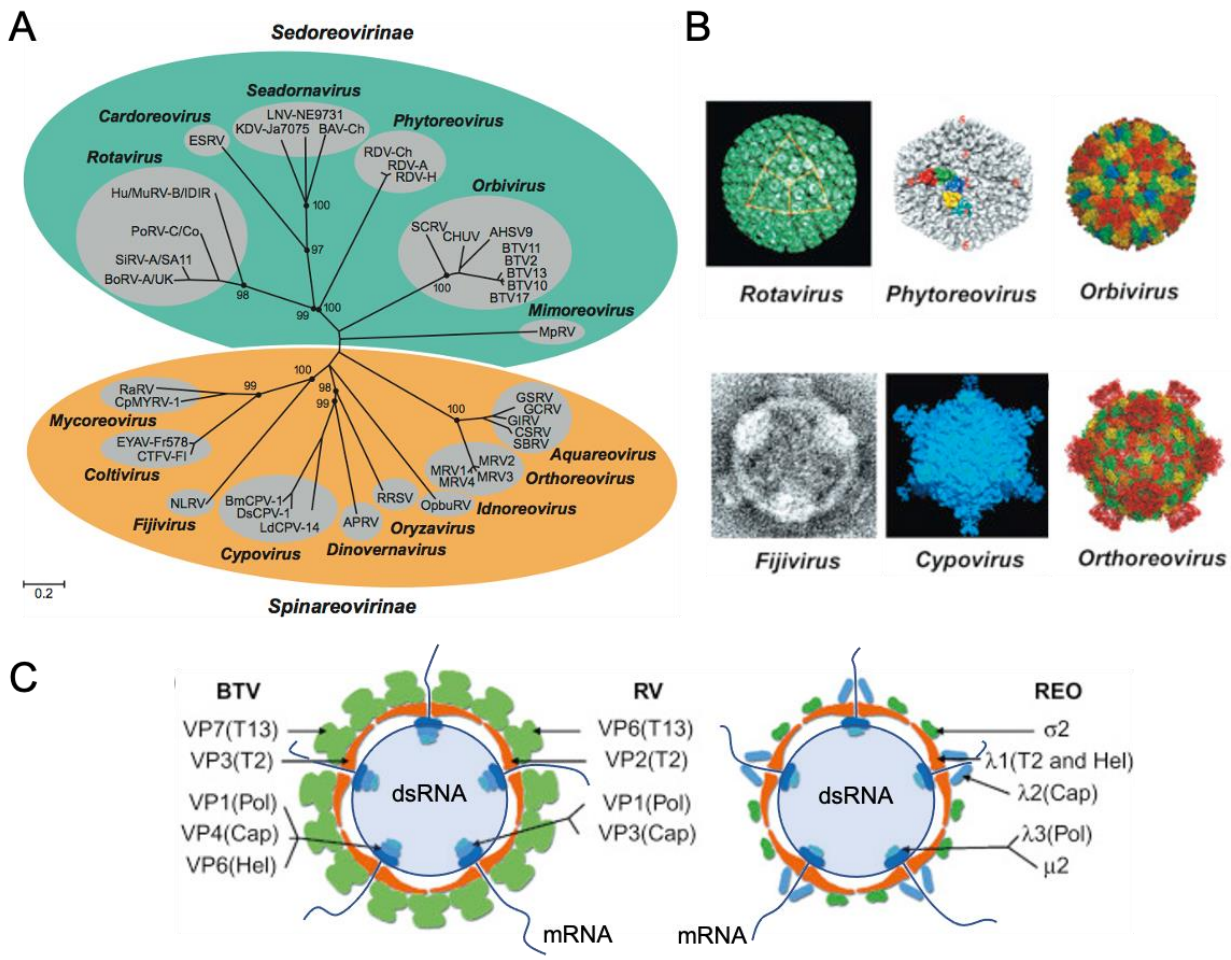

Figure 1. Reoviridae family of viruses

(A) Phylogenetic tree of *Reoviridae* viruses prepared by analyzing amino acid sequences of viral RNA-dependent RNA polymerases. Values at the nodes represent confidence levels. Viral subfamilies grouped by capsid morphology are indicated in green and orange. Smooth capsids are classified in the subfamily Sedoreovirinae, and turreted capsids are classified in the subfamily Spinareovirinae. (B) Morphology of viral capsids determined by electron microscopy or X-ray crystallography. (C) Illustration of blue tongue virus (BTV), rotavirus (RV), and reovirus (REO) cores transcribing mRNAs with viral proteins indicated. Proteins with capping (Cap), helicase (Hel), or polymerase (Pol) activity are listed. Triangulation numbers (T13 or T2) also are indicated. Figure adapted with permission from ICTV 9th Report (2011).

1.2.2 *Reoviridae* mRNAs

Reoviridae mRNAs differ from cellular mRNAs. Since *Reoviridae* mRNAs are transcribed in the cytoplasm, they are neither polyadenylated nor spliced (23). Host mRNAs that lack polyadenylated 3' termini usually are not efficiently translated and have poor stability (24). However, *Reoviridae* mRNAs are efficiently translated by a process that remains largely unknown. *Reoviridae* virions package capping enzymes and, as such, *Reoviridae* mRNAs can be capped (25). Additional common features of *Reoviridae* mRNAs are that they contain short, conserved 5' and 3' untranslated regions (UTRs). The mRNAs are hypothesized to form panhandles through long-range UTR interactions, but mRNA structural studies to test this hypothesis have not been reported (26). Despite lacking polyadenylate tails, not always being capped, and containing short UTRs, viral mRNAs are efficiently translated to yield increasing levels of viral proteins as infection progresses (27). Once the viral mRNAs are transcribed and translated, viral factories begin to form in the cytoplasm.

1.2.3 *Reoviridae* factories

Viral factories are intracellular structures formed during infection that promote production of progeny virions. These neoorganelles concentrate viral and host components to establish discrete intracellular environments optimal for viral genome replication and packaging and often immune evasion or suppression (28). Viral factories may appear to form with only a few key components, but these structures are not completely functional and are usually called factory-like structures (29, 30). To be

recognized as a functioning factory, the structures must house all of the required viral and host components to produce progeny virions. The basic components of *Reoviridae* virions are viral proteins and dsRNA. While viral proteins and nucleic acids concentrate in factories, mechanisms by which these viral components are recruited to these structures are not well understood, especially for viruses that contain dsRNA genomes.

Membrane enclosure is an effective mechanism for intracellular compartmentalization, as lipid bilayers form efficient barriers to passive diffusion. Many viruses modify membranes to corral and concentrate factors required for replication (31). Positive-sense RNA viruses like coronavirus, flaviviruses, and nodaviruses form spherules from cellular membranes to promote viral RNA synthesis and virion assembly (32). Membranes used in this fashion protect negative-sense RNA intermediates from cellular nuclease degradation (33). However, not all viruses require membranes to form replication factories. For example, *Reoviridae* factories are not enclosed by lipid bilayers (34) (Fig. 2A and 2B). Although such factories lack a physical barrier, they are self-contained entities that can concentrate components necessary for viral replication and packaging (35). While *Reoviridae* virions do not require factories to assemble empty capsids, factories are required for packaging viral genomes into capsids (36).

A mechanism that could explain how *Reoviridae* replication complexes form is liquid-liquid phase separation (LLPS), a process that facilitates reversible intracellular compartmentalization (37). LLPS allows certain components to separate from the surrounding environment through weak multivalent interactions (37). Because components of LLPS condensates interact preferentially with each other over others in a given environment, physical partitioning occurs (Fig. 2C). Condensates are attractive

viral factory structures since they form easily, concentrate required components, exclude nonessential components, and increase reaction kinetics (Fig. 2D).

There are two types of components of phase-separated condensates. *Scaffolds* form the matrix of a condensate, and *clients* are recruited to the matrix through direct or indirect interactions with scaffolds. Through preferential interactions between scaffolds and clients, condensates can be exclusive or trap diffusive components by forming meshed networks (38). In cells, scaffolds can be proteins, nucleic acids, or both (39). A common feature of protein scaffolds is the presence of intrinsically disordered regions (IDR) that are flexible and capable of transient interactions (40). Nucleic acids (usually RNA) are also common scaffolds because their long negatively charged backbone can nucleate numerous electrostatic interactions (41). When sufficient multivalent interactions occur, a distinct condensate forms.

Depending on environmental conditions like temperature and pressure, matter can undergo phase transitions from gas to liquid to solid. Interestingly, LLPS condensates can undergo similar thermodynamic transitions, between liquid and solid states. Increasing interactions between condensate components by physically crowding the environment with noncondensate components or increasing the concentration of condensate-forming components drives LLPS. Key concentrations and conditions, (e.g., salt, solubility, pH, and temperature) that promote phase separation are experimentally determined to develop phase-transition diagrams (42). There is not yet a unified methodology for experimentally defining whether a component can drive LLPS, but the current standard includes: building phase-transition diagrams to define minimal components to induce LLPS, live-cell microscopy to observe fusion, fission, and surface

tension of condensates, fluorescence recovery after photobleaching (FRAP) assays to determine dynamics of condensates, and treatment of condensates with LLPS-dissolving drugs (43). Once specific saturation conditions are achieved, condensates form and sometimes progress to gel-like or solid aggregates. Solid aggregates, like transactive response DNA-binding protein-43 (TDP-43) in neurons, can be pathogenic drivers of disease, but solid states do not directly correlate with disease, as some nonpathogenic condensates can have solid cores (44, 45).

As interest in LLPS has increased, important biological processes have been recognized to use LLPS as a mechanism of intracellular partition. Ribosomal biogenesis occurs in nucleoli, which are multi-layer condensates that form by high-valency protein-RNA interactions. If the structural organization and biophysical properties of this condensate are disrupted, ribosomal biogenesis is dysregulated, which contributes to a variety of diseases (46). Cellular responses to stress also require condensate organization. Stress granules (SGs) are one of the most well-studied biomolecular condensates (44). SGs store translationally stalled mRNAs when cells are stressed. When stress events are resolved, SGs quickly dissolve, allowing translation of stalled transcripts to proceed. Biomolecular condensates promote transcription by forming on transcriptionally active genes. Cellular transcriptional regulators can coalesce by LLPS on enhancer elements along with the core transcriptional machinery to enhance transcription (47). While there are many types of condensates, their functions depend on the biomolecules within and their resultant biophysical properties.

It comes as no surprise that viruses use LLPS to build replication factories to promote viral replication. The paramyxoviruses measles virus (MeV) and respiratory

syncytial virus (RSV) are notable examples of viruses that use LLPS to form factories (48, 49). MeV forms LLPS condensates using two proteins, nucleoprotein and phosphoprotein. When mixed with viral RNA, the formation of nucleocapsid-like structures is enhanced within the condensates, suggesting that LLPS is required for packaging of viral genomic RNA (50). In addition to containing components required for viral replication, RSV-induced LLPS condensates also sequester NF-κB, an innate-immune-response activating protein (51). Inhibiting the dynamics of RSV factories by hardening the condensates with a steroidal alkaloid cyclopamine analog (A3E) decreases viral replication (52).Studies of viral factories formed by LLPS have led to new avenues of research for antiviral drug development focused on antagonizing viral factory formation or function. There are challenges targeting viral condensates since LLPS is a common cellular mechanism, and drugs that antagonize these processes can be nonspecific or toxic. However, there have been promising initial animal studies and formation of biotech companies that are making strides towards accomplishing such goals (52, 53).

Before the start of this dissertation, it was not known if *Reoviridae* virus factories were LLPS condensates. However, properties that suggested factories were formed by condensates were known yet underappreciated. The evidence included the observations that factories lack a constraining outer membrane, factory morphologies resemble LLPS condensates, and factories undergo dynamic fusion and fission events (54). Experimental evidence was published last year suggesting that rotavirus factories, also known as viroplasms, are LLPS condensates (55). Rotavirus nonstructural proteins, NSP2 and NSP5, are key components that drive LLPS in cells and *in vitro*

(55). The formation of factory-like structures was thought to occur only when both proteins were present, but NSP5 can form condensates *in vitro* without NSP2 (55). Other *Reoviridae* virus nonstructural proteins, when expressed in uninfected cells, form similar factory-like structures (Table 1). While some properties of these nonstructural proteins are known, definitive mechanisms underlying factory formation are lacking.

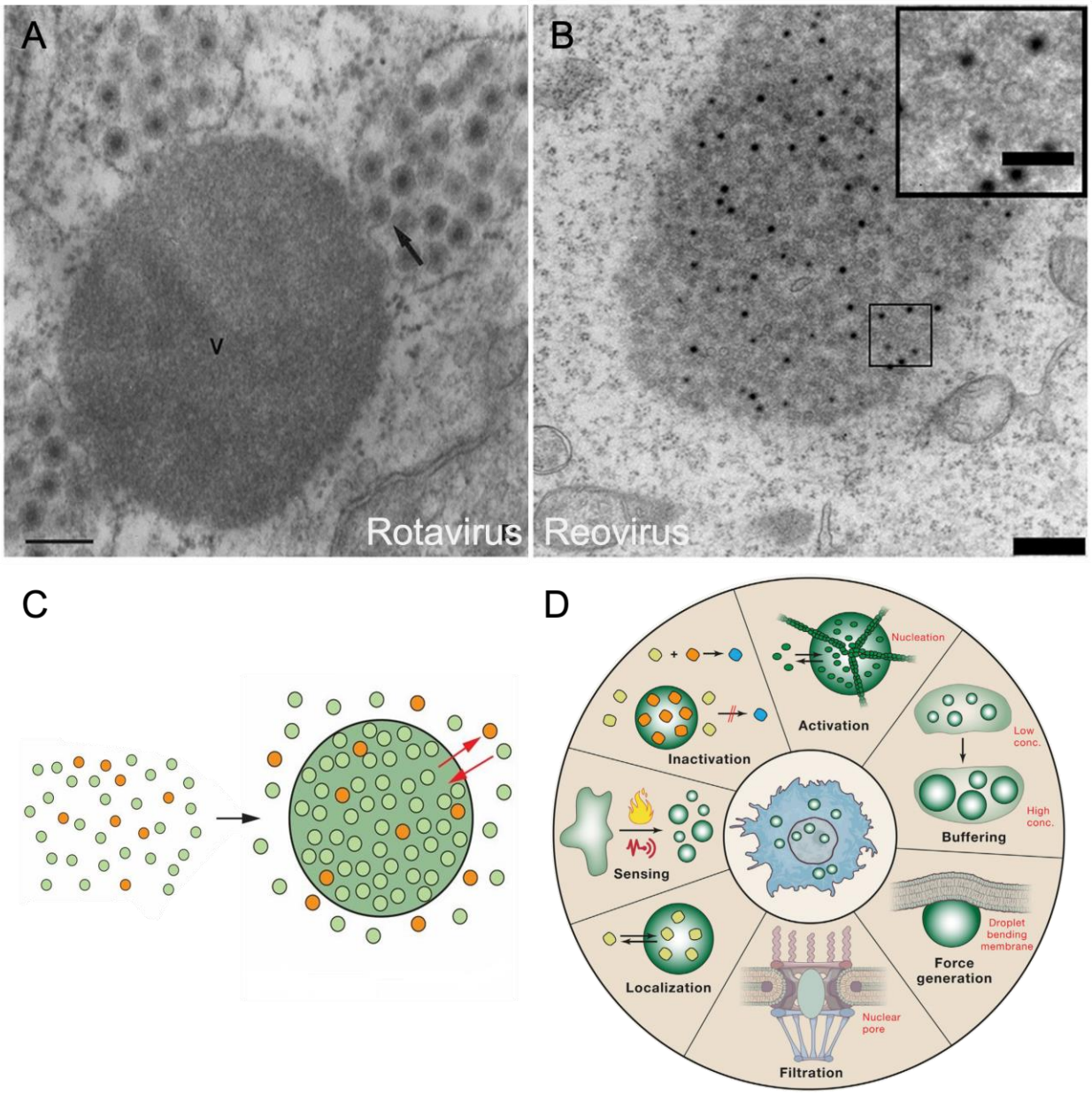

Figure 2. Reoviridae factories are liquid-liquid phase-separated condensates

(A) EM image of rotavirus-infected cells 12 hours post-adsorption. Arrows indicate viruses budding from viroplasms (V) into the endoplasmic reticulum (ER). Scale bar = 0.2 µm. (B) EM image of reovirus-infected cells 18 hours post adsorption. Scale bar = 1 and 0.3 µm (inset). (C) Simplified schematic of a two-component system undergoing liquid-liquid phase separation to form condensates. (D) Potential functions for cellular condensates. Figure adapted with permission from (35, 43, 56).

Virus	Protein	Mass (kDa)	Properties	Can form factory-like-structures when expressed alone
Rotavirus	NSP2	36.7	RNA-binding protein, NTPase activity, can be phosphorylated	No
Rotavirus	NSP5	21.7	RNA-binding protein	Yes
Bluetongue virus	NS2	41	RNA-binding protein, forms cytoplasmic factories, can be phosphorylated	Yes
Mammalian orthoreovirus	μNS	80	Forms cytoplasmic factories and can interact with viral capsid proteins	Yes
Mammalian orthoreovirus	σNS	41	Nonspecific RNA-binding protein	No

Table 1. Examples of *Reoviridae* nonstructural proteins necessary for functional viral factory formation

1.3 Reovirus

Mammalian orthoreovirus (reovirus) is a well-studied member of the *Reoviridae* family. Reovirus does not commonly induce symptomatic infection in humans, but it has been implicated as an environmental trigger for celiac disease (5, 57). Due to its low virulence in humans and capacity to preferentially infect transformed cells, reoviruses are being investigated as oncolytic therapeutics (5, 57). There are three serotypes of reovirus that are grouped based on antibody neutralization. Prototype strains of the three serotypes are named by the last names of children from which the viruses were isolated, Type 1 Lang (T1L), Type 2 Jones (T2J), and Type 3 Dearing (T3D) (58). Reoviruses are a tractable research model for dsRNA viruses and, with the availability of a robust reverse genetics system, reovirus research has expanded knowledge of dsRNA viruses (59).

Mature reovirus virions contain two concentric shells, termed outer capsid and core. Ten segments of unique dsRNA are packaged in the viral core (60). When reovirus dsRNA genome segments are purified from virions and separated by size using polyacrylamide gel electrophoresis, three distinct classes of RNA are observed—large (L), medium (M), and small (S) (Fig. 3A). Reovirus gene segments in each class are numbered by size (Fig. 3B). The proteins encoded by each gene segment are designated by Greek symbols—large (λ), medium (μ), and small (σ), corresponding to the segment size class. However, the protein numbering does not correspond to size or gene-segment numbering. Nonstructural proteins are designated “NS” (Fig. 3C). The arrangement of reovirus structural proteins in the reovirus particle types is shown in Fig 3D. Reovirus particle types will be described in the next section.

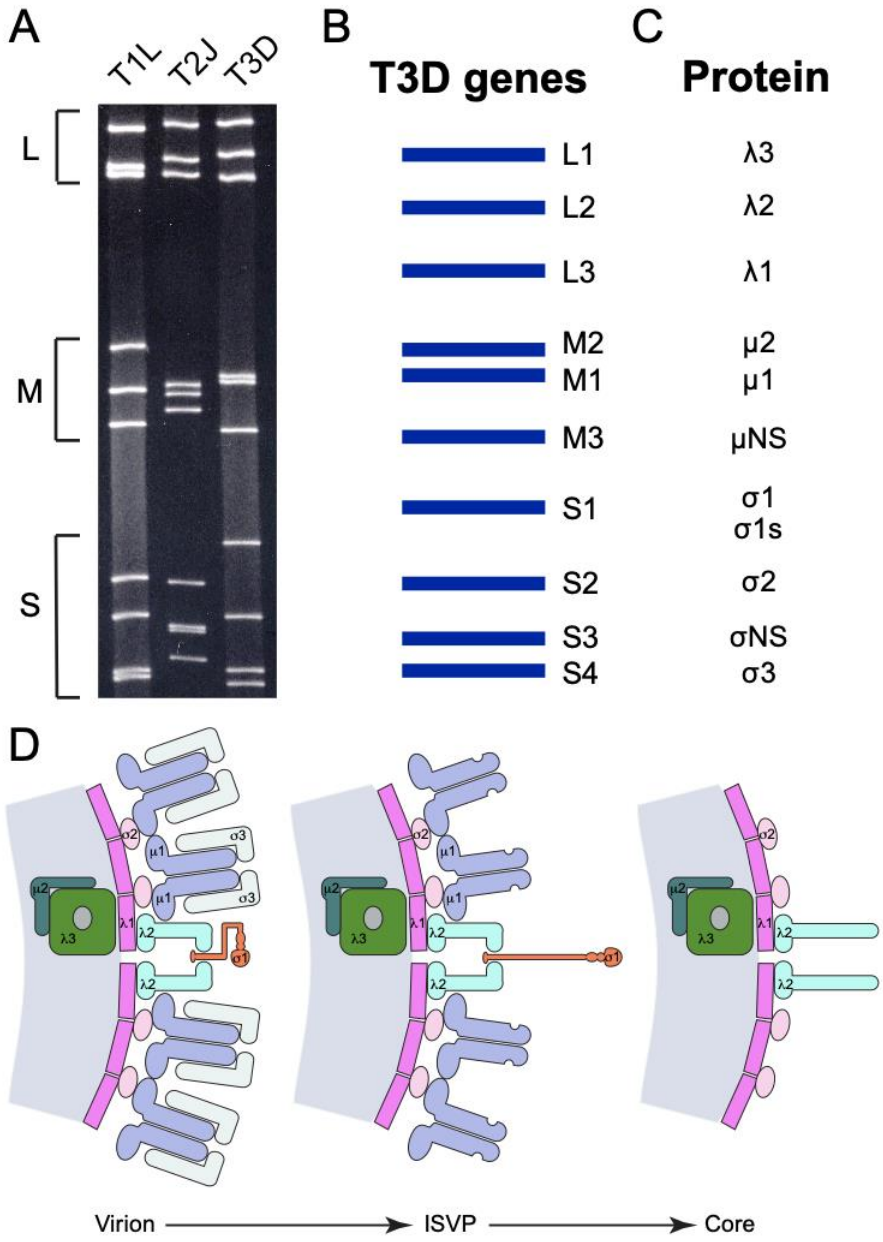

Figure 3. Reovirus genome and capsid structure

(A) Size-dependent separation of purified reovirus dsRNA from strains T1L, T2J, and T3D by SDS-polyacrylamide gel electrophoresis. (B) Schematic of electrophoretic profile of T3D dsRNA with corresponding name of gene segment indicated. (C) Major viral proteins encoded by corresponding dsRNA gene segments. (D) Schematics of reovirus particle cross sections undergoing transformation from virion to infectious subvirion particle to core. Figures adapted with permission from Fields Virology (60)

1.4 Reovirus replication cycle

Reovirus can infect a wide range of hosts. Its broad tropism is dependent on the capacity to interact with numerous cell-surface attachment factors and receptors. Reovirus binds many cell types. Known attachment factors are sialic acid and proteinaceous receptors junctional adhesion molecule A (JAM-A), which is found at cellular tight junctions, and Nogo receptor (NgR1), which is expressed on the surface of neurons. Other proteinaceous receptors likely exist for reovirus, as viral replication can occur in cells that lack the known reovirus receptors (61).

Once reovirus binds to the cell surface, particles are internalized by receptor-mediated endocytosis induced by integrins in most cells or macropinocytosis in neurons (62). Within an endocytic compartment, virions undergo a series of disassembly events that allow viral escape into the cytoplasm. The outer capsid is proteolytically removed by cathepsins to form infectious subvirion particles (ISVPs), which then transition to cores. Degradation products of outer-capsid proteins drive pore formation at endosomal membranes (63). Pore formation allows cores to penetrate into the cytoplasm (64).

Reovirus cores can initiate transcription in the cytoplasm due to the absence of outer-capsid proteins, which sterically block channels at the icosahedral fivefold vertices. The reovirus RdRp, packaged adjacent to the icosahedral vertices, transcribes viral mRNAs using (-) sense strands of packaged dsRNA segments as templates. As viral mRNAs are transcribed, they are extruded through core channels. Transcription by infecting cores is referred to as primary rounds of transcription. All viral mRNAs are transcribed at similar rates and thought to accumulate inversely to the length of each segment, i.e., S-class mRNAs more abundant that M- and L-class mRNAs (65).

Viral mRNAs are translated by host ribosomes. Newly synthesized viral proteins reorganize the cytoplasm, establishing dynamic factories (54, 66). How reovirus factories form is not well known, but prior experiments indicate that they are comprised of viral proteins (67), host factors (68), endoplasmic reticulum (ER) membranes(69), and viral RNA. Cleaved membranes derived from the ER are embedded in factories (54, 66, 69, 70). However, the importance of these membranes has not yet been established. Formation of factories requires two nonstructural proteins, μNS and σNS, which are expressed at early stages of infection (67).

As the concentration of viral proteins and mRNAs increase within factories, nascent particles are assembled and package a single copy of each viral RNA segment in a highly selective and specific manner (14). Concurrently or soon thereafter, (-) sense RNA strands are synthesized using the mRNA segments as templates, forming dsRNA (71). Newly formed viral cores are transcriptionally active and synthesize secondary viral mRNA transcripts, which further perpetuate the replication cycle (72). Outer-capsid proteins eventually coalesce onto the newly formed cores to produce mature virions. Addition of outer-capsid proteins silences transcription of viral mRNAs, and the mature virions exit cells through lytic or nonlytic mechanisms, completing a replication cycle (Fig. 4).

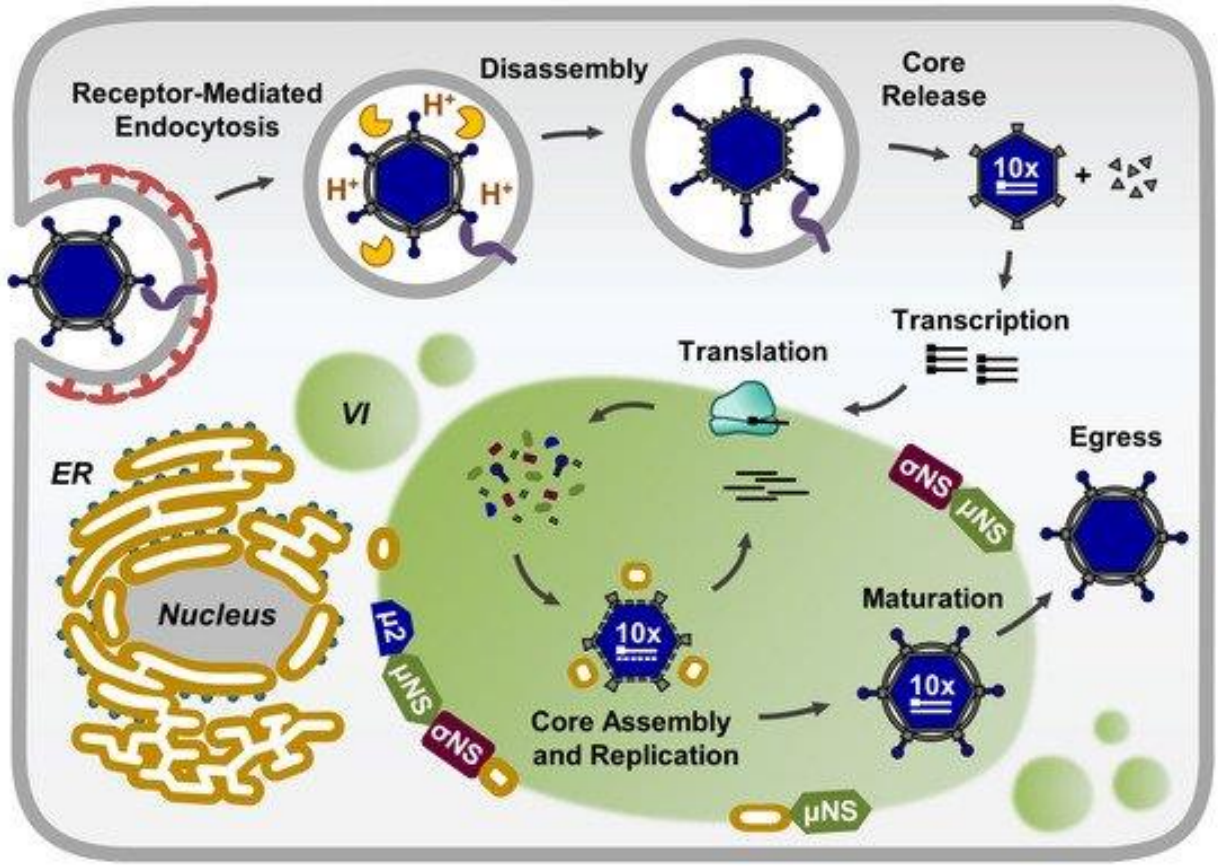

Figure 4. Reovirus replication cycle

Reovirus is internalized into cells by receptor-mediated endocytosis. In the endocytic pathway, the outer capsid is proteolytically degraded by cathepsin proteases. Activated cores are released into the cytoplasm and transcribe viral mRNAs using the (-) sense strands of packaged dsRNA as templates. The mRNAs are released through pores at the vertices of the core. Viral mRNAs are translated into proteins that promote reorganization of the host cell to stimulate viral replication. An accumulation of viral proteins and viral mRNA leads to formation of viral factories, which house viral replication functions. Complexes of viral proteins and mRNAs within factories selectively package one copy of each viral RNA segment. Concurrently or soon thereafter, (-) sense RNA strands are synthesized using mRNA templates, forming dsRNA (genome replication). Progeny cores can transcribe viral mRNA in secondary rounds of transcription, which amplify the replication cycle. Outer-capsid proteins coalescence onto progeny cores, forming mature virions. The outer capsid sterically blocks the pores by which transcripts are released. Mature virions exit cells, completing a replication cycle.

1.5 Reovirus μNS

Reovirus μNS protein forms the scaffold for viral factories (73) (Fig. 5A). This function is essential for reovirus replication. Expression of μNS alone in cells leads to formation of dynamic globular structures that resemble liquid-liquid phase-separated condensates (66, 74) (Fig. 5B). Interestingly, μNS globular structures can form in mammalian, yeast, and bacterial cells (75, 76). These structures do not require other reovirus proteins to form and appear similar in morphology to reovirus factories (67). As such, μNS condensates in uninfected cells are called factory-like structures (77).

The structure of reovirus μNS has not been reported. However, avian reovirus μNS forms crystals in transfected Sf9 insect cells, and promising initial structural features have been deduced using X-ray free-electron lasers (XFFL) (78). Mutagenesis has identified sequences of mammalian reovirus μNS that are required for its function (Fig. 5C). Formation of μNS globular structures requires a predicted C-terminal coiled-coil domain (79). If this domain is deleted or mutated, μNS does not coalesce and instead distributes diffusely in the cytosol (80). Coiled coils are secondary structures composed of at least two α-helices that wind around each other. Coiled coils can promote protein interactions that can drive oligomerization and hydrogel formation (81, 82). Interestingly, coiled coils are often found in proteins that form LLPS condensates (83). In addition to forming a scaffold for viral factories, μNS also recruits viral structural proteins to factories. Reovirus core proteins are enriched in factories to enhance the efficiency of viral capsid assembly. Core proteins co-expressed with μNS in uninfected cells are recruited to factory-like structures (Fig. 5D) (29). These proteins interact with

the N-terminal region of μNS, suggesting that μNS concentrates reovirus proteins essential for viral assembly (29).

μNS has been suggested to bind viral mRNA (84). However, the only evidence suggesting this interaction comes from immunoprecipitation studies of μNS in infected cells (84). There is not conclusive evidence to suggest a direct interaction. An indirect interaction is possible, as other known RNA-binding reovirus proteins that interact with μNS were present in the samples, such as σNS and the reovirus RdRp.

Cellular proteins also interact with μNS. An innate-immune response protein, interferon regulatory factor 3 (IRF3), is sequestered within μNS scaffolds, which prevents translocation of IRF3 into the nucleus where it activates transcription of innate immune response genes (85). It is not clear whether μNS and IRF3 directly interact, but expression of μNS alone promotes IRF3 sequestration into factory-like structures. Additionally, other factors that could aid viral replication, including protein chaperones (heat shock protein 70 [hsp70]) and ER membrane fragments, have been observed to be recruited to μNS scaffolds (86). These interactions could enhance the function of μNS as an integral factory formation protein.

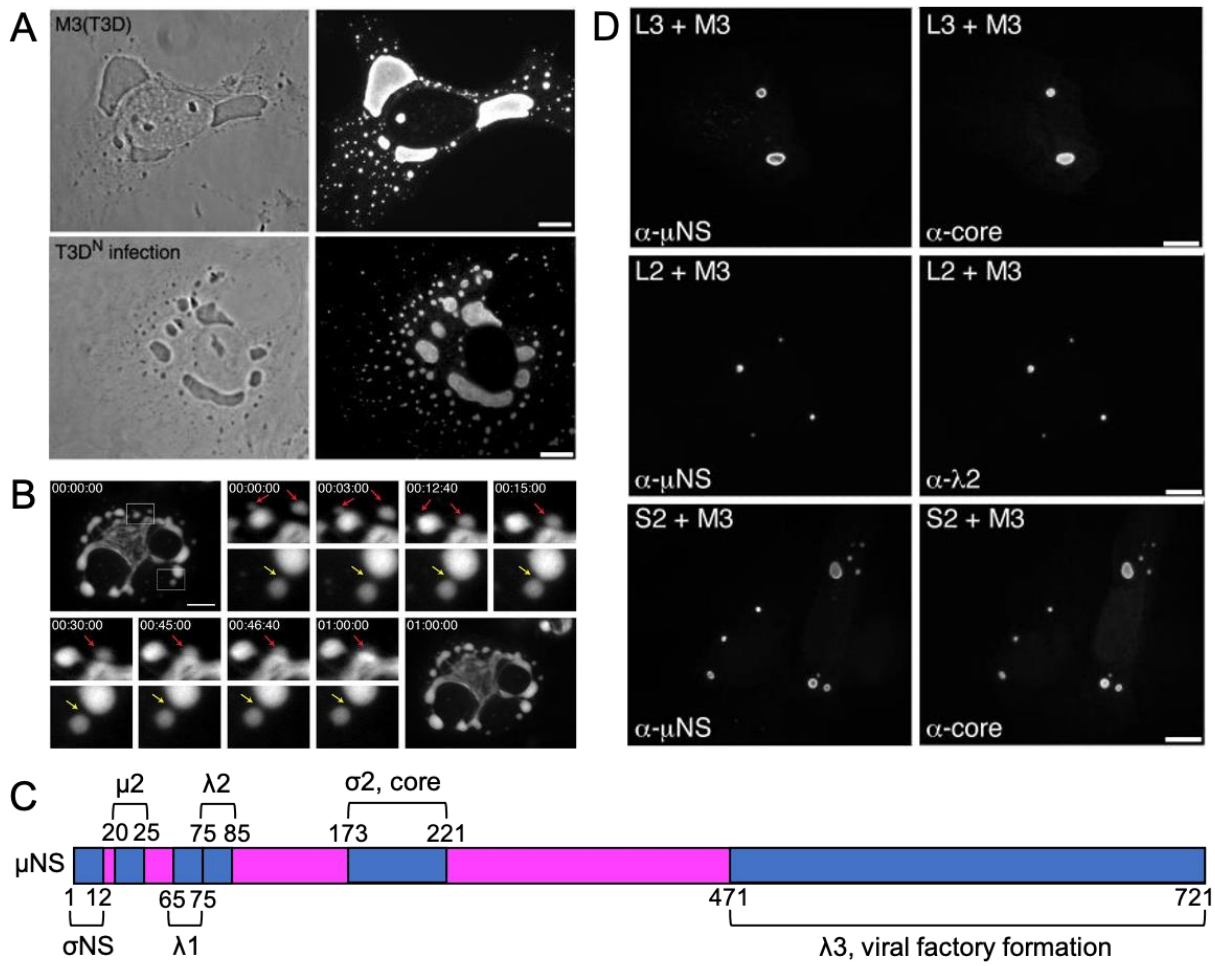

Figure 5. Reovirus μNS protein

(A) Distribution of μNS in cells. Cells were transfected with a μNS expression plasmid [M3(T3D)] or infected with reovirus [T3D infection], and 18 hours post-transfection or post-infection, cells were processed for phase-contrast microscopy or immunofluorescence imaging using antibodies specific for μNS. Scale bar = 10 μm. (B) Still frames from a 1-hour video of fluorescein arsenical helix binder, bis-EDT adduct (FlAsH-EDT2)-labeled μNS in viral factories. Cells were infected with reovirus that encodes FlAsH-EDT2-labeled μNS and, at 18 hours post-adsorption, processed for live microscopy. Viral factory fusion is indicated with red arrows, and fusion events are indicated with yellow arrows. (C) Regions of μNS required for interactions with other reovirus proteins and viral factory formation. (D) Distribution of reovirus core proteins in cells co-transfected with μNS. Cells were co-transfected with expression plasmids encoding λ1 (L3), λ2 (L2), or σ2

(S2) along with μNS (M3) for 18 hours and processed for immunofluorescence imaging using antibodies specific for the proteins shown. Figure adapted with permission from (29, 66, 73).

1.6 Reovirus σNS

In addition to a vital role for reovirus μNS in viral factory formation, nonstructural protein σNS is required to form functional reovirus factories. σNS was discovered in 1971 by Bill Joklik's research team and originally named σ2a because it migrated slightly faster than the reovirus σ2 structural protein in SDS-polyacrylamide gels. Since the protein is not incorporated into mature virions it was renamed σNS in 1978 to convey its identity as a nonstructural reovirus protein (87).

In infected cells, σNS is detectable soon after μNS and integrates into the matrix of viral factories (73). In uninfected cells, exogenous σNS distributes diffusely in the cytoplasm when expressed alone but localizes to factory-like structures in the presence of μNS (Fig. 6A) (67). Recruitment of σNS to μNS factory-like structures requires the N-terminal regions of both proteins (88). Since localization is essential for the function of many proteins, σNS has been hypothesized to serve a critical function in factory formation. Without σNS, reovirus replication stalls at a replication step that precedes or encompasses dsRNA synthesis (Fig. 6B) (89). This observation suggests that σNS is directly or indirectly required for dsRNA synthesis. However, the precise function of σNS in viral replication has been enigmatic.

The first function ascribed to σNS was direct engagement in dsRNA synthesis . However, this conclusion was likely a mistake. When fractions of radiolabeled reovirus

proteins purified from infected L-cells were incubated *in vitro* with homopolymer templates (polyriboadenylate [poly(A)], polyribouridylate [poly(U)], polyriboguanylate [poly(G)], and polyribocytidylate [poly(C)]), fractions containing σNS most effectively synthesized a poly(G) strand using poly(C) templates, forming dsRNA (90). Since the fractions largely contained σNS, the polymerase activity was thought to be attributable to σNS. However, subsequent studies using recombinant σNS showed that the purified protein did not have polymerase activity, while λ3, the reovirus RdRp did mediate this activity (18, 20). These data suggest that σNS forms complexes with λ3 that facilitate formation of genome replication complexes.

An indirect way that σNS could be involved in a replication step that precedes dsRNA synthesis is by enhancing translation of viral proteins. In some cases, low concentrations of σNS can enhance translation of non-reovirus mRNAs *in vitro* by a mechanism that is unknown (89). However, the benefits to translation are lost as the concentration of σNS reaches saturating conditions (89). Studies to determine whether these *in vitro* concentrations are reproduced in infected cells have not been reported. It has been hypothesized that translation-enhancing concentrations could be achieved early during infection and, as infection progresses, translation diminishes, since intracellular [σNS] increases (89). While regulating translation could be a theoretical function of σNS, no direct evidence exists that reovirus mRNAs are translated more efficiently in the presence of σNS.

Other indirect evidence suggesting that σNS enhances viral translation comes from studies that probed σNS interactions with cellular factors. Protein complexes containing either phosphorylated ribosomal protein S6 (pRPS6), which is a part of the

40S ribosomal complex, or eukaryotic translation initiation factor 3 subunit A (eIF3A) captured by immunoprecipitation from reovirus-infected cells include σNS. Interestingly, these translation proteins are observed by immunofluorescence within reovirus factories (68). Interactions between σNS and these translation proteins could be direct or indirect. ER membranes, which can include membrane-bound ribosomes, also are modified by σNS, and expression of σNS in cells can induce ER tubulation (70). The mechanism by which σNS causes ER reorganization or the functional consequence of this change are not clear (70)

Ras-GAP SH3 domain binding protein 1 (G3BP1) is another cellular protein that closely associates with σNS. G3BP1 is an important host protein that mediates cellular stress responses. In stressed cells, G3BP1 binds and sequesters mRNAs with stalled polysomes, initiating stress granule formation (91). Using proximity-ligation assays (PLAs), σNS is detected near G3BP1 (92). However, genetic ablation of G3BP1 in mouse embryotic fibroblasts does not alter reovirus replication, suggesting that essential functions of σNS do not depend on interactions with G3BP1 (92).

One well-established property of σNS is its capacity to bind nucleic acid (93). Purified σNS interacts preferentially with single-stranded (ss) RNA and is not thought to display sequence specificity (94). It is not known whether σNS binds ssRNA nonspecifically in infected cells. However, σNS can co-immunoprecipitate all 10 viral mRNAs from reovirus-infected cells and protects specific regions of viral mRNAs from degradation (84, 95). Using RNase-protection assays, it appears that σNS binding can cover 20-nucleotide regions of RNA (94).

The N-terminal 38 residues of σNS are required for RNA binding (89), suggesting that this region forms an RNA-binding domain. Computational structural analyses suggest that the N-terminal region consists of an alpha-helix (96). It is not known whether this region directly or indirectly engages RNA. σNS binds RNA with positive cooperativity and can form oligomers (89). Imaging σNS-RNA complexes using cryo-electron microscopy (EM) reveals long filamentous structures. The mechanism by which σNS binds RNA or the function of its RNA-binding capacity in viral replication are unknown. However, since this reovirus protein binds ssRNAs and localizes to viral factories, I hypothesized that an essential function of σNS is to recruit viral mRNAs to factory scaffolds where they could be packaged into progeny cores.

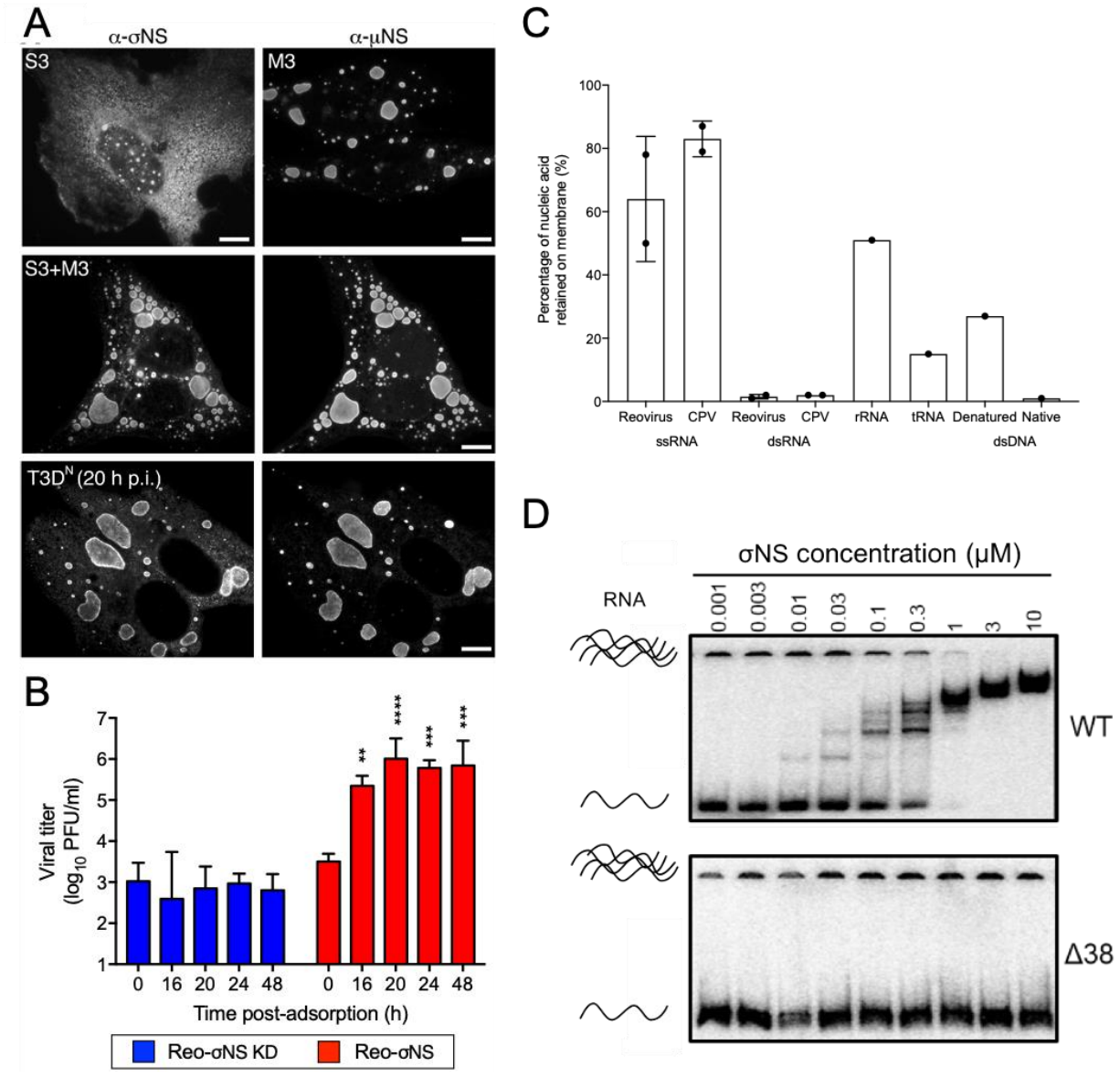

Figure 6. Reovirus σNS protein

(A) Distribution of σNS in cells. Cells were transfected with σNS (S3) or μNS (M3) expression plasmids, co-transfected with both plasmids (S3 + M3), or infected with reovirus (T3D). At 18 hours post-transfection or 20 hours post-adsorption, cells were processed for immunofluorescence imaging using antibodies specific for σNS or μNS. Scale bar = 10 μm. (B) Cells expressing σNS-specific siRNAs were adsorbed with reovirus susceptible (Reo-σNS KD) or resistant to σNS-targeted siRNAs (Reo-σNS). At the time points shown, cell lysates were prepared, and viral titers in lysates were quantified by plaque assay. The results shown are mean viral titers ± SD (n=3). One-way ANOVA with Tukey's multiple comparisons test was conducted to

identify titers that significantly differed from the titer at 0 h (**, $P < 0.01$; ***, $P < 0.001$; ****, $P < 0.0001$). (C) Purified recombinant σNS was incubated with the ^{32}P-labedled RNA species shown at 4º C for 15 minutes, and complexes were filtered on nitrocellulose membranes. Radioactivity was quantified using a liquid-scintillation spectrophotometer. RNAs for the binding assay were purified from reovirus, cytoplasmic polyhedrosis virus (CPV), and yeast for ribosomal RNA (rRNA) and transfer RNA (tRNA). A linearized *E. coli* cloning plasmid was used for double-stranded DNA (dsDNA). (D) σNS binds ssRNA**.** Increasing concentrations of purified σNS and Δ38-σNS were incubated for 10 minutes at RT with P^{32}-radiolabeled 7SK stem I RNA (108 nt) that had been previously denatured. Aggregates of RNA are trapped in wells at the top of the gels, and the laddering effect of RNA is due to different quantities of bound σNS. Figure adapted with permission from (88, 89, 97).

1.7 Significance of research

Viral replication requires the formation of neoorganelles in infected cells to concentrate essential viral and host replication components. However, for many viruses, it is unclear how these components coalesce into neoorganelles to form factories for viral replication. I discovered that two mammalian reovirus nonstructural proteins act in concert to form functional viral factories. Reovirus μNS protein assembles into exclusive factory scaffolds that require reovirus σNS protein for efficient viral mRNA incorporation. My results demonstrate a role for σNS in RNA recruitment to reovirus factories and, more broadly, show how a cytoplasmic, non-membrane-enclosed factory is formed by an RNA virus. Understanding mechanisms of viral factory formation could help identify new targets for antiviral therapeutics that disrupt assembly of these structures and inform the use of nonpathogenic viruses for biotechnological applications.

2.0 Reovirus nonstructural protein σNS recruits viral RNA to replication factories

2.1 Introduction

Reovirus requires σNS to replicate, but its precise functions are not well defined (89). In the absence of σNS, reovirus factories are small and incapable of producing progeny virions (89). I hypothesized that altering known biochemical properties of σNS and studying subsequent effects on viral replication would allow me to identify how σNS supports viral factory formation.

The N-terminal 38 residues of σNS (Fig. 7A) are required for binding to RNA *in vitro* (89). These residues are conserved in available σNS sequences (98), and three of these residues (R6, R14, and R29) are conserved in the σNS proteins of other *Orthoreovirus* species (Fig. 8). Protein-RNA contacts occur by electrostatic or base-stacking interactions (99), and approximately 25% of the residues in this region of σNS are capable of mediating either of these interactions. I hypothesized that disrupting electrostatic or base-stacking interactions would prevent σNS from binding RNA and inhibit σNS functions. To test this hypothesis, I exchanged conserved basic and aromatic residues in the N-terminus with alanine and evaluated the resultant mutant proteins for the capacity to support reovirus replication. Additionally, I examined whether viral mRNAs distributed to viral factories and factory-like structures when σNS was absent or incapable of binding RNA. The results show viral mRNAs only incorporate into viral factories or factory-like structures when σNS can bind RNA, suggesting that σNS recruits viral RNA to factory scaffolds for packaging into progeny virions.

The reverse genetics experiments to recover σNS mutant viruses were assisted by Janie French. Analysis of the imaging data was conducted with the assistance of Drs. Krishnan Raghunathan and Gwen Taylor. Immunogold-labeling studies to assess intra-factory distribution of σNS were conducted by Drs. Raquel Tenario and Dr. Isabel Fernandez in Dr. Cristina Risco's laboratory. Reagents required for the work described in this chapter, including μNS-specific antibodies, were provided by Dr. John Parker.

2.2 Results

2.2.1 Engineering σNS mutants deficient in RNA binding

To determine whether the RNA-binding capacity of σNS is required for reovirus replication, we engineered σNS mutants deficient in binding RNA. We engineered seven alanine substitution mutations individually into a σNS expression plasmid, resulting in seven σNS mutants (R6A, K11A, R14A, Y25A, R29A, K35A, and R38A). We also engineered a triple mutant to disrupt a cluster of positively charged residues in the N-terminus (K11A, K13A, R14A; termed TriA) and a mutant lacking the N-terminal 38 residues (Δ38).

To verify that the engineered σNS mutations do not disrupt protein folding, we characterized the mutants using three independent approaches. First, we conducted limited proteolysis of WT and mutant σNS proteins recovered from coupled *in vitro* transcription and translation reactions using rabbit reticulocyte lysates supplemented with S^{35} methionine. Following *in vitro* expression, WT and mutant proteins were

digested with proteinase K, and digestion reactions were resolved by polyacrylamide gel electrophoresis (PAGE) (Fig. 7B). The only mutant that differed from WT σNS in digestion kinetics or resultant protein fragments was Δ38 σNS. Based on these results, we conclude that Δ38 σNS is not properly folded and excluded this mutant from subsequent analyses. Second, we used σNS conformation-specific monoclonal antibody 2A9 (100) to immunoprecipitate σNS expressed in HEK293T cells (Fig. 7C). While varying levels of protein expression were apparent, all of the mutants were immunoprecipitated by this conformation-specific antibody, suggesting that the mutations do not disrupt an epitope in σNS recognized by this antibody. Third, we tested whether the mutant σNS proteins were capable of co-immunoprecipitation (co-IP) with a known σNS-binding partner, reovirus μNS protein. The two proteins were co-expressed in HEK293T cells, and co-IPs were conducted using monoclonal antibody 3E10, which also is directed against σNS (100) (Fig. 7D). Each of the mutants was capable of immunoprecipitating μNS. Surprisingly, replacing positively charged residues in σNS with alanine residues promoted more efficient immunoprecipitation of μNS. Collectively, the σNS alanine substitutions and the TriA σNS mutant yielded folding phenotypes comparable to WT σNS and were capable of interacting with a known σNS-binding partner, suggesting that the mutations do not substantially alter σNS structure.

We next evaluated the RNA-binding capacity of the σNS mutants using an RNA-dependent electrophoretic mobility shift assay (EMSA). In these experiments, we employed a property of σNS to form oligomeric ladders with RNA when expressed *in vitro* (89). These ladders collapse following treatment with RNase A (Fig. 9A), indicating that RNA binding is required for ladder formation. WT and mutant σNS proteins were

expressed in rabbit reticulocyte lysates in the presence of ^{35}S methionine. Half of each protein sample was resolved using native PAGE to separate complexes of σNS and RNA, while the other half was electrophoresed using denaturing PAGE to compare protein levels (Fig. 9B). Based on the molecular weight of monomeric WT σNS (~ 37 kDa), σNS appears to migrate in the presence of RNA as a hexamer and correspondingly larger species that vary by two monomers of σNS each. Treatment of the σNS-RNA complexes with RNase A yielded a band that migrates at approximately the 66 kDa molecular-weight marker, which likely represents a dimer of σNS not bound to RNA. Mutant forms of σNS produced bands that migrated at comparable molecular weights to the dimer, but the intensities varied, inversely correlating with the intensities of the higher molecular weight bands. The percentage of RNA-dependent oligomers for each σNS protein was determined by dividing the total density of bands migrating between ~ 200 and 1,000 kDa (Fig. 9A, green bar) by the sum of the densities of all bands observed in the gel (Fig. 2A, green and orange bars). Two mutants, R6A and TriA σNS, did not display any detectable RNA-dependent oligomerization (Fig. 9A). The RNA-binding capacity of the other charged-to-alanine mutants was less than that of WT or Y25A σNS (Fig. 9C). However, all σNS-RNA complexes were sensitive to RNase A treatment. Most mutants yielded dominant dimer bands following RNase A treatment, but the Y25A mutant did not. Instead, Y25A σNS appeared to aggregate at the top of the gel following RNase A treatment (Fig. 10). These results suggest that positively-charged residues in the σNS N-terminus are required for RNA binding. However, predicted base-stacking interactions mediated by Y25 appear dispensable for this property, but without RNA, the Y25A mutant appeared more prone to aggregation.

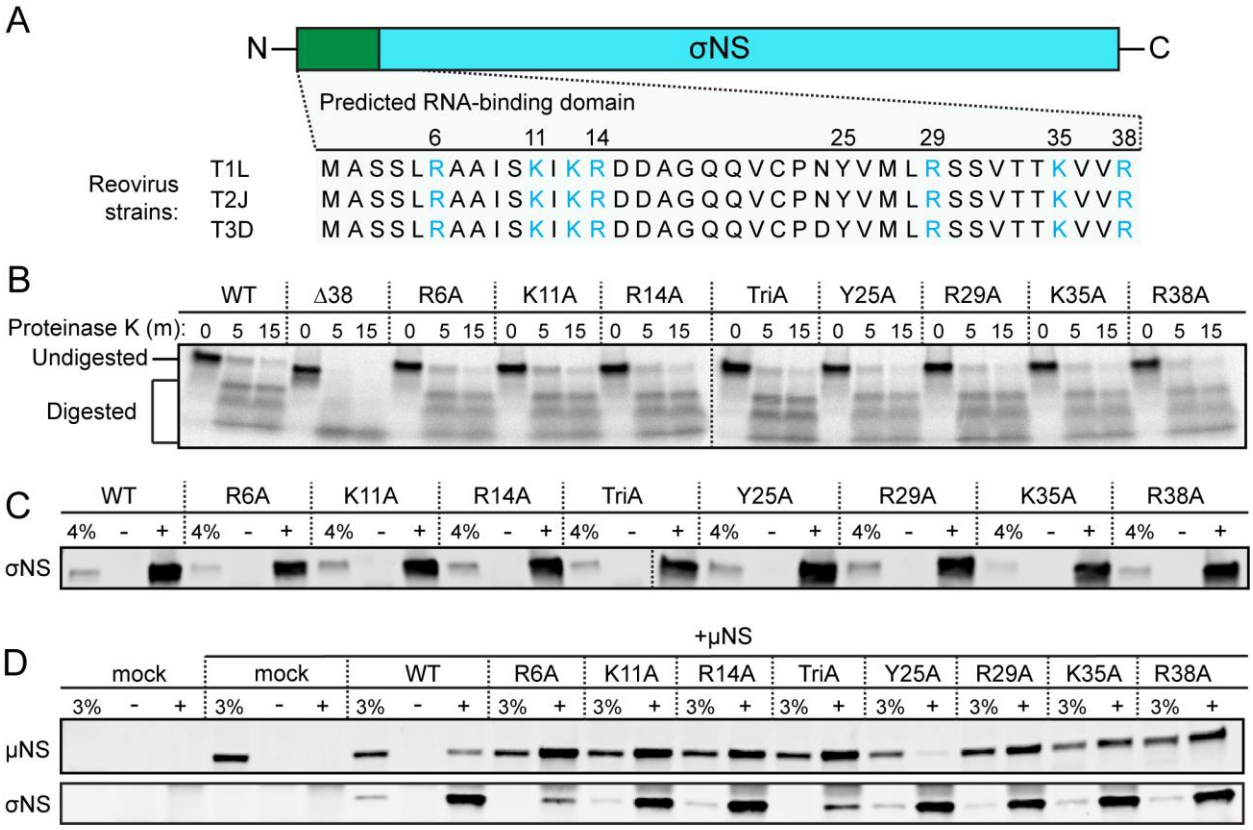

Figure 7. Mutations in σNS do not appear to alter protein folding

(A) Sequence alignment of the N-terminal 38 amino acids (green bar) of σNS encoded by mammalian reovirus strains T1L, T2J, and T3D. Positively charged residues are shown in blue. (B) ^{35}S-labeled, *in vitro*-expressed σNS was incubated with proteinase K for the times shown, resolved by SDS-PAGE, and visualized by autoradiography. 293T cells were transfected with σNS alone (C) or co-transfected with σNS and μNS (D) and incubated for 24 h. Total protein in cell lysates was immunoprecipitated using an IgG isotype antibody (-), conformation-specific σNS-specific monoclonal antibody 2A9 (C; +), or σNS-specific monoclonal antibody 3E10 (D; +), resolved by SDS-PAGE, and immunoblotted using antisera directed against σNS (C, D) or μNS (D). Percentages of total lysates in the immunoprecipitation reactions (4% [C] or 3% [D]) were used as loading controls.

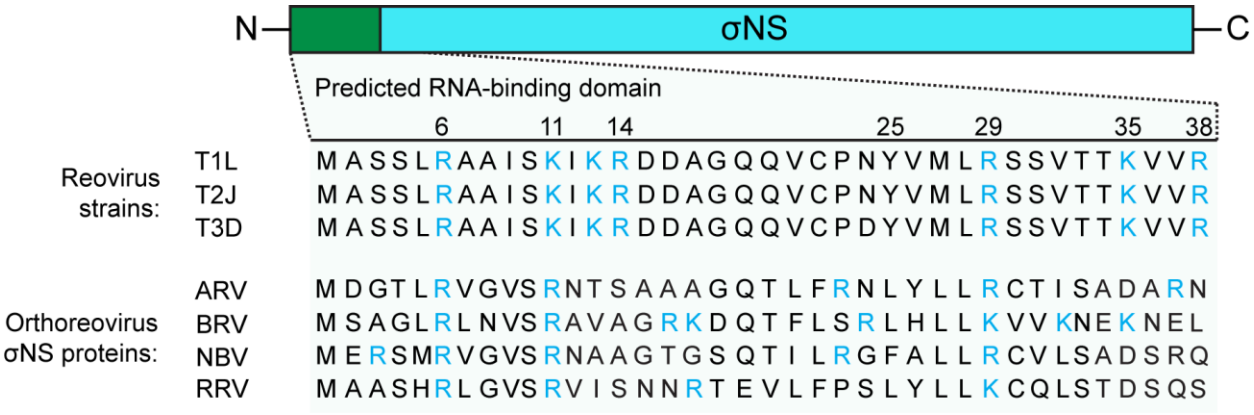

Figure 8. Sequence alignment of the N-terminal 38 amino acids (green bar) of σNS proteins encoded by *Orthoreovirus* species.

Shown are σNS sequences from mammalian reovirus strains T1L, T2J, and T3D, avian reovirus (ARV), baboon reovirus (BRV), Nelson Bay orthoreovirus (NBV), and reptilian reovirus (RRV). Positively charged residues are shown in blue.

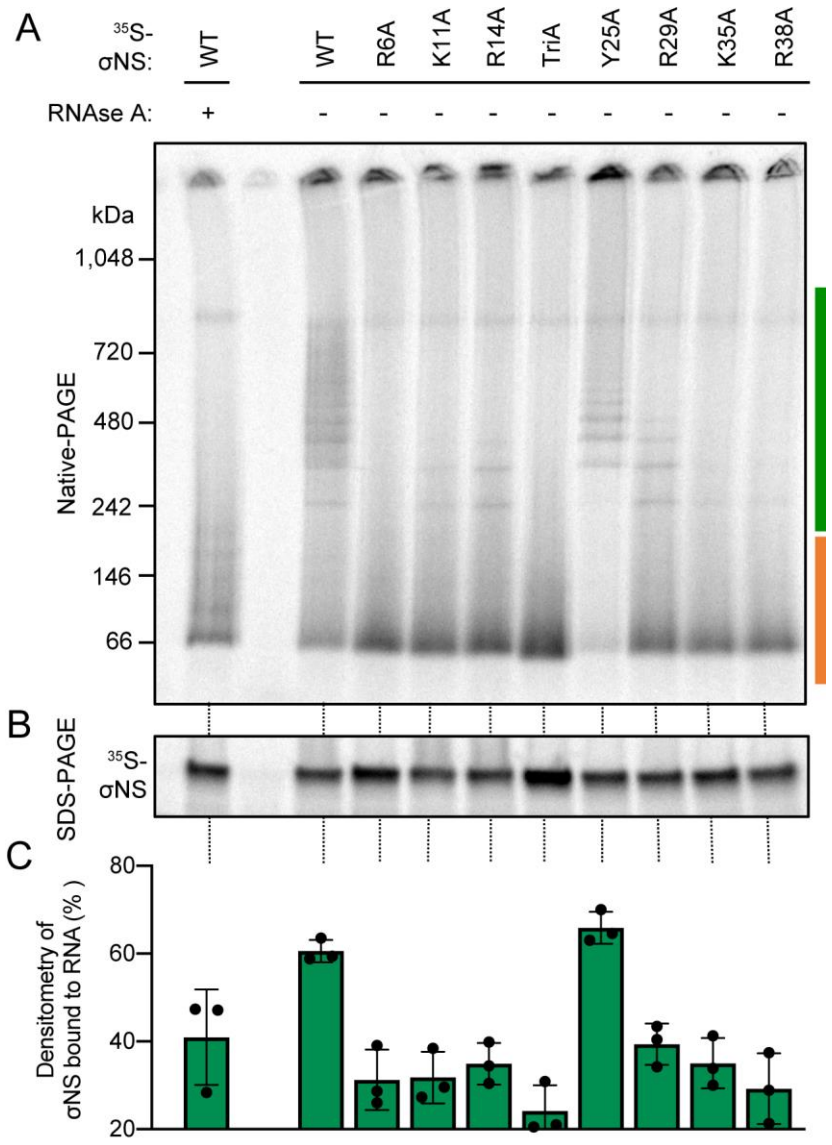

Figure 9. Alanine substitution of positively charged residues in a predicted RNA-binding domain of σNS alters RNA-dependent oligomerization

^{35}S-labeled σNS was expressed in RRLs and incubated with or without RNase A. Samples were resolved by (A) native PAGE to preserve oligomeric species or (B) SDS-PAGE to monitor protein expression and visualized by autoradiography. The scale bar to the right of the native polyacrylamide gel (A) marks the kilodalton (kDa) ranges used for densitometric analysis of each σNS construct. The green scale bar marks σNS bound to RNA, whereas the orange scale bar marks unbound σNS. (C) The efficiency with which each σNS construct forms RNA-dependent oligomers was calculated by dividing the density of

σNS bound to RNA (Fig. 2A; green scale bar) by the total density of σNS present in the gel (Fig. 2A; green and orange scale bar)

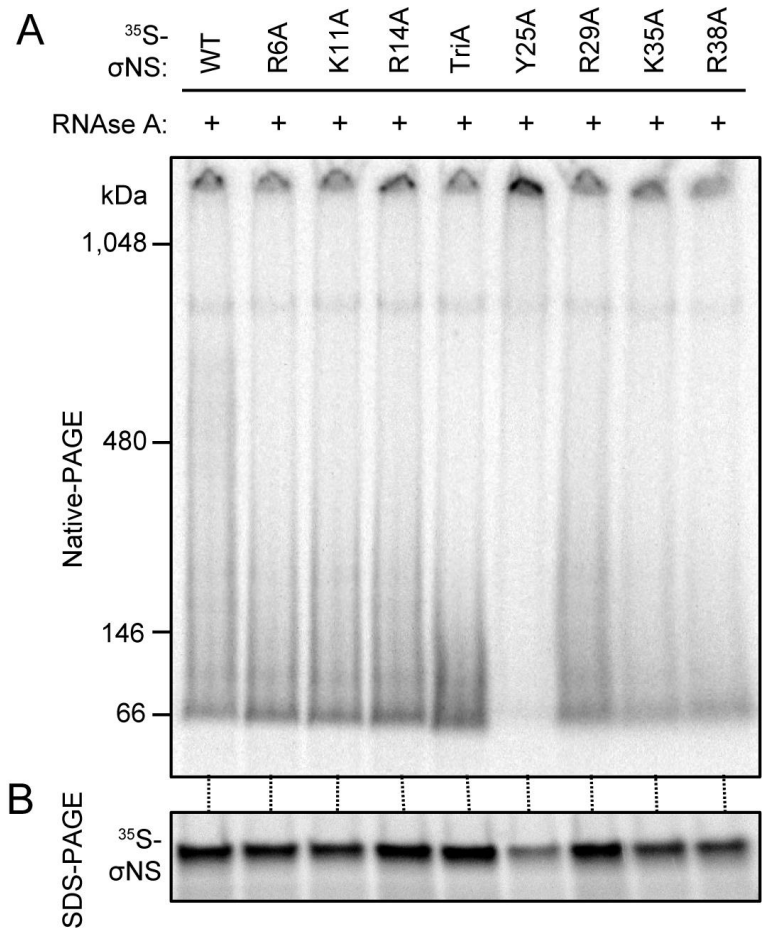

Figure 10. RNase A treatment of σNS mutants disrupt RNA-dependent oligomerization

^{35}S-labeled σNS was expressed in RRLs and incubated with RNase A. Samples were resolved by (A) native PAGE to preserve oligomeric species or (B) SDS-PAGE to monitor protein expression and visualized by autoradiography

2.2.2 Mutants of σNS incapable of RNA binding fail to complement σNS knockdown during infection

To test whether σNS RNA-binding capacity contributes to reovirus replication, we first attempted to recover reoviruses encoding the R6A, K11A, or R29A mutations in σNS using reverse genetics. Plaque-forming mutant viruses could not be recovered in three independent attempts, suggesting that residues required for RNA-binding also are required for viral replication. To define the step in reovirus replication facilitated by the RNA-binding capacity of σNS, we established a complementation system in which WT or mutant forms of the proteins could be tested for the capacity to overcome inhibition of σNS expression. First, we evaluated the capacity of expressed WT or mutant σNS proteins to complement σNS knockdown in σNS-siRNA cells (89). As a control, we used HEK293T cells constitutively expressing siRNAs directed against GFP (GFP-siRNA cells) (89). We transfected these cells with expression plasmids encoding GFP as a negative control, WT σNS, or σNS incorporating synonymous mutations in the siRNA recognition site (σNS mismatch [σNS-MM]). Transfected cells were incubated for 24 h, after which time, cells were adsorbed with reovirus at a low multiplicity of infection (MOI). We used a low MOI in these experiments to enable the constitutively expressed siRNAs to diminish the expression of virus-encoded σNS transcripts. As anticipated, at 24 h post-adsorption, σNS protein levels (Fig. 11A) and reovirus replication (Fig. 11B) were unaffected by the GFP-restricting siRNA. However, σNS protein expression was not detected and reovirus replication was substantially impaired by the σNS-restricting siRNA, and neither σNS expression nor reovirus replication was complemented by GFP. σNS protein expression was greater following σNS-MM transfection relative to

that following WT σNS transfection (Fig. 11A), demonstrating the susceptibility of WT σNS transcripts to siRNA-mediated knockdown in these cells. However, transfection of WT σNS into reovirus-infected σNS-siRNA cells allowed reovirus yields comparable to those following transfection of σNS MM, indicating that increased levels of σNS allowed by the mismatch mutations in the siRNA target sequence do not lead to increased production of viral progeny (Fig. 11B). Both WT and MM σNS were capable of promoting reovirus replication in σNS-siRNA cells relative to complementation with GFP. These results indicate that overexpression of σNS prior to infection can rescue reovirus replication in cells expressing σNS-specific siRNAs and that rescue is independent of mismatch mutations in the σNS siRNA target sequence.

To determine whether the engineered σNS mutants can complement reovirus replication in cells expressing σNS-specific siRNAs, we transfected GFP-siRNA and σNS-siRNA cells with the σNS mutants, adsorbed with reovirus, and monitored viral yields by plaque assay (Fig. 12A). Following infection of GFP-siRNA cells, viral yields were only modestly altered by expression of WT or mutant σNS (Fig. 12B). In contrast, following infection of σNS-siRNA cells, viral yields were reduced to a maximum of 10,000-fold following expression of the σNS mutants incapable of binding RNA relative to expression of WT σNS (Fig. 12B). Additionally, Y25A σNS complemented reovirus replication more efficiently than the other mutants, albeit at lower levels than did WT σNS. Transfection of GFP-siRNA and σNS-siRNA cells with σNS mutants resulted in variable levels of σNS protein after 24 h of incubation (Fig. 12C). R6A σNS and TriA σNS displayed the lowest levels of expression, which was surprising, as expression of these mutants was similar to WT σNS in rabbit reticulocyte lysates (Fig. 9B). However,

levels of σNS present prior to infection did not correlate with the capacity of the mutants to complement σNS siRNA-mediated knockdown (Fig. 12B). K11A σNS, which was expressed at levels comparable to WT σNS, and R14A σNS, which was expressed at higher levels than WT σNS, were incapable of restoring viral replication. These results suggest that the capacity of σNS to support viral replication is not contingent on levels of σNS expression and instead on properties of the protein that were altered following mutagenesis, likely the capacity to bind RNA.

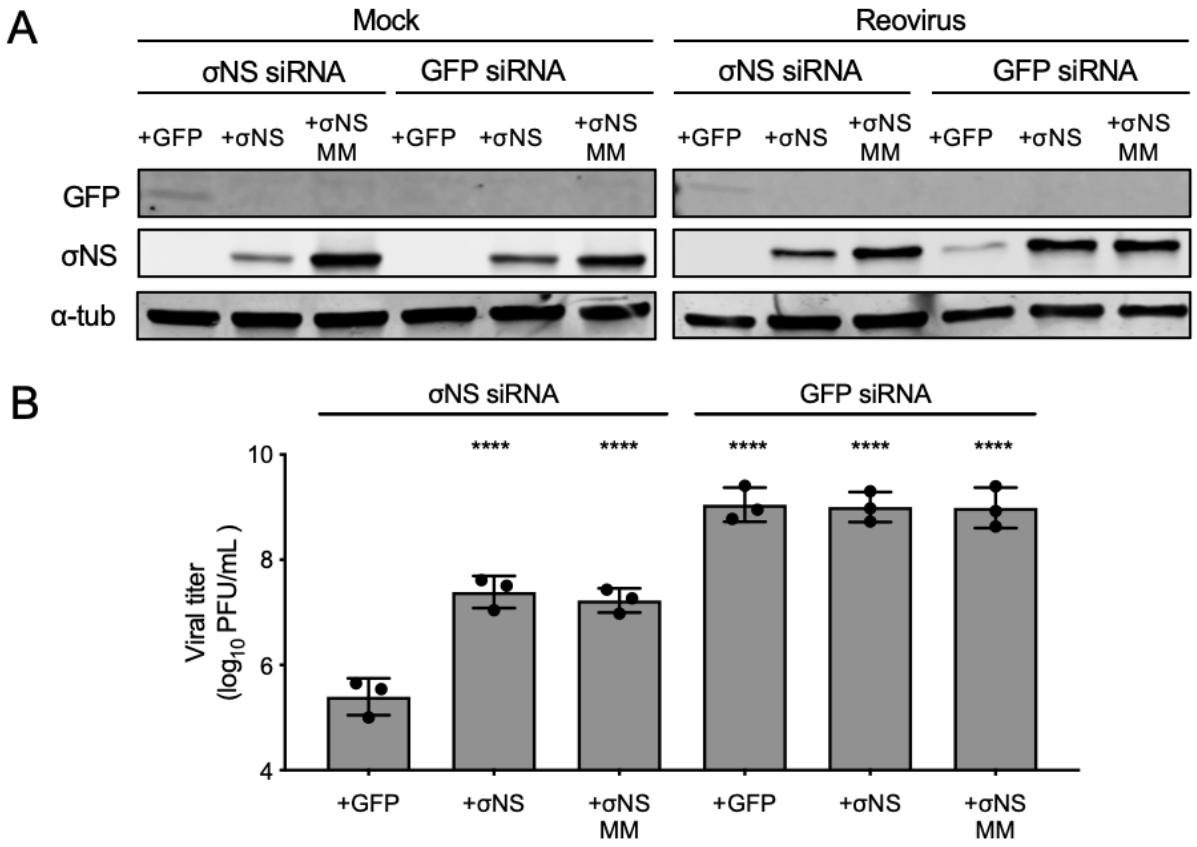

Figure 11. Overexpression of σNS complements siRNA knockdown of σNS during infection

Cells that constitutively express siRNAs directed against σNS or GFP were transfected with expression plasmids encoding GFP, WT σNS (σNS), or WT σNS with σNS-siRNA-resistant sequences (σNS MM) and incubated for 24 h. Cells were adsorbed with reovirus strain T3D at an MOI of 5 PFU/cell and incubated for 24 h. Cell lysates were collected for (A) immunoblotting and (B) infectious virus quantification by plaque assay. (A) Immunoblot analysis of proteins expressed following complementation. Protein expression was evaluated using monoclonal antibodies specific for GFP or alpha-tubulin (α-tub) and guinea-pig sera specific for σNS. (B) Infectious virus quantification following complementation. Titer values that differ significantly from those obtained from cells expressing siRNAs against σNS complemented with GFP by one-way analysis of variance (ANOVA) with Dunnett's multiple-comparison test are shown (****, $P < 0.0001$).

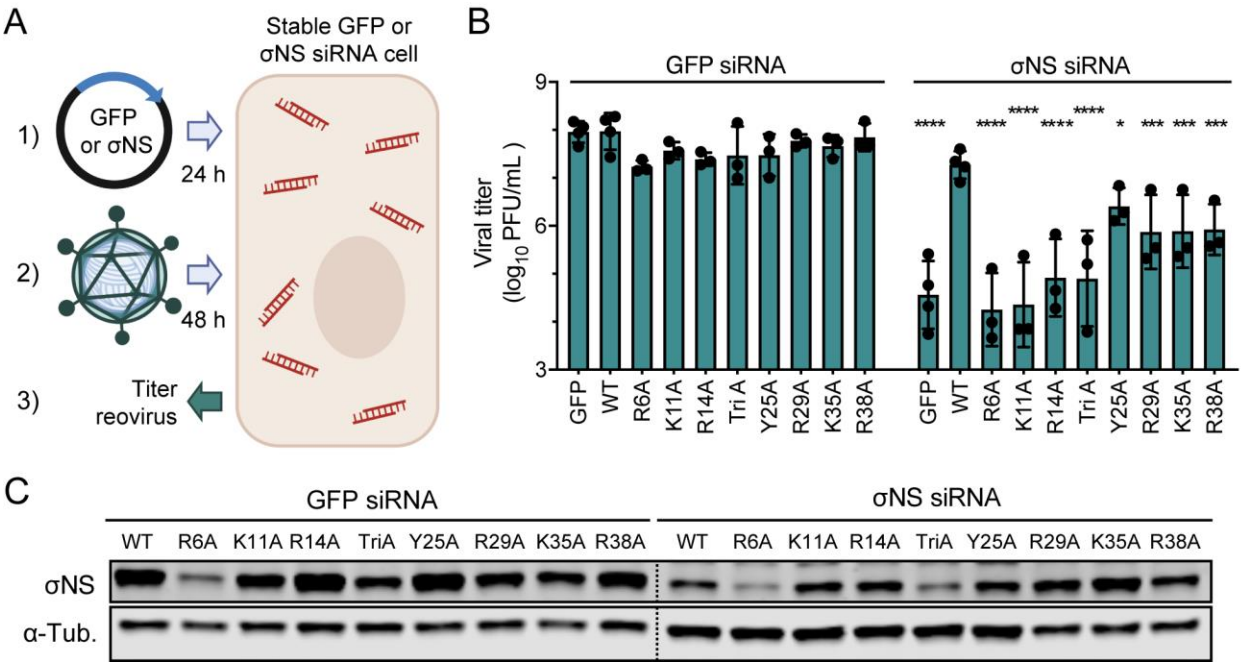

Figure 12. Mutants of σNS incapable of RNA binding fail to complement reovirus replication in cells expressing σNS-specific siRNAs

(A) Cells that constitutively express siRNAs directed against GFP or σNS were transfected with expression plasmids encoding GFP or the σNS constructs shown and incubated for 24 h. Cells were adsorbed with reovirus strain T3D at an MOI of 5 PFU/cell and incubated for 48 h. (B) Cell-culture supernatants were collected for infectious virus quantification by plaque assay. Titer values that differ significantly from those obtained from cells expressing siRNAs against GFP complemented with GFP by one-way ANOVA with Dunnett's multiple-comparison test are shown (**, $P < 0.0021$; ***, $P < 0.0002$; ****, $P < 0.0001$). (C) Cells that constitutively express siRNAs against GFP or σNS were transfected with expression plasmids encoding the σNS constructs shown and incubated for 24 h. Cell lysates were resolved by SDS-PAGE and immunoblotted using antisera directed against σNS and monoclonal antibodies specific for alpha-tubulin (α-Tub).

2.2.3 σNS incorporation into reovirus factories is disrupted by mutations that alter RNA binding

In reovirus-infected cells, σNS preferentially localizes to viral factories (100). To determine whether σNS distribution in cells contributes to its function, we assessed the intracellular distribution of WT and mutant forms of σNS during infection. We selected three mutants (R6A, Y25A, and R29A) to represent our panel of σNS mutants in this and subsequent experiments. The R6A and R29A mutants display little to no RNA-dependent oligomerization and fail to complement σNS knockdown in infected σNS-siRNA cells. The Y25A mutant displays RNA-dependent oligomerization comparable to WT σNS and complements σNS knockdown in infected σNS-siRNA cells more efficiently than the other σNS mutants. To evaluate the distribution of mutant σNS during infection, we transfected σNS-siRNA cells with WT or mutant forms of σNS, infected the cells with reovirus, stained fixed cells with antibodies specific for σNS and μNS, and imaged the cells using confocal indirect immunofluorescence microscopy (Fig. 13A). Viral factory structures were demarcated by intense μNS staining. Factories formed in all conditions and retained a globular morphology, which is characteristic of the type 3 Dearing (T3D) strain of reovirus used in these experiments (101). However, factories formed in the absence of σNS expression or in the presence of the R6A or R29A σNS mutants were smaller than those formed in the presence of WT or Y25A σNS. Immunofluorescence signals for WT and Y25A σNS were more frequently detected in viral factories, while those produced by the R6A and R29A σNS mutants were more frequently detected outside of viral factories (Fig. 13B). Collectively, these

observations suggest that mutations impairing RNA binding limit viral factory maturation and alter σNS distribution to viral factories.

To confirm that the preferential distribution of σNS to the periphery of larger viral factories was not solely due to poor penetration of σNS-specific antibodies into factories of fixed and permeabilized cells, we processed reovirus-infected cells for Tokuyasu cryosections, stained σNS with gold-labeled σNS-specific antibodies, and imaged the cells using transmission electron microscopy (Fig. 14). Small puncta containing σNS were observed throughout the cytoplasm in the majority of infected cells. These small puncta were not coated at the periphery with σNS, but instead, σNS was distributed diffusely in these structures (Fig. 14, A and B). However, in larger, electron-dense factories, σNS was concentrated at the factory periphery (Fig. 14, C and D), consistent with previous results (68). These observations suggest that σNS distributes to the factory periphery as these structures enlarge.

To determine whether incorporation of σNS into reovirus factories depends on viral replication, we used a simplified factory-like structure model system (67, 73). We transfected HEK293T cells with μNS and WT or mutant forms of σNS and processed the cells for confocal immunofluorescence microscopy to visualize σNS and μNS (Fig. 15A). WT and Y25A σNS were efficiently incorporated into factory-like structures (Fig. 15B). The morphology and size of these structures resembled viral factories observed during reovirus infection (Fig. 15B). In contrast, the R6A and R29A σNS mutants were poorly incorporated into factory-like structures (Fig. 15B) and recapitulated phenotypes observed during complementation of reovirus-infected cells (Fig. 13B). Based on data presented thus far, we conclude that RNA promotes oligomerization of σNS, which

could enable a greater number of σNS molecules to incorporate into factory structures, overcoming saturation limits of μNS binding.

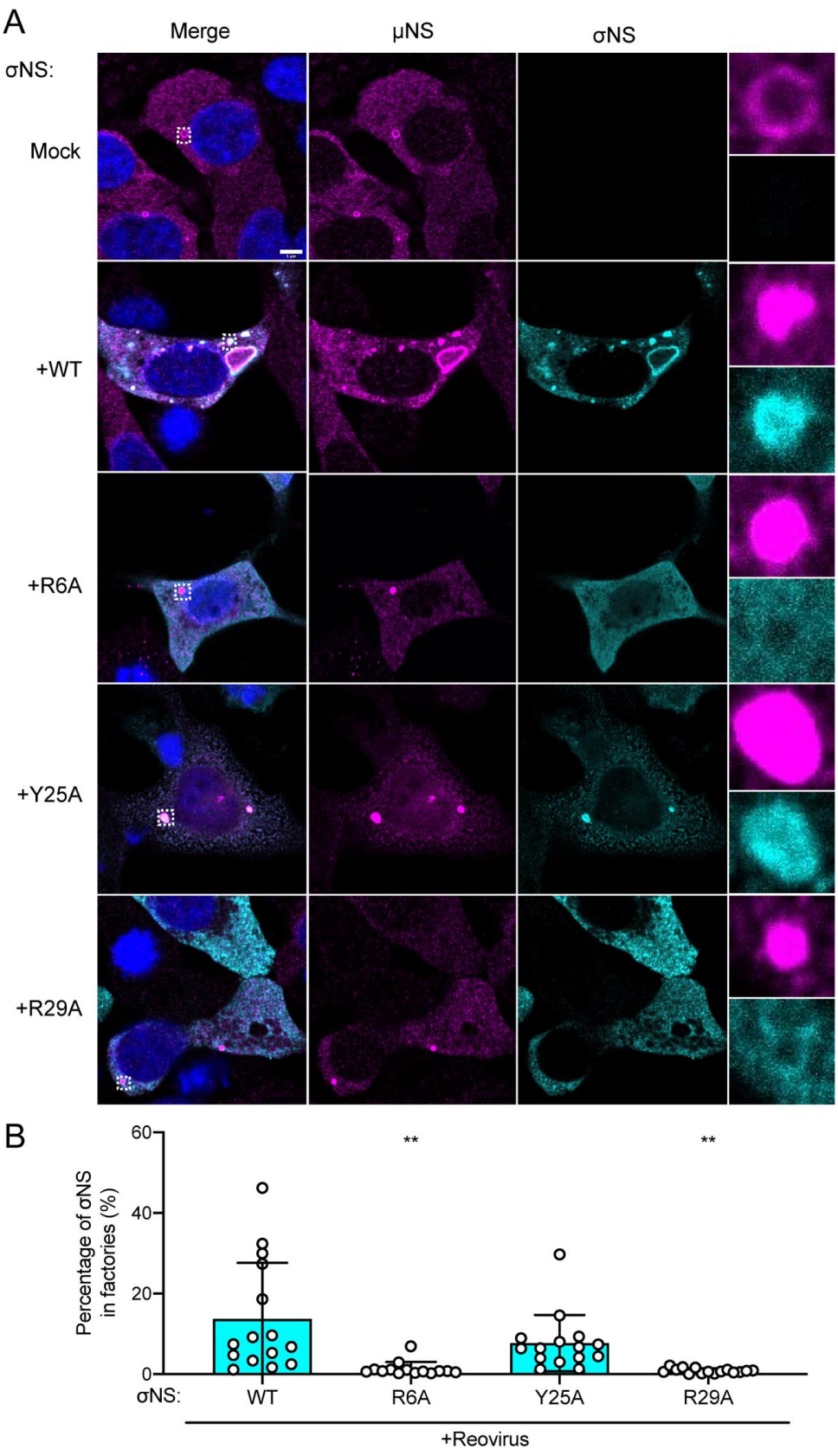
A
Merge
μNS
σNS
σNS:
Mock
+WT
+R6A
+Y25A
+R29A
B
Percentage of σNS in factories (%)
60
40
20
0
**
**
σNS:
WT
R6A
Y25A
R29A
+Reovirus

Figure 13. Mutations in σNS that compromise RNA binding disrupt incorporation of the protein into reovirus replication organelles

(A) Cells that constitutively express siRNAs directed against σNS were transfected with expression plasmids encoding the σNS constructs shown and incubated for 24 h. Cells were adsorbed with reovirus strain T3D at an MOI of 5 PFU/cell, incubated for 48 h, fixed, stained using σNS-specific monoclonal antibody 3E10 (cyan), μNS-specific antiserum (magenta), and DAPI (blue), and imaged using confocal microscopy. Regions selected for magnification are indicated by dotted white boxes. Bar, 5 μm. (B) The percentage of σNS immunofluorescence signal in reovirus factories was quantified by dividing the sum of σNS signal in reovirus factories by the sum of cytoplasmic σNS signal. Individual data points represent single cells. Percentage values that differ significantly from those obtained from WT σNS-transfected, reovirus-infected cells by one-way analysis of variance (ANOVA) with Dunnett's multiple-comparison test are shown (**, $P < 0.0021$).

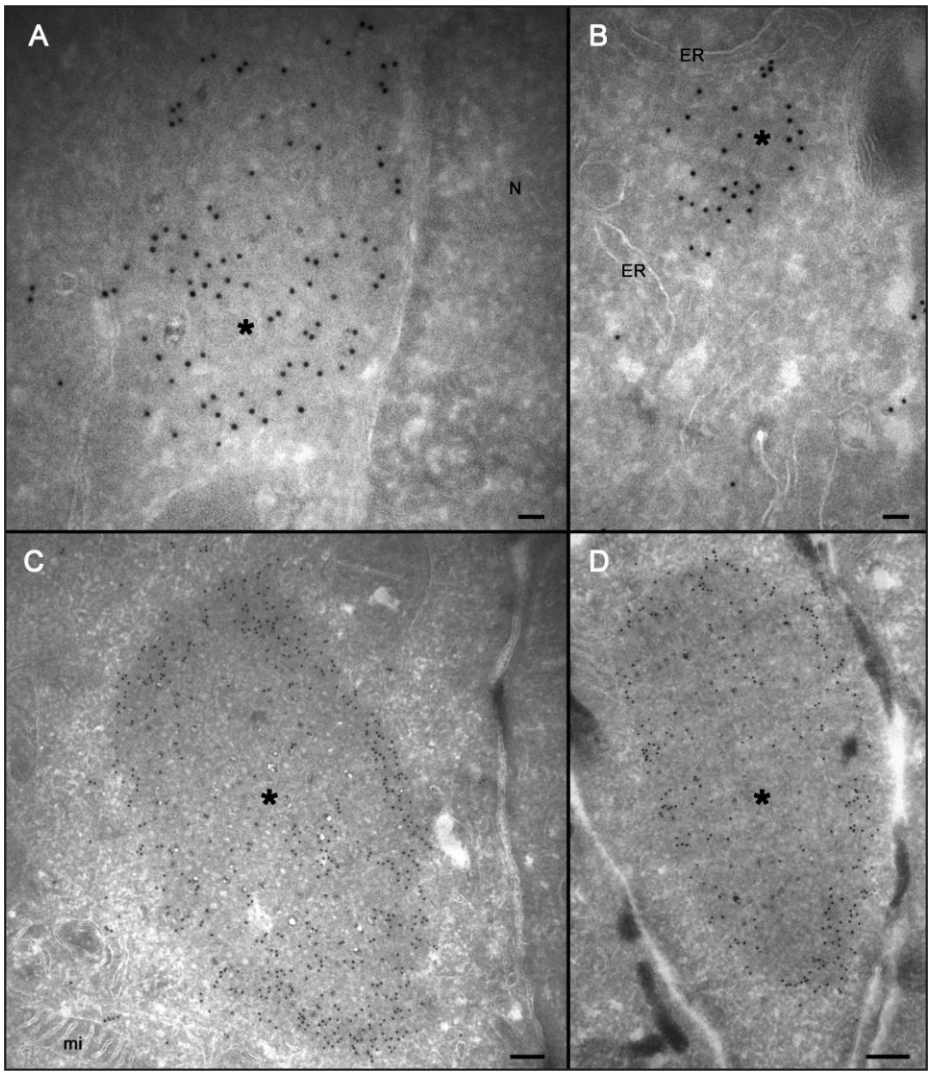

Figure 14. Immunogold labeling of σNS proteins in Tokuyasu cryosections of reovirus-infected cells

Cells were adsorbed with reovirus strain T1L M1 P208S at an MOI of 1 PFU/cell, incubated for 14 h, frozen in liquid nitrogen, and sectioned at -120°C. Thawed cryosections were processed for immunogold labeling using σNS-specific monoclonal antibody 2F5, followed by a secondary antibody bound to 10 nm colloidal gold spheres. Cryosections were imaged using transmission electron microscopy. Panels A and B show representative images of small, punctate, viral factories, and panels C and D show representative images of larger mature factories. Nucleus (N), endoplasmic reticulum (ER), and mitochondria (mi) are labeled when visible surrounding a viral factory (*). Bars, 50 nm (A and B), 200 nm (C and D).

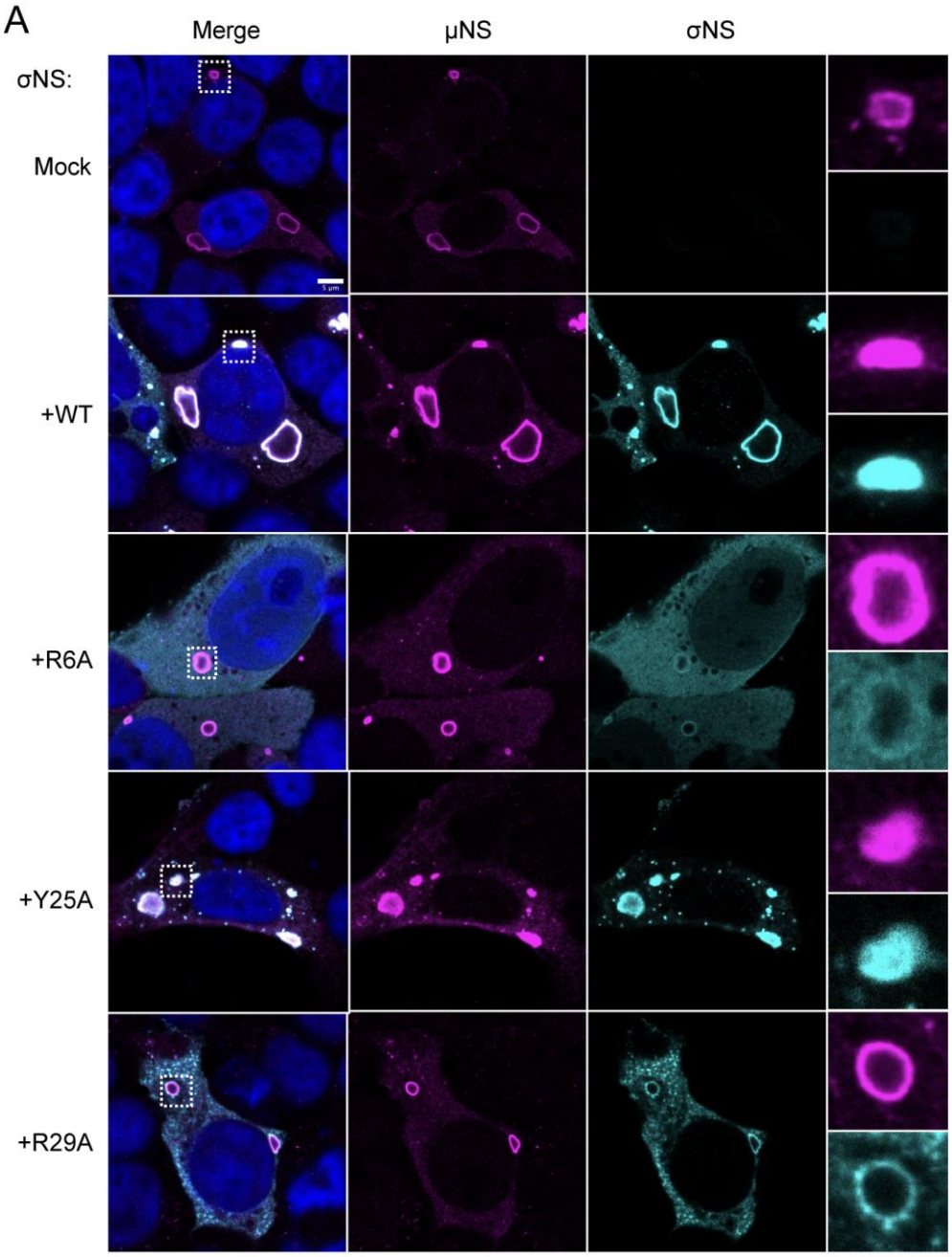
A
Merge
μNS
σNS
σNS:
Mock
+WT
+R6A
+Y25A
+R29A
B
Percentage of σNS in FLS (%)
100
80
60
40
20
0
****
****
σNS:
WT
R6A
Y25A
R29A
+μNS

Figure 15. Mutations in σNS that compromise RNA binding disrupt incorporation of the protein into factory-like structures

(A) Cells were transfected with expression plasmids encoding the σNS constructs shown along with μNS and incubated for 24 h. Cells were fixed, stained using σNS-specific monoclonal antibody 3E10 (cyan), μNS-specific antiserum (magenta), and DAPI (blue), and imaged using confocal microscopy. Regions selected for magnification are indicated by dotted white boxes. Bar, 5 μm. (B) The percentage of σNS immunofluorescence signal in reovirus factory-like structures was quantified by dividing the sum of σNS signal in reovirus factory-like structures by the sum of cytoplasmic σNS signal. Individual data points represent single cells. Percentage values that differ significantly from those obtained from WT σNS and μNS co-transfected cells by one-way analysis of variance (ANOVA) with Dunnett's multiple-comparison test are shown (****, $P < 0.0001$).

2.2.4 Mutations in σNS that alter RNA binding diminish mRNA incorporation in reovirus factories

Since the R6A and R29A σNS mutants are altered in RNA binding and incorporation into viral factories, we hypothesized that viral mRNAs also are mislocalized in infected σNS-siRNA cells transfected with these mutants. To test this hypothesis, we transfected σNS-siRNA cells with WT or mutant forms of σNS, infected with reovirus, and processed the cells 48 h post-adsorption for fluorescence in situ hybrirdization coupled with immunofluorescence detection of μNS to visualize reovirus factories (Fig. 16A). FISH probes were designed to specifically detect either the reovirus σNS-encoding mRNA (σNS mRNA) or the reovirus σ3-encoding mRNA (σ3 mRNA), which encodes outer-capsid protein σ3. Following infection of σNS-siRNA cells by reovirus, viral mRNAs were not detected in viral factories. Expression of WT and Y25A

σNS prior to infection led to formation of larger viral factories relative to untransfected cells and, importantly, both σNS and σ3 mRNAs were detected in cells. Interestingly, σ3 mRNAs were not concentrated in factories to the same extent as σNS mRNAs, but both σNS and σ3 mRNAs were observed to co-localize in discrete high-intensity puncta in viral factories, suggesting a suborganization in the factory structures. While expression of WT and Y25A σNS promoted conditions to allow detection of viral mRNAs in factories, expression of the R6A and R29A σNS mutants did not. R6A and R29A σNS mRNAs were detected in cells containing small factories, but these mRNAs were not observed in the factory structures. These results suggest that viral mRNAs are not efficiently produced or do not distribute to factories when σNS is incapable of interacting with RNA.

We were surprised that σ3 mRNAs were not concentrated in functioning factories to the same extent as σNS mRNAs. We hypothesized that differences in σNS and σ3 mRNA localization could be dependent on the time point at which we fixed cells for imaging. To test this hypothesis, we infected HEK293T cells with reovirus, and processed the cells at 9, 24, and 48 h post-adsorption for FISH coupled with immunofluorescence detection of μNS to visualize reovirus factories (Fig. 17). Both σ3 and σNS mRNAs were concentrated in factories at 9 and 24 h post adsorption. However, at 48 h post-adsorption, σ3 mRNAs distributed less prevalently to factories, while σNS mRNAs maintained a predominantly factory distribution. These results suggest that as viral factories mature, some viral mRNAs distribute to different intracellular sites.

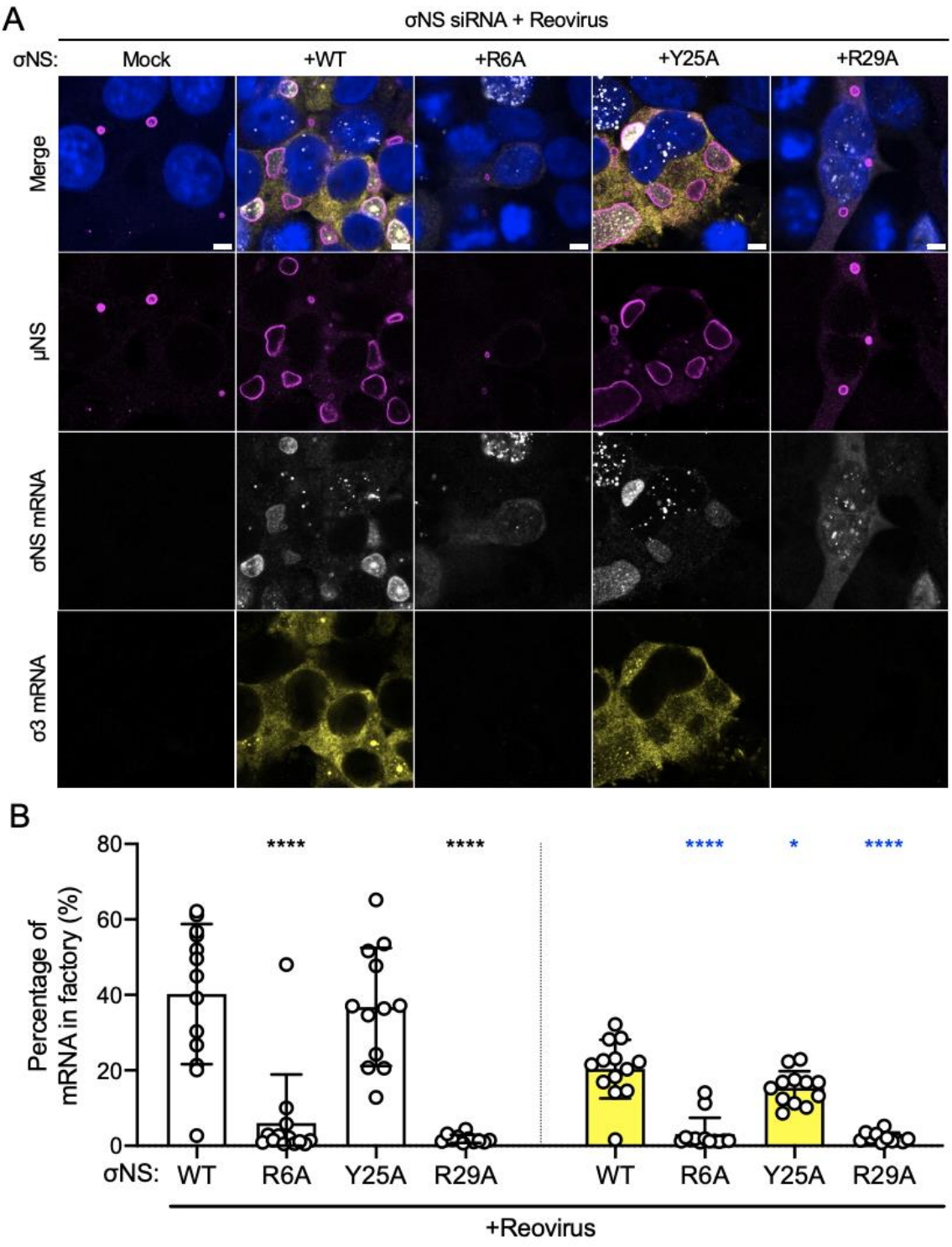

Figure 16. Reovirus transcripts are present in viral factories only when σNS is capable of binding RNA

Cells that constitutively express siRNAs directed against σNS were transfected with expression plasmids encoding the σNS constructs shown and incubated for 24 h. Cells were adsorbed with reovirus strain T3D at an MOI of 5 PFU/cell, incubated for 48 h, fixed, stained using RNA FISH probes specific for σNS mRNA (white) or σ3 mRNA (yellow), μNS-specific antiserum (magenta), and DAPI (blue), and imaged using confocal microscopy. Bar, 4.8 μm. The percentage of cytoplasmic (B, white bars) σNS-mRNA and (B, yellow bars) σ3-mRNA FISH signals in reovirus factories was quantified by dividing the sum of FISH signal in reovirus factories by the sum of cytoplasmic FISH signal. Individual data points represent single cells. Percentage values that differ significantly from those obtained from WT σNS-transfected, reovirus-infected cells by one-way analysis of variance (ANOVA) with Dunnett's multiple-comparison test are shown (*, $P < 0.0332$; ****, $P < 0.0001$)

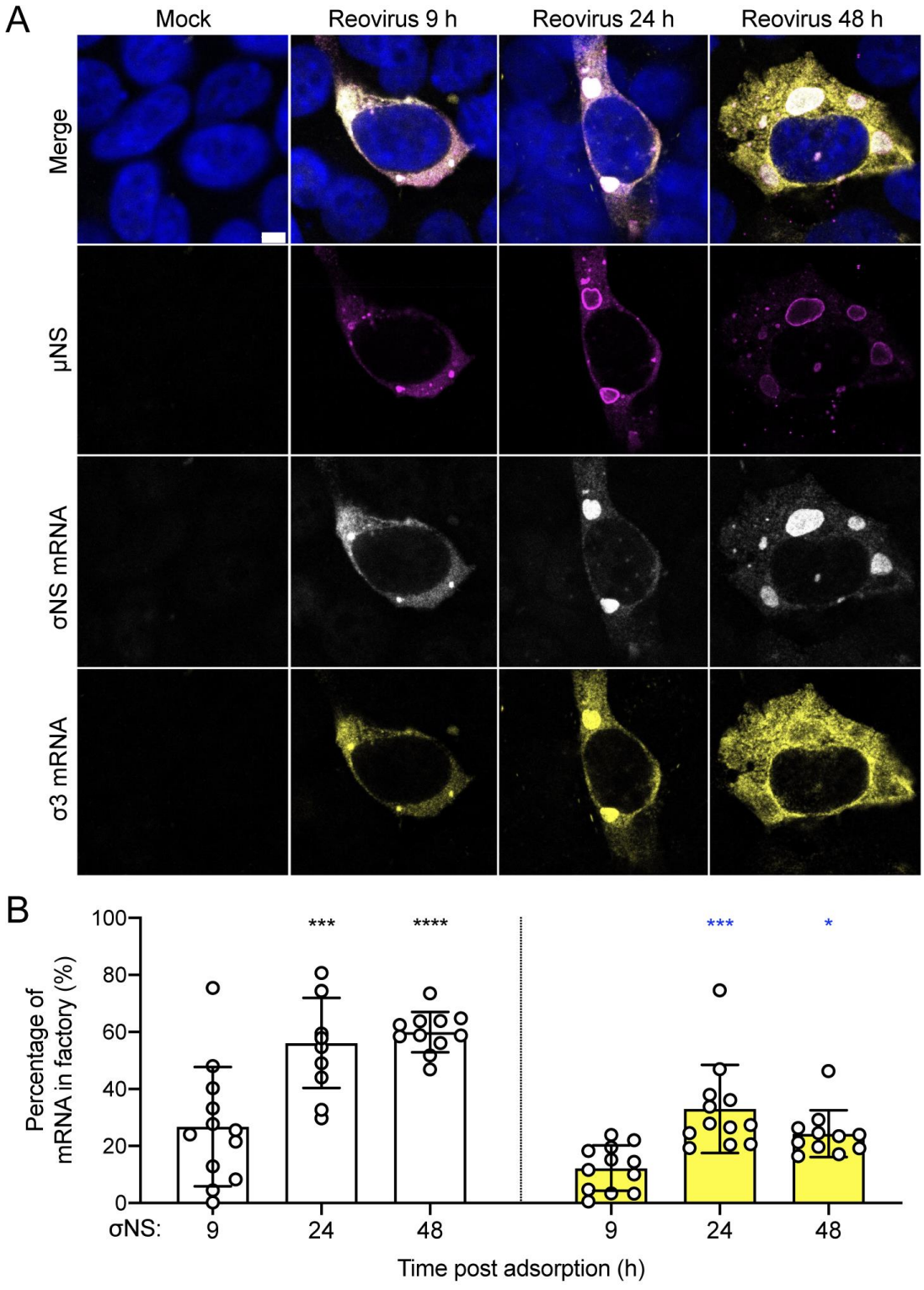

Figure 17. Reovirus transcripts differentially localize in viral factories at late timepoints post-adsorption

HEK293T cells were adsorbed with reovirus strain T3D at an MOI of 20 PFU/cell, incubated for 9, 24, and 48 h, fixed, stained using RNA FISH probes specific for σNS mRNA (white) or σ3 mRNA (yellow), μNS-specific antiserum (magenta), and DAPI (blue), and imaged using confocal microscopy. Bar, 5 μm. The percentage of cytoplasmic (B, white bars) σNS-mRNA and (B, yellow bars) σ3-mRNA FISH signals in reovirus factories was quantified by dividing the sum of FISH signal in reovirus factories by the sum of cytoplasmic FISH signal. Individual data points represent single cells. Percentage values that differ significantly from those obtained from 9 h post-adsorption by one-way analysis of variance (ANOVA) with Dunnett's multiple-comparison test are shown (*, $P < 0.0332$; ***, $P < 0.0002$; ****, $P < 0.0001$).

2.2.5 WT σNS and μNS are sufficient to recruit viral mRNA to factory-like structures

The lack of viral mRNAs in factories formed in the presence of mutant σNS could be independent of viral mRNA incorporation into viral factories and instead due to impaired viral replication, leading to reduced secondary rounds of viral transcription. To uncouple viral mRNA distribution from viral replication, we transfected HEK293T cells with different combinations of expression plasmids encoding μNS, WT or mutant forms of σNS, and σ3, fixed and stained for FISH, and imaged the cells using confocal immunofluorescence microscopy (Fig. 18A). The σ3 protein binds double-stranded RNA but not single-stranded RNA (93) and, thus, would not be expected to retain viral mRNA in factory-like structures. Concordantly, expression of μNS and σ3 was insufficient to promote incorporation of σ3 mRNAs into factory-like structures (Fig. 18B, yellow). However, expression of μNS and σ3 along with WT or Y25A σNS led to concentration of σ3 mRNAs (Fig. 18B, yellow) as well as σNS mRNAs in these structures (Fig. 18B, white). Neither σNS nor σ3 mRNAs concentrated in factory-like structures following

expression of the R6A or R29A σNS mutants with μNS and σ3. Instead, viral mRNAs appeared to be excluded from the interior of factory-like structures in the presence of these mutant σNS proteins. Since the plasmids are transcribed in the nucleus, these data suggest that σNS functions to recruit viral mRNAs into cytoplasmic factory-like structures. Collectively, these results suggest that σNS is required to recruit viral mRNAs to reovirus factories.

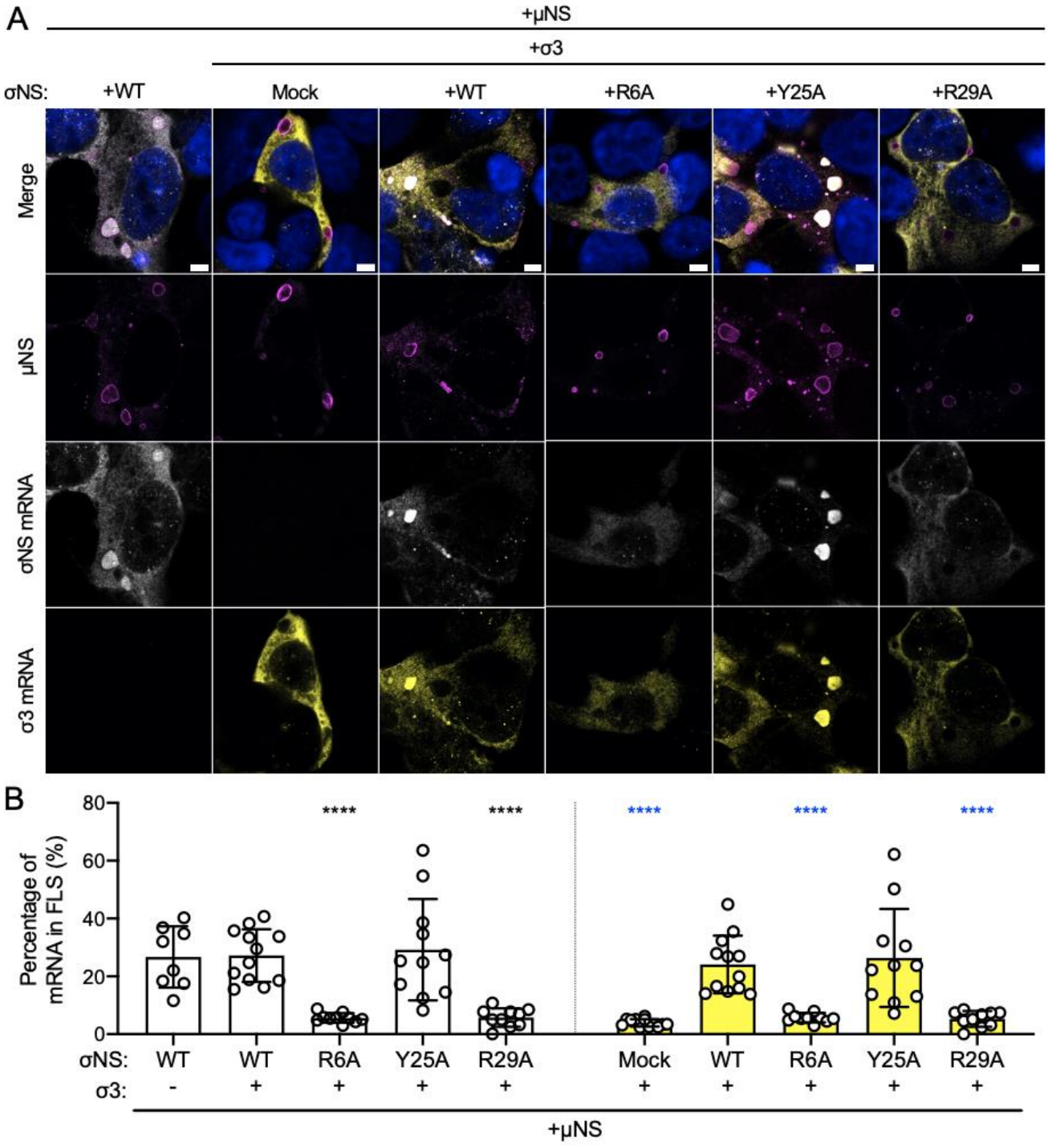

Figure 18. Reovirus mRNAs are recruited to factory-like structures by σNS

Cells were transfected with expression plasmids encoding μNS, σ3, and the σNS constructs shown and incubated for 24 h. Cells were fixed, stained using RNA FISH probes specific for σNS mRNA (white) or

σ3 mRNA (yellow), μNS-specific antiserum (magenta), and DAPI (blue), and imaged using confocal microscopy. Bar, 4.8 μm. The percentage of cytoplasmic (B, white bars) σNS-mRNA and (B, yellow bars) σ3-mRNA FISH signals in factory-like structures was quantified by dividing the sum of FISH signal in factory-like structures by the sum of cytoplasmic FISH signal. Individual data points represent single cells. Percentage values that differ significantly from those obtained from cells co-transfected with WT σNS, σ3, and μNS by one-way analysis of variance (ANOVA) with Dunnett's multiple-comparison test are shown (****, $P < 0.0001$).

2.3 Discussion

In this study, we discovered a function for σNS in reovirus factory formation. We found that σNS requires electrostatic interactions to bind RNA and that RNA is not required to facilitate σNS-μNS interactions. We also observed that impeding σNS-RNA binding disrupts viral mRNA incorporation into viral factory scaffolds. Reovirus factories that form in the presence of σNS mutants incapable of binding RNA do not produce progeny viral particles. A model of σNS recruiting viral mRNAs for reovirus factory formation is shown in Fig. 19.

The manner in which RNA-binding proteins interact with RNA can influence the biological function of the resulting ribonucleoprotein complexes. Our data suggest that electrostatic interactions are required for reovirus σNS to bind RNA (Fig. 9). These interactions could occur between an RNA base or the RNA phosphate backbone and positively charged residues in the N-terminal region of σNS. Similarly, avian reovirus σNS also requires positively charged residues in its N-terminus (R6 and R11) to bind ssRNAs *in vitro* (102). Avian reovirus σNS additionally displays RNA chaperone activity

in vitro (15), suggesting another potential function for σNS is to fold viral mRNAs. Certain mRNA structures could enhance RNA-RNA interactions between different viral mRNA segments, allowing precise packaging of 10 unique viral mRNAs into progeny viral particles (103). Rotavirus NSP2, which has been hypothesized to be a functional homolog of σNS (15), also binds RNA using electrostatic interactions and, analogous to avian reovirus σNS, chaperones rotavirus mRNAs (102). NSP2 regulates RNA-binding using residues that electrostatically repulse RNA (104). While we have identified residues required for σNS to bind RNA, questions about the regulation and specificity of RNA-binding remain. σNS may displace RNA similarly to NSP2 or by some type of post-translational modification (105). Outside of cellular contexts, σNS does not preferentially bind viral mRNAs (94). However, in the context of viral infection, we hypothesize that σNS preferentially binds and concentrates viral mRNAs in factories. Concentrating host mRNAs in viral factories may compromise viral packaging, as viral mRNAs would have to compete with cellular mRNAs for RNA-RNA interactions. In support of this idea, RNA-binding specificity of other RNA-binding proteins differs when compared *in vitro* and in cells (106). Future studies of σNS-RNA binding could help fill these knowledge gaps and explain how σNS controls the selective uptake of viral mRNAs into reovirus factories. Such a mechanism of control could be exploited to modulate the types of RNAs recruited into factory-like structures (107).

The charge-to-alanine mutations in the N-terminus of σNS engineered in this study do not impair interactions of σNS with μNS as detected by co-immunoprecipitation (Fig. 7D). However, mutant forms of σNS incapable of RNA binding are not recruited to factories (Fig. 13A) or factory-like structures nucleated by μNS (Fig. 15A). There are

three possible explanations for the inconsistency of our co-immunoprecipitation and co-localization results. First, since the same general N-terminal region of σNS (residues 1-11) is required for binding to RNA and μNS (77, 96), mutations that disrupt RNA binding may allow enhanced accessibility of that region to interact with μNS. Second, σNS could bind μNS proteins that have not integrated into the factory scaffolds. Third, σNS could bind μNS more avidly during cell lysis. The process of cell lysis likely disrupts the stability of factories and factory-like structures, which would allow increased access of σNS to μNS than that expected in viral factories.

Reovirus σNS is required for a step or steps in viral replication at or prior to dsRNA synthesis by the viral polymerase (89). Based on previous results, σNS interactions with viral mRNAs could enhance the stability of mRNAs bound at early stages of infection (89). However, based on our findings, we think that σNS is also required for the formation of functional viral factories, which precedes dsRNA synthesis (108). The morphology of viral factories does not change dramatically in the absence of σNS, but factories are notably smaller when σNS is absent (89) (Fig. 13). During viral factory morphogenesis, σNS likely alters factory scaffold properties to allow RNA incorporation. Viral mRNAs are thought to be packaged into nascent core particles in viral factories during assembly of reovirus progeny. σNS mutants incapable of binding RNA retain the capacity to be recruited to factory structures, albeit to a lesser degree. However, σNS distribution to factories is insufficient for its function in reovirus replication. σNS additionally requires RNA-binding capacity, which mediates incorporation of viral mRNAs into factories. The accumulation of viral mRNAs (recruited by σNS) and viral structural proteins (recruited by μNS) within factories establishes an

environment replete with viral components. Progeny virions then can form and amplify viral replication to yield much larger factories.

While our findings enhance an understanding of σNS function during early steps in reovirus replication, questions remain about other potential functions of this protein. In addition to a potential role as an RNA chaperone, it is possible that σNS enhances interactions between the viral polymerase and mRNAs, as observed for other viral RNA-binding proteins (109-113). Any of these observed or potential functions require that σNS dissociate from viral mRNAs, as σNS is not contained in mature viral particles (114). The mechanism underlying mRNA release from σNS is not known, nor is it apparent at precisely what site in the cell such dissociation would occur. As factories enlarge, σNS concentrates at the factory periphery (68) (Fig. 14), suggesting that σNS dissociates from RNA at that site. However, it also is possible that σNS dissociates from RNAs in the factory center, as the protein is detectable throughout factories, albeit in more limited quantities, especially in larger factories.

Formation of functional reovirus factories also requires cellular factors, many of which are unknown. Therefore, it is possible that σNS modifies host components in some way to promote factory formation and viral replication. Expression of σNS in the absence of other viral proteins induces ER tubulation (70). This morphological change is hypothesized to culminate in formation of the ER fragments embedded in reovirus factories during infection. σNS could facilitate the incorporation of ER fragments into factories by binding ER-resident RNAs or proteins or engaging ER lipids. While the function of the ER fragments within factories has not been established, we think that the membranes provide a physical matrix to allow viral packaging, as observed for many

RNA viruses (115). Proteins essential for the integrated stress response also are implicated in reovirus replication (116-118). In stressed cells, σNS recruits G3BP1 and other stress-granule proteins to factory-like structures (92). The recruitment of stress-granule proteins to factories depends on RNA and could lead to recruitment of the translational machinery, usually found within stress granules, to viral factories (68). These activities could occur concomitantly with viral mRNA recruitment by σNS.

Membrane enclosure is the most broadly known mechanism for organelles to compartmentalize intracellular components required for efficient molecular interactions and functions. However, organelles can form using a process of liquid-liquid phase separation (119). Liquid-liquid phase separation leads to the development of dynamic organelles, called condensates, that are stabilized by multivalent interactions between proteins, nucleic acids, or both (119). These organelles can separate from the intracellular environment, selectivity package discrete constituents, and allow biochemical activities, such as viral genome replication and capsid assembly, to be coordinated with high efficiency (120). Many RNA viruses use this mechanism to form viral factories (34, 48, 50, 121, 122). While development of many types of liquid-liquid phase separated condensates of both viral and cellular origin depend on RNA, formation of reovirus factories may differ (123). Since reovirus mRNAs are excluded from the factory-like structures formed solely by μNS, it is likely that μNS does not require RNA to phase-separate. In this way, reovirus factory-like structures resemble other condensates that do not require RNA to mediate multivalent interactions (124, 125). For example, formation of measles virus factories also does not require RNA, and a viral RNA-binding protein, N protein, can recruit RNA to factory-like structures to

efficiently form RNP complexes within (50). Future studies will identify the minimal constituents and conditions required to form reovirus factory condensates and define the biophysical changes that occur when other components are added.

Experiments reported here indicate that σNS incorporates viral mRNAs into reovirus factory scaffolds that naturally exclude viral mRNAs. Our work begins to uncover how a dsRNA virus factory controls the selectivity of its composition. Next steps include defining the specificity of σNS interactions with RNA and identifying additional molecular interactants that enable σNS to promote viral genome replication and packaging. These studies are anticipated to illuminate new targets to impede dsRNA virus replication, which may have broad utility.

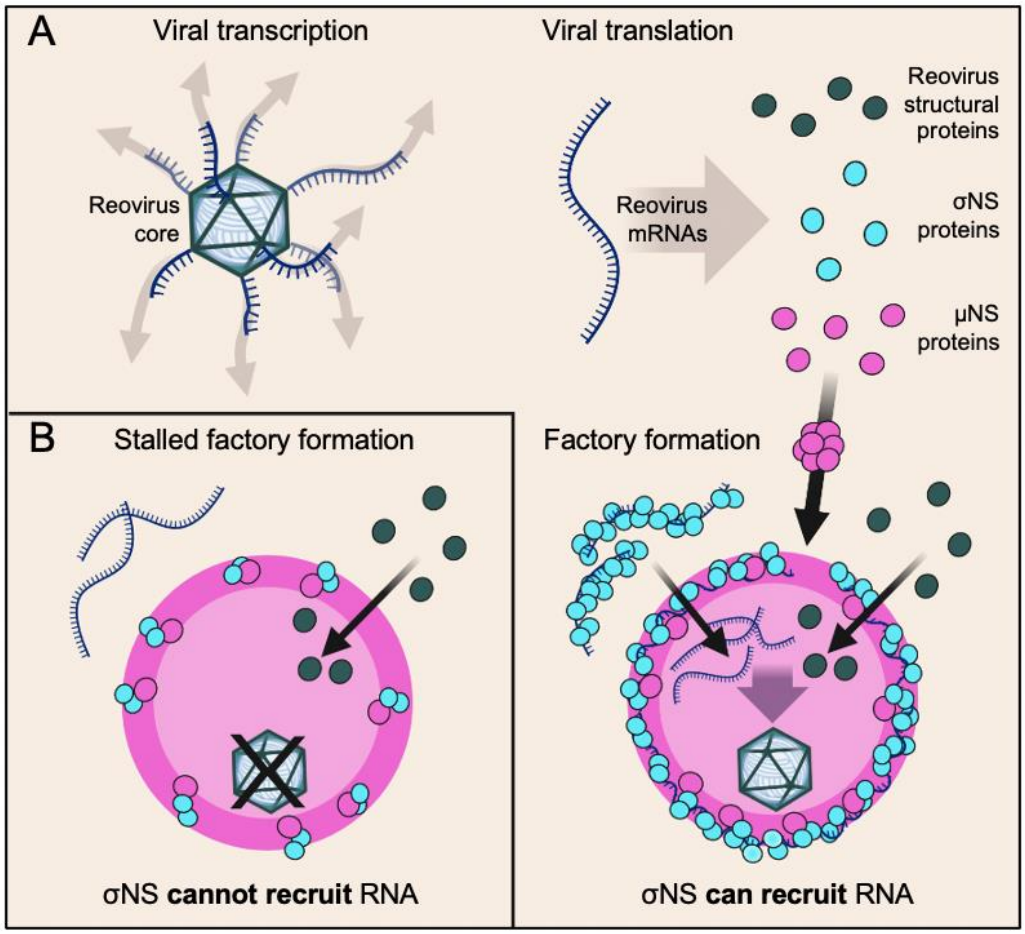

Figure 19. Model of σNS mRNA recruitment for reovirus factory formation

(A) Following viral attachment and internalization, reovirus cores enter the cytoplasm and transcribe viral mRNAs that are translated to yield structural and nonstructural (NS) proteins. Factory scaffolds are formed by μNS (large magenta sphere), which recruits reovirus structural proteins. Viral mRNAs in the cytoplasm are bound by σNS and delivered to factory scaffolds. Viral components that form nascent viral cores are concentrated in factories, promoting viral packaging and core maturation for secondary rounds of transcription and translation. (B) Mutations in σNS that compromise RNA-binding capacity also impede recruitment of mRNAs to factories and stall factory enlargement, as nascent cores do not form and are thus incapable of amplifying viral replication

3.0 Structural analysis of σNS

3.1 Introduction

The physical structure of a protein is filled with clues that can yield insights about protein function. Structural features like specific folds in domains, electrostatic surfaces, or solvent-exposed side chains can define how proteins interact with ligands or catalyze reactions. Thus, studies of σNS functions in reovirus replication would be aided by an examination of the structural basis of σNS interacting with RNA or other ligands. The N-terminal region of σNS is required to interact with RNA and μNS (96) (88). Additionally, σNS forms oligomers in the presence of RNA (94). It is not clear how these interactions occur, and we thought that analyzing the structure of σNS purified from bacteria would yield explanations.

Investigators in the laboratory of Dr. B. V. V. Prasad, with whom we collaborate, determined the crystal structure of another *Reoviridae* nonstructural protein, rotavirus NSP2 (126). Their expertise and prior success suggested it would be possible to determine the structure of reovirus σNS. However, initial attempts to determine the structure of σNS were unsuccessful. While purified σNS formed crystals, the crystals did not diffract to a sufficiently high resolution to determine the structure. Based on the low diffraction, we hypothesized that σNS nonspecifically binds RNA when expressed in *E. coli*. Attempts to remove the contaminating RNA with high-salt washes were not successful, which is a common problem in purifying RNA-binding proteins free of contaminants.

To overcome these obstacles, we purified and crystalized a previously characterized RNA-binding mutant of σNS, R6A, from *E. coli* and determined the structure using single-wavelength dispersion (SAD).

The experimental work reported in this chapter was conducted by Dr. Liya Hu and Boyang Zhao in Dr. Prasad's lab.

3.2 Results

3.2.1 Crystal structure of R6A σNS

RNA-dependent oligomerization of σNS is disrupted by replacing Arg6 with alanine. We hypothesized that this mutation would allow us to purify σNS free of contaminating cellular RNAs. R6A σNS expressed in *E. coli* purified as a dimer, suggesting that σNS dimers can form in the absence of RNA. To confirm that purified R6A σNS does not bind RNA, we conducted an *in vitro* RNA-binding assay. Purified WT or R6A σNS was incubated with magnetic beads coated with *in vitro* transcribed reovirus S3 mRNAs. Following incubation, bead-bound protein was purified and identified using immunoblotting. As anticipated, WT σNS bound to beads coated with RNA, while R6A σNS did not (Fig. 20A). Based on this analysis, we conclude that purified R6A σNS does not bind RNA.

Following purification, we propagated R6A σNS crystals using hanging-drop vapor diffusion. The resultant crystals diffracted to 2.8 Å resolution, which was substantially better than previous results using WT σNS crystals. Since we lacked a

homologous structure as a search model, we could not phase the diffraction data using molecular replacement methods. Therefore, we purified R6A σNS incorporating seleno-methionine (SeMet) from *E. coli* strain B834(DE3). We collected X-ray diffraction data at 2.8 Å of the SeMet-substituted R6A protein for single-wavelength anomalous diffraction (SAD) phasing. Most of the structure was unambiguously determined, except residues 219-230, which displayed flexibility. While the crystal structure was determined using R6A σNS, modeling analysis suggests that replacing Ala6 with arginine does not change the monomer or dimer structure we observed.

An R6A σNS monomer contains 15 α-helices and 10 β-strands (Fig. 20B) and can be depicted as a hand forming a “finger gun” (Fig. 20C and 20D). The first α-helix (residues 4-11) resides in a flexible N-terminal region that protrudes from the central core. This flexible N-terminus (residues 1-18) forms the “index finger.” The other α-helices, which vary in length, gather around the longest α-helix (residues 242-272) to form a globular core, which forms the “fist.” Ten β-strands interact to form three distinct β-sheets that reside near the periphery of the central core. The first three β-strands (residues 19-47) form a β-sheet that we refer to as the “thumb,” since it extends from the core perpendicularly to the “index finger.” The C-terminus is tucked within the “fist.”

R6A σNS monomers combine to form dimers with a curved surface. Dimers form when two mirrored monomers, pointing in opposite directions, interact near the base of the fists (Fig. 21). The interaction forms a buried surface area of 1853 Å. Based on the crystal structure, we hypothesize that mutations at key residues could destabilize the dimer, while still maintaining proper protein folding. To identify residues for mutagenesis, we used a computational program, mCSM-PPI2, which predicts the

effects of missense mutations on protein-protein interaction affinity (127). The top-four predicted mutations were L60A, R67A, G148A, and H164A. Each mutation was predicted to change the free energy of dimer binding by 0.998, 1.147, 1.013, and 1.349 kcal/mol, respectively. We hypothesized that these mutations would prevent dimers from forming when expressed *in vitro* using RRLs. We discovered that these mutations did not change proteinase K digestion patterns, suggesting that the mutant proteins were similarly folded (data not shown). However, the mutations did not disrupt dimer formation when evaluated using native-PAGE analysis (data not shown). These results suggest that altering these residues at the interface would not likely disrupt the large, buried surface area of the σNS dimer.

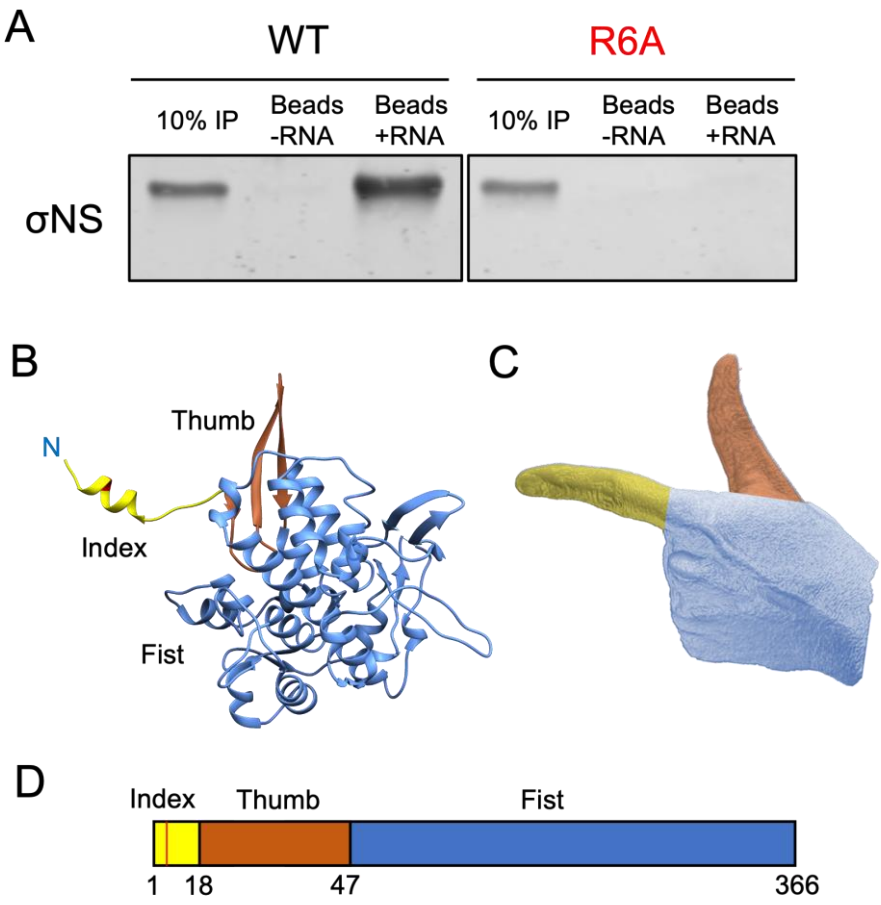

Figure 20. Crystal structure of purified R6A σNS

(A) WT or R6A σNS purified from *E. coli* was incubated with magnetic beads coated with (+RNA) or without (-RNA) reovirus S3 mRNA. Total protein bound to beads was purified and resolved by SDS-PAGE and immunoblotted using σNS-specific antiserum. Ten percent of the protein incubated in a reaction (10% IP) was used as a positive control for immunodetection. (B) Representative crystal structure of the R6A σNS monomer. (C) Schematic of hand shaped into a “finger gun” that represents an analogous σNS structure. (D) Bar diagram of σNS domain organization based on similarities to the finger gun model. The R6A mutation is indicated in red, and residues at the edge of domains are numbered.

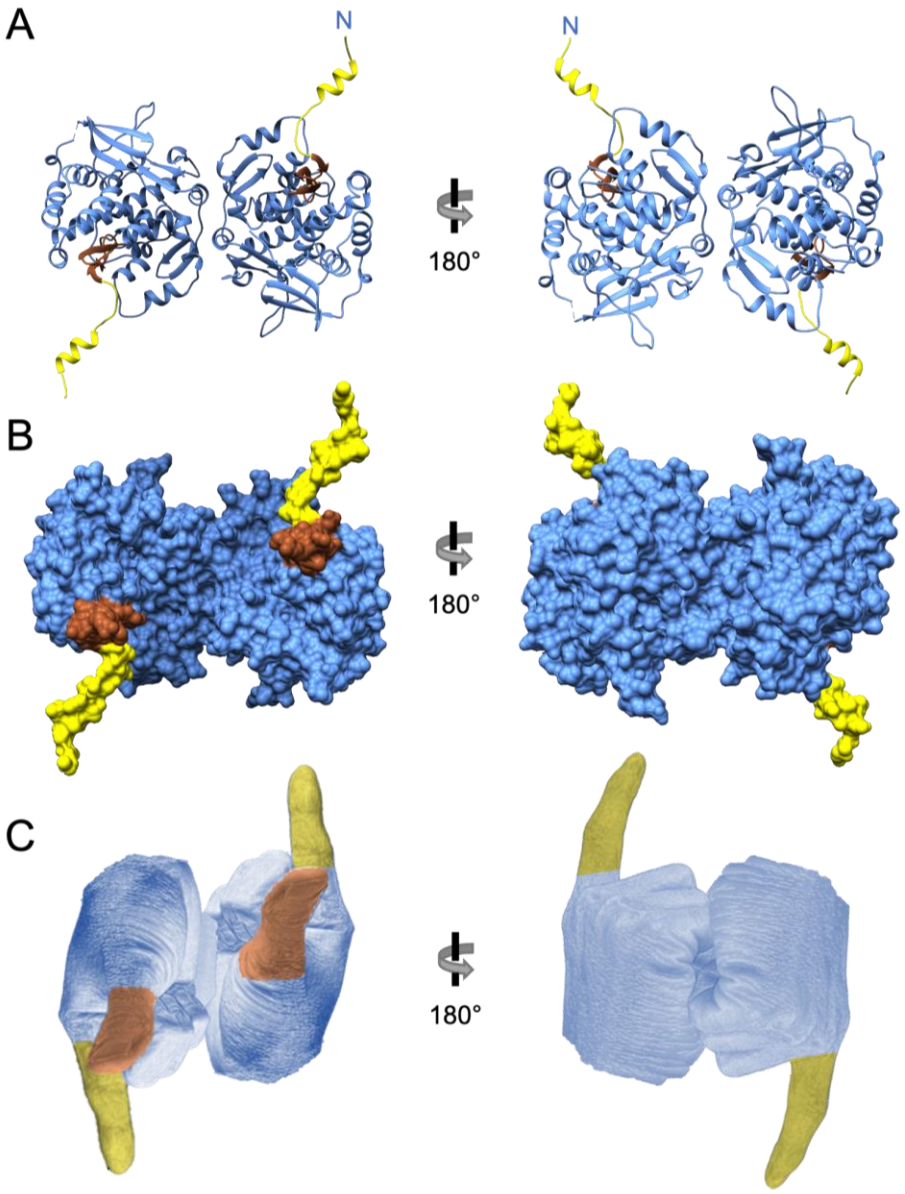

Figure 21. Structures of σNS dimer

(A) Representative structure of the R6A dimer shown as a ribbon diagram, rotated 180º around y-axis. (B) Representative structure of the R6A σNS dimer with surface rendering, rotated 180º around the y-axis. (C) Simplified representation of the R6A σNS dimer as two opposing mirrored finger guns.

3.2.2 σNS oligomerization forms helical structures

In addition to forming dimers, SeMet R6A σNS packs within a crystal to form helical structures (Fig. 22A). A σNS dimer is the minimum building block for helical oligomerization. The helix rotates 360º per 6 dimers and has an interior diameter of ~ 43 Å. Since helical packing was not observed in R6A σNS crystals, the addition of SeMet stabilized σNS to facilitate this packing arrangement, even in the absence of RNA. We hypothesized that WT σNS also forms similar structures when incubated with RNA. Concordantly, *in vitro* expressed WT σNS forms RNA-dependent oligomers, which are disrupted by RNase A treatment (89). Purified WT σNS-RNA complexes also form long filaments that do not form when σNS is incapable of binding RNA (89). To determine whether WT σNS-RNA complexes also form helical filaments, WT σNS was purified from *E. coli*, incubated with reovirus S4 mRNA, and processed for single-particle cryo-EM. Preliminary class-averaging of σNS-RNA complexes suggest formation of helices similar to SeMet R6A σNS (data not shown). Collectively, these data suggest that WT σNS forms helical filaments stabilized with RNA.

To form oligomers, a flexible σNS “index finger” of a dimer wraps around the “fist” of an adjacent dimer (Fig. 22A). We attempted to append WT σNS with a GFP tag at the N-terminus (data not shown). However, this mutant did not complement the function of WT σNS using cells expressing siRNAs targeting σNS (1) (data not shown). Based on the σNS structure, GFP likely sterically hinders the index finger from properly interacting with its binding pocket to stabilize oligomerization.

Mutations in σNS that disrupt RNA-dependent oligomerization (R6A, K11A, R13A, R14A, R29A, K35A, and R38A) alter residues that reside in different regions of

the protein. The location of these residues provide clues about how the mutations might alter RNA-dependent oligomerization. Instead of residing in a more solvent-exposed region, four of these residues (R6, K11, R13, R14) reside within the flexible index finger domain. These residues bind a groove on the adjacent fist that contains negatively charged residues that likely stabilize the interaction (Fig. 22B). R29A is capable of forming oligomers, albeit less efficiently than WT σNS. This observation is consistent with the location of Arg29 at a distance from the groove in the fist domain. Lys35 and Arg38 are located within the inner surface of the helix and more solvent exposed, suggesting that these residues directly contact RNA. Therefore, based on the σNS structure, the index finger likely does not directly interact with RNA but instead facilitates σNS oligomerization.

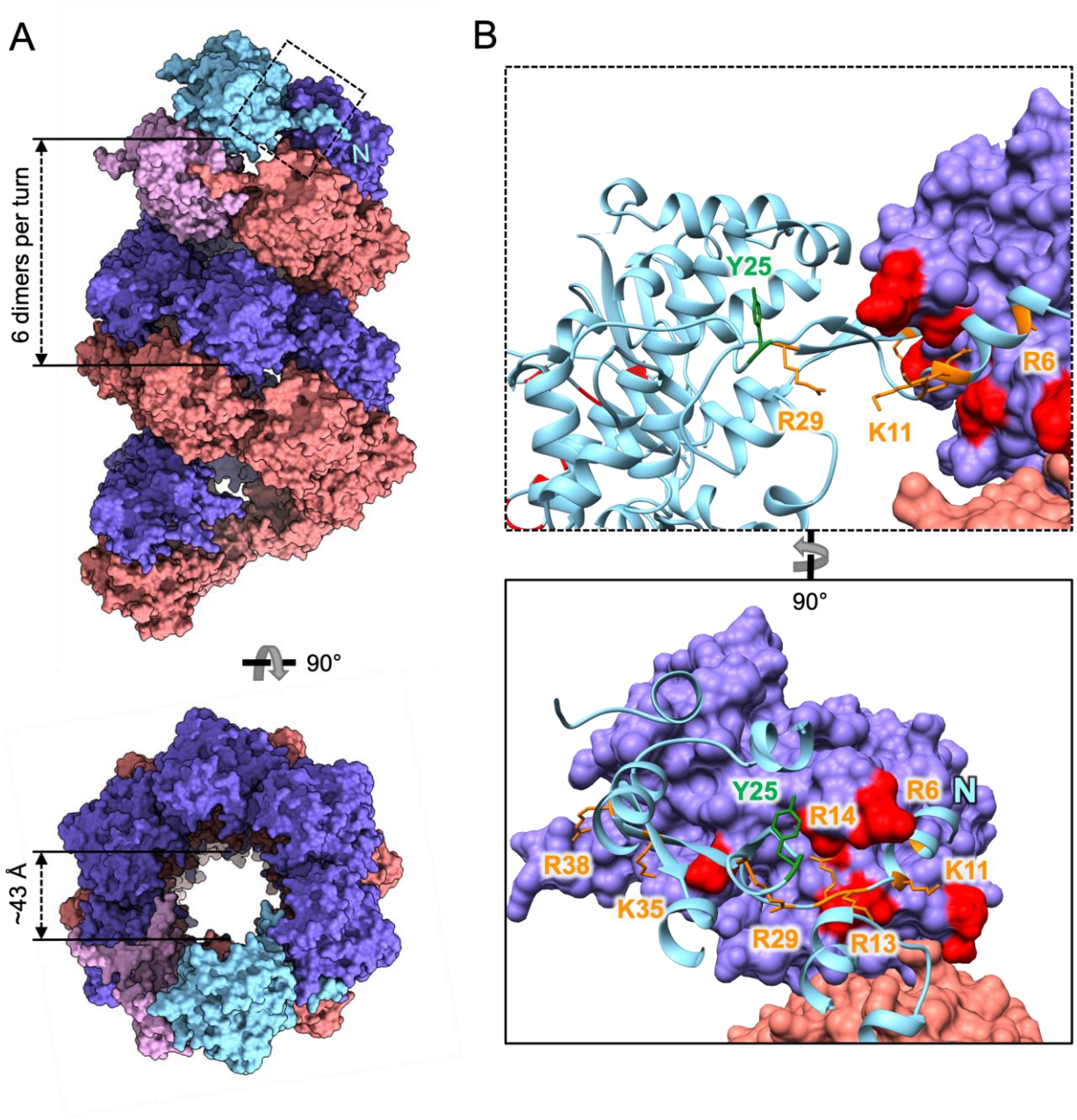

Figure 22. σNS oligomerizes into a helix

(A) Molecular surface model of the R6A σNS oligomer arranged as a helix. One monomer of a representative dimer is shown in cyan and the other in magenta. The inner channel of the helix is approximately 43 Å wide. One full rotation of the helix occurs when six dimers oligomerize. (B) Enlargement of the region depicted in the dashed box in panel A that focus on the interface between two monomers of adjacent σNS dimers. Residues shown in orange and green were mutagenized in Chapter 2. Replacement of residues shown in orange with alanine disrupted RNA-dependent oligomerization,

while replacement of residues shown in green did not (1). Surfaces shown in red are formed by negatively-charged residues.

3.2.3 Surface electrostatic potential of R6A σNS predicts RNA binding surfaces

Incubation of σNS in high-salt conditions or altering positively-charged residues in the σNS N-terminus to neutral residues disrupts σNS-RNA binding, suggesting that σNS interacts with RNA using electrostatic interactions (1). To define possible RNA-binding sites on σNS, we mapped the electrostatic potential of σNS residues onto a surface-shaded model of the structure. The curvature of σNS dimers leads to formation of two faces. The convex face is mainly electronegative, whereas the concave face is electropositive (Fig. 23A). Solvent-exposed residues within the concave face include R6, R29, R35, R38, R46, K64, R65, R86, R288, E348, R346, and R365. Thus, the concave σNS face forms a cylindrical electropositive interior in σNS helices (Fig. 23C). Because of the strong electropositive potential, we hypothesized that RNAs bind within the inner channel of σNS helices. Computational placement of a model 26-nucleotide ssRNA within the channel yielded an acceptable fit with ample space for RNA binding (Fig. 23D). To better model interactions of σNS and RNA, we used yeast tRNA (PDB: 1VTQ) (128), which binds σNS *in vitro*. The top 10 models predicted by the HDOCK protein-docking algorithm showed binding of yeast tRNA within the inner face of a σNS dimer (Fig. 23E). There are no known RNA-binding motifs in this region, but residues responsible for the positive electrostatic potential interact with yeast tRNA in the models. Interestingly, Arg29 and Lys35 participate in the interaction. R29A and K35A disrupt σNS RNA-binding capacity (1).

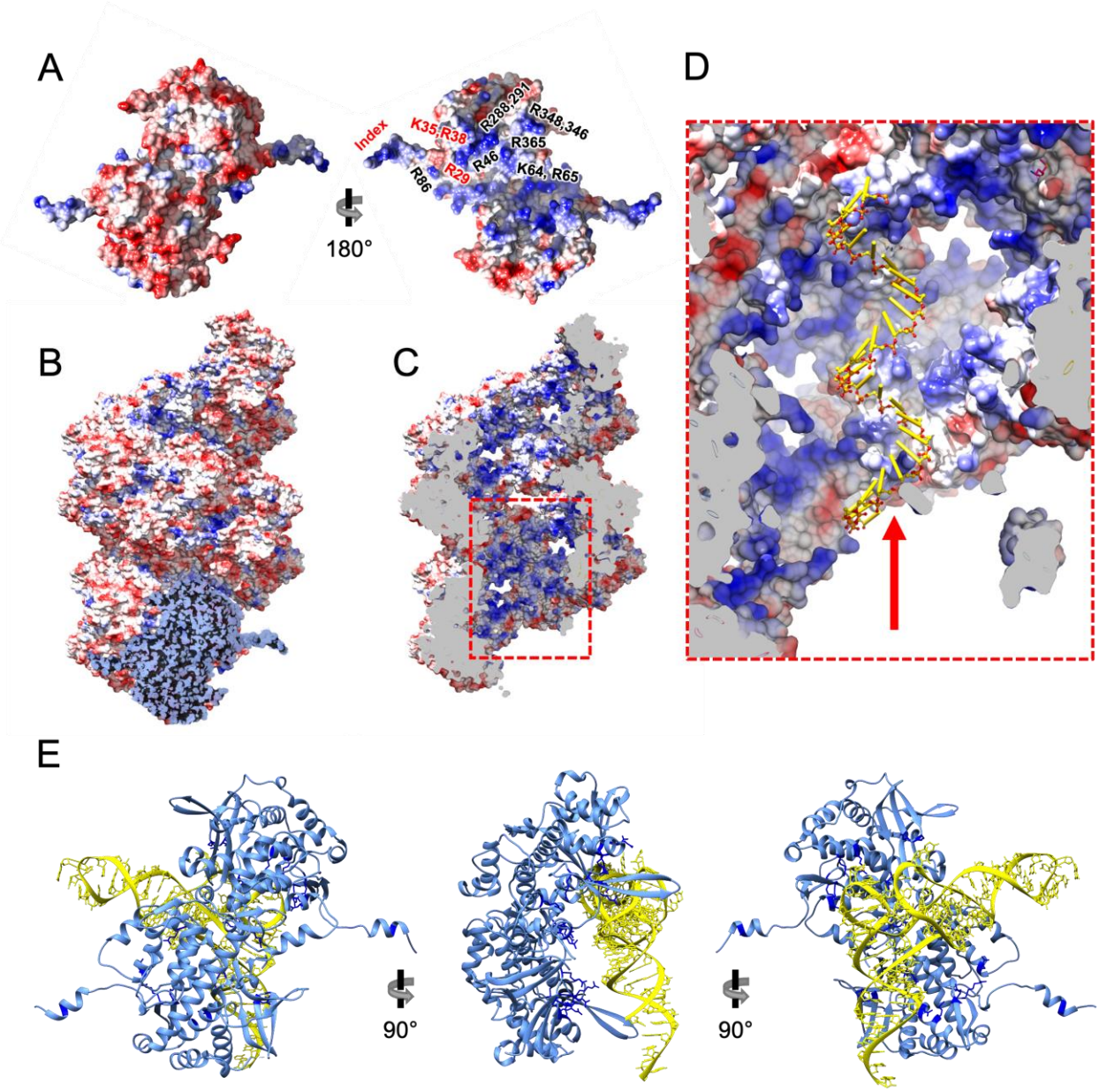

Figure 23. σNS dimers interact with RNA through a positively-charged concave surface

(A) Electrostatic potential of residues mapped onto the surface of a σNS dimer. Positively and negatively charged areas are colored blue and red, respectively. The most electropositive residues on the concave surface are labeled. (B) Electrostatic potential of residues mapped onto the outer surface of a σNS helix. A σNS dimer is shown in light blue to display the relative size of an oligomer. (C) Cross section of a σNS helix surface model along the helical axis with the interior channel colored by electrostatic potential of

residues. (D) A 26-nucleotide poly-A RNA is placed within interior channel to depict relative sizes. (E) Highest-scoring HDOCK model of yeast tRNA (yellow) placed onto the surface of R6A σNS dimer (light blue).

3.2.4 Location of a temperature-sensitive mutation on σNS

Temperature-sensitive mutant virus *tsE320* has an M260T mutation in σNS (100). This virus does not replicate efficiently at temperatures above 37º C (Fig. 25A) (100). Infection of cells with *tsE320* at elevated temperatures leads to formation of small cytoplasmic granules of σNS (Fig. 25B). Additionally, reovirus factories are not observed in *tsE320*-infected cells (Fig. 25B), and reovirus proteins are distributed diffusely in the cytoplasm. To determine how the M260T mutation might affect the function of σNS, we defined the location of residue 260 in the crystal structure. Met260 is in the middle of the longest α-helix that forms the globular core of σNS. Mutation of Met260 to threonine increases the estimated α-helix free energy, suggesting that the stability of this central column is more disrupted at higher temperatures (129). Based on these data, it appears that the structural integrity of σNS is disrupted by this mutation at higher temperatures, which could prevent RNA-binding or interactions with other ligands like μNS.

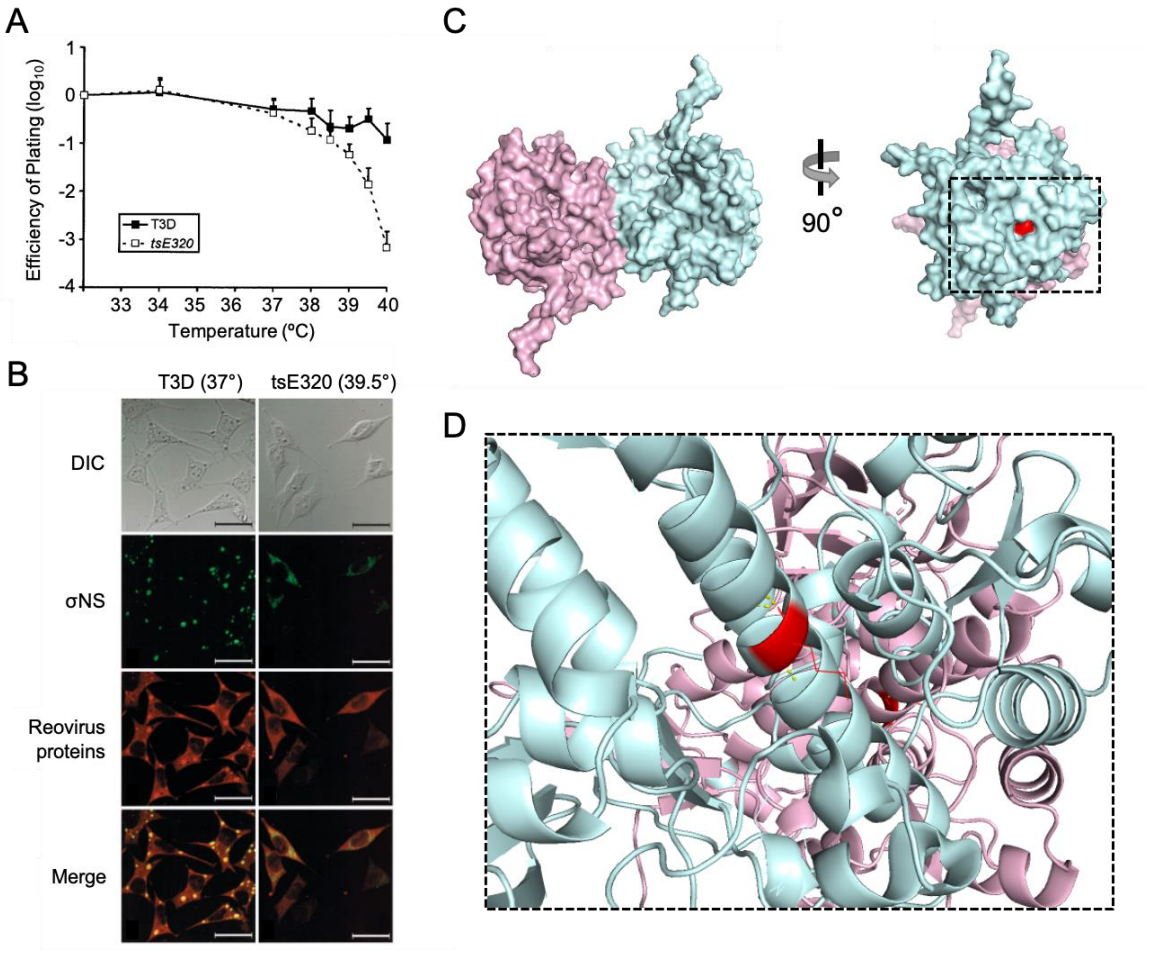

Figure 24. M260T mutation destabilizes σNS core alpha helix at high temperatures

(A) L cells were infected with WT reovirus T3D or temperature-sensitive mutant *tsE320* at the temperatures shown for 24 hours. Efficiency of plating is expressed as the viral titer at the indicated temperature divided by the viral titer at 32º C. Results are presented as the mean of six experiments. (B) L cells were infected with T3D or *tsE320* at either 37º C or 39.5º C, respectively, for 24 hours. Cells were fixed, stained with mAb specific for σNS (green) and polyclonal antiserum specific for reovirus virions (red), and imaged using confocal microscopy. (C) Surface model of a σNS dimer (one monomer shown in cyan and the other in magenta) with M260 colored in red. (D) Enlargement of the region depicted in the dashed box showing M260 (red) in the middle of the longest α-helix within the σNS core. Figures 25A and 25B were adapted from (100).

3.3 Discussion

In this chapter, I describe a 2.8 Å resolution structure of R6A σNS, which was determined using X-ray crystallography. While the structure was determined using R6A σNS, computationally replacing Ala6 with arginine does not appear to alter the monomer or dimer structure we observed. We found that σNS monomers fold into the shape of a hand forming a finger gun. Two mirrored monomers, pointed in opposite directions, interact to form curved dimers. The σNS dimers can oligomerize to form a helix when SeMet R6A σNS is packed into crystals or WT σNS is incubated with ssRNA. These findings suggest that σNS must be stabilized to form oligomers.

We previously discovered that σNS oligomerization requires RNA and is sensitive to RNAse treatment or high salt conditions (1). Surface-shaded representations of σNS helices show openings between dimers along the helical axis and at the helix top and bottom. These spaces are sufficiently large for RNase A to penetrate, which explains our observation that RNase A destabilizes RNA-dependent σNS oligomerization (1, 89). Structural analysis of σNS dimers suggests that the electropositive inner face binds RNA and that subsequent helical assembly propagates along an RNA strand (Fig. 26). σNS oligomerization requires flexible index finger domains of σNS that interact with adjacent σNS subunits, and positively-charged residues in this domain aid in stabilizing inter-dimer contacts. While we initially hypothesized that these positively-charged residues directly interact with RNA (1), the σNS helical structure suggests that these residues stabilize inter-dimer interactions. Our data further suggest that electrostatic σNS-RNA and σNS-σNS interactions aid in the formation of σNS helices.

The helical oligomerization of σNS resembles oligomers formed by the P9-1 nonstructural protein of black rice-streaked dwarf virus (RBSDV), which is a member of the *Reoviridae* family (130). P9-1 protein forms vertically elongated octamers that require flexible C-terminal arms of P9-1 dimers to interact with adjacent dimers. The interior surface of P9-1 octamers similarly binds RNA using electrostatic interactions, and P9-1 is hypothesized to form higher-ordered oligomers along RNA (131). Interestingly, P9-1 is recruited to factory-like structures made by RBSDV P6 protein, suggesting further analysis of structural similarities between σNS and P9-1 could explain how σNS binds μNS (132). Similarities of RNA-binding surfaces and oligomerization using flexible terminal arms of dimers are not shared by all RNA-binding nonstructural proteins of the *Reoviridae* family. For example, rotavirus NSP2 forms a doughnut-shaped octamer, but unlike σNS or P9-1, it binds RNA along positively charged crevices between dimers on the exterior of an octamer (126). Moreover, this binding cleft is responsible for the RNA-chaperone activity of NSP2 (104). Avian reovirus σNS has RNA-chaperone activity (15), and mammalian reovirus also has been suggested to catalyze this function (15, 89). It is possible that σNS dimers act as an RNA chaperone to unwind RNAs, but instead of using an exterior crevice on an octamer like NSP2, σNS may use the concave face of a dimer. Following RNA unwinding, σNS could oligomerize to form helices by binding the RNAs it unwinds. Unwinding RNA structures could promote RNA-RNA interactions among the viral RNA segments for assortment or facilitate interactions of the viral mRNAs with the viral RNA polymerase in preparation for genome replication.

Interestingly, other viral and mammalian proteins form helical oligomers that resemble the structure of σNS. Negative-sense ssRNA genomes of *Bunyaviridae* and *Orthomyxoviridae* viruses are coated with nucleoproteins to form RNP complexes along with polymerase subunits (133, 134). The nucleoproteins oligomerize on viral RNA molecules and form helical structures that enhance viral genome replication and transcription (135). While it was thought that influenza genomic RNA segments might be fully sequestered within the helical structures, biochemical studies suggest that portions of the viral RNA segments protrude from these structures, which could allow RNA-RNA interactions for specific packaging of the segmented genome (136). Regions of reovirus mRNAs also may reside outside of the helical oligomers formed by σNS to promote assortment. MDA-5 also forms helical filaments, but unlike the previous examples, MDA-5 oligomerizes on dsRNA (137, 138). MDA-5 helical assembly also is a criterion for measuring the length of naked nucleic acids, allowing innate immune sensors to discriminate self from non-self nucleic acids (137). It is unclear whether σNS also can form helical oligomers on dsRNA, but there appears to sufficient space within the central cavity to accommodate dsRNA (Fig. 23). As helical assemblies are ubiquitous in biology, finding common features among these structures may facilitate understanding of σNS structure and function.

Understanding the structure of σNS will inform future studies of σNS interactions with other reovirus proteins and RNA. The σNS and μNS proteins serve essential functions in reovirus replication (139). σNS requires its N-terminal arms to interact with μNS (88), suggesting that μNS binding could compete with σNS to block self-oligomerization. While the structure of μNS has not been determined, preliminary folding

models using AlphaFold could help develop hypotheses for this interaction. These results also may yield insights into how σNS and the RNAs it binds are recruited to reovirus factory scaffolds formed by μNS. Additionally, we have preliminary evidence suggesting that σNS interacts with the λ3 polymerase, which is not surprising given that other *Reoviridae* RNA-binding nonstructural proteins interact with their respective viral polymerases (140, 141). Definition of the precise function for these interactions will require further studies. Investigating σNS-μNS and σNS-λ3 interactions will help define how σNS recruits RNAs to μNS scaffolds and facilitates synthesis of the viral genome.

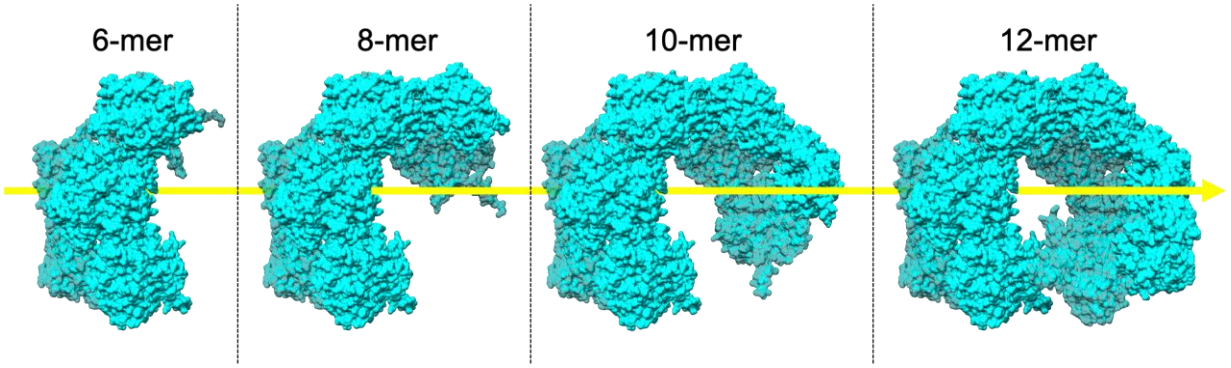

Figure 25. Model of σNS oligomerizing on RNA

Model of assembly steps showing σNS dimers incrementally oligomerizing along a horizontal helical axis. The horizontal axis represents a ssRNA (yellow). The multimerization status of σNS is indicated above each oligomer.

4.0 Parental reovirus cores embed within early-stage reovirus factories

4.1 Introduction

RNA-RNA interactions are hypothesized to drive the assortment of many segmented viruses, including reovirus and rotavirus (103). Reovirus factories likely provide specialized environments that enhance intersegmental interactions between viral mRNAs and prevent spurious interactions with cellular RNAs. In this case, factories should concentrate more viral than host RNAs. Since σNS recruits viral mRNAs to factories, we hypothesize that it uses a mechanism to enrich for viral RNAs in factories.

The σNS protein preferentially binds ssRNA over dsRNA. However, purified σNS indiscriminately binds reovirus or non-reovirus ssRNAs (97). It is speculated that σNS preferentially binds certain regions of viral ssRNA, including the 3'-termini (95). However, competition assays do not provide definitive evidence that σNS displays RNA-binding specificity for reovirus 3'-termini (94). Collectively, these results suggest that σNS does not have strong ssRNA-binding preferences. As such, we wondered how σNS selectively recruits viral mRNAs to factories. We hypothesized that σNS localizes to newly synthesized viral mRNAs, which would enhance interactions with viral mRNAs relative to host RNAs.

RNAs are not uniformly distributed within cells (142). The distribution of RNAs depends in part on the distribution of RNA-binding proteins (143). Consequently, large RNP complexes have low cytoplasmic diffusion rates (144) but can quickly redistribute using cytoskeletal transport machinery (145). While the cytoskeletal transport network is

expansive, the majority of mRNAs are stationary or corralled within small areas of the cytoplasm (146). Reovirus mRNAs are transcribed by cores within the cytoplasm, but the displacement of viral mRNAs from cores is not well understood. We hypothesized that reovirus mRNAs accumulate near transcribing cores, which promotes proximally-translated σNS to bind nascent viral transcripts. To test this hypothesis, we investigated whether early-stage reovirus factories concentrate viral vs. host mRNAs and assessed the distribution of parental reovirus cores in relation to early-stages factories.

4.2 Results

4.2.1 Endogenous host mRNA is not concentrated in reovirus factories

Since reovirus mRNAs are enriched in viral factories, assortment is thought to occur within these structures. Other non-essential RNAs, including many host mRNAs, should be excluded from these structures to prevent competing RNA-RNA interactions. I chose glyceraldehyde 3-phosphate dehydrogenase (GAPDH) as a surrogate host mRNA since it is easily detectable and its levels do not change during reovirus infection (147). To test whether GAPDH mRNA is excluded from viral factories or factory-like structures, I infected HEK293T cells with reovirus or transfected cells with plasmids encoding μNS and σNS. After 24 h, cells were processed for FISH coupled with immunofluorescence detection of μNS to visualize reovirus factories and factory-like structures (Fig. 26). FISH probes were designed to specifically detect either the reovirus σNS-encoding mRNA (σNS mRNA) or human GAPDH mRNA (1). σNS mRNA

concentrated in both factories and factory-like structures. In contrast, GAPDH mRNA was diffusely distributed in the cytoplasm and notably not present within viral factories. Additionally, endogenous GAPDH mRNA was not concentrated within factory-like structures (Fig. 26), suggesting host mRNAs are not recruited to factories.

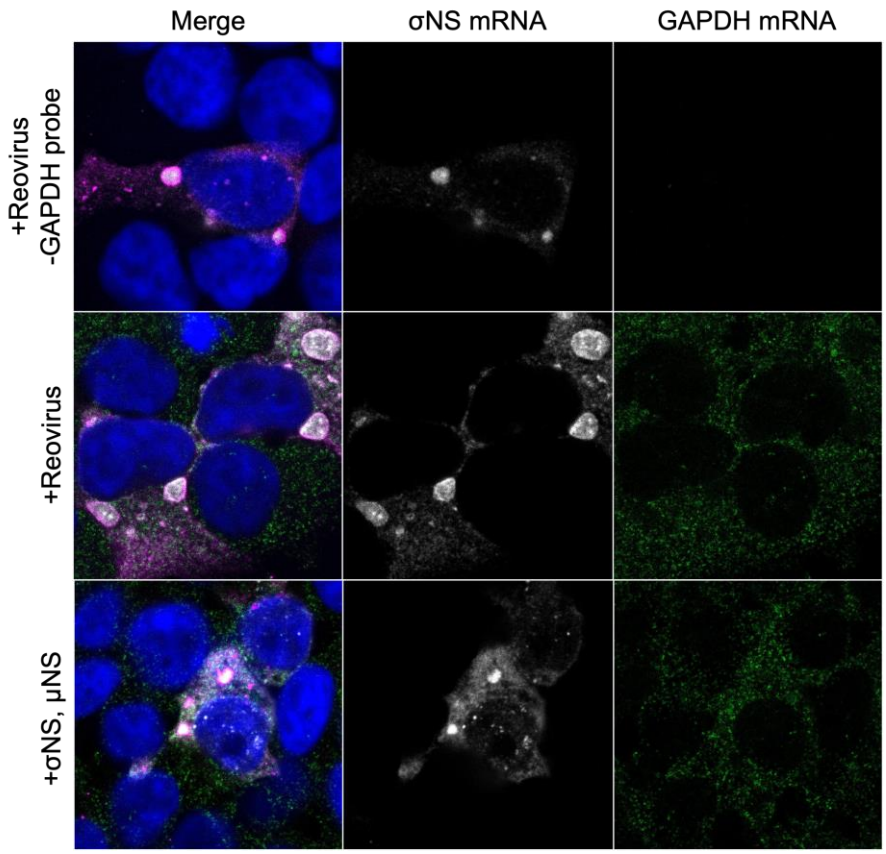

Figure 26. Endogenous host mRNA is not concentrated within reovirus factories

HEK293T cells were adsorbed with reovirus strain T3D at an MOI of 10 PFU/cell or co-transfected with expression plasmids encoding σNS and μNS and incubated for 24 h, fixed, stained using RNA FISH probes specific for σNS mRNA (white) or GAPDH mRNA (green), μNS-specific antiserum (magenta), and DAPI (blue), and imaged using confocal microscopy.

4.2.2 Reovirus factories but not factory-like structures exclude overexpressed host mRNA

Since endogenous GAPDH mRNA is not enriched in viral factories, I tested whether overexpressed GAPDH mRNA also is not present in factories or factory-like structures. To determine whether overexpressed GAPDH mRNA distributed to factories, I transfected HEK293T cells with plasmids encoding GAPDH and, at 24 h post-transfection, adsorbed cells with reovirus. Cells also were transfected with plasmids encoding μNS, WT or R6A σNS, and GAPDH to test whether overexpressed GAPDH mRNA distributed to factory-like structures. At 24 h post-adsorption or 48 h post-transfection, cells were processed for FISH coupled with immunofluorescence detection of μNS to visualize reovirus factories and factory-like structures. FISH probes were designed to specifically detect either the reovirus σNS-encoding mRNA (σNS mRNA) or human GAPDH mRNA.

Overexpressed GAPDH mRNA did not concentrate within reovirus factories, whereas viral mRNA was observed in these structures. However, overexpressed GAPDH mRNA did not distribute diffusely in the cytoplasm. Instead, GAPDH mRNA clumped in micrometer-sized puncta that docked onto the factory periphery (Fig. 27). Similar structures enriched with GAPDH mRNA also docked onto scaffolds formed by μNS when expressed alone or along with R6A σNS (Fig. 27). Interestingly, these structures were absent when GAPDH was co-expressed with μNS and WT σNS. Instead, GAPDH mRNA concentrated within factory-like structures formed by μNS and σNS. These findings suggest that σNS nonspecifically binds highly-expressed mRNAs for collection within factory-like structures. I hypothesized that the discrepant

recruitment of overexpressed GAPDH mRNAs into factory-like structures and not factories is attributable to the recruitment of actively-transcribing parental cores to early-stage factories. This hypothesis is based on the idea that early-stage factories are “sponges” that absorb RNAs (29). Thus, viral mRNAs transcribed from cores embedded within factories should preferentially concentrate in factories relative to RNAs recruited from the factory exterior.

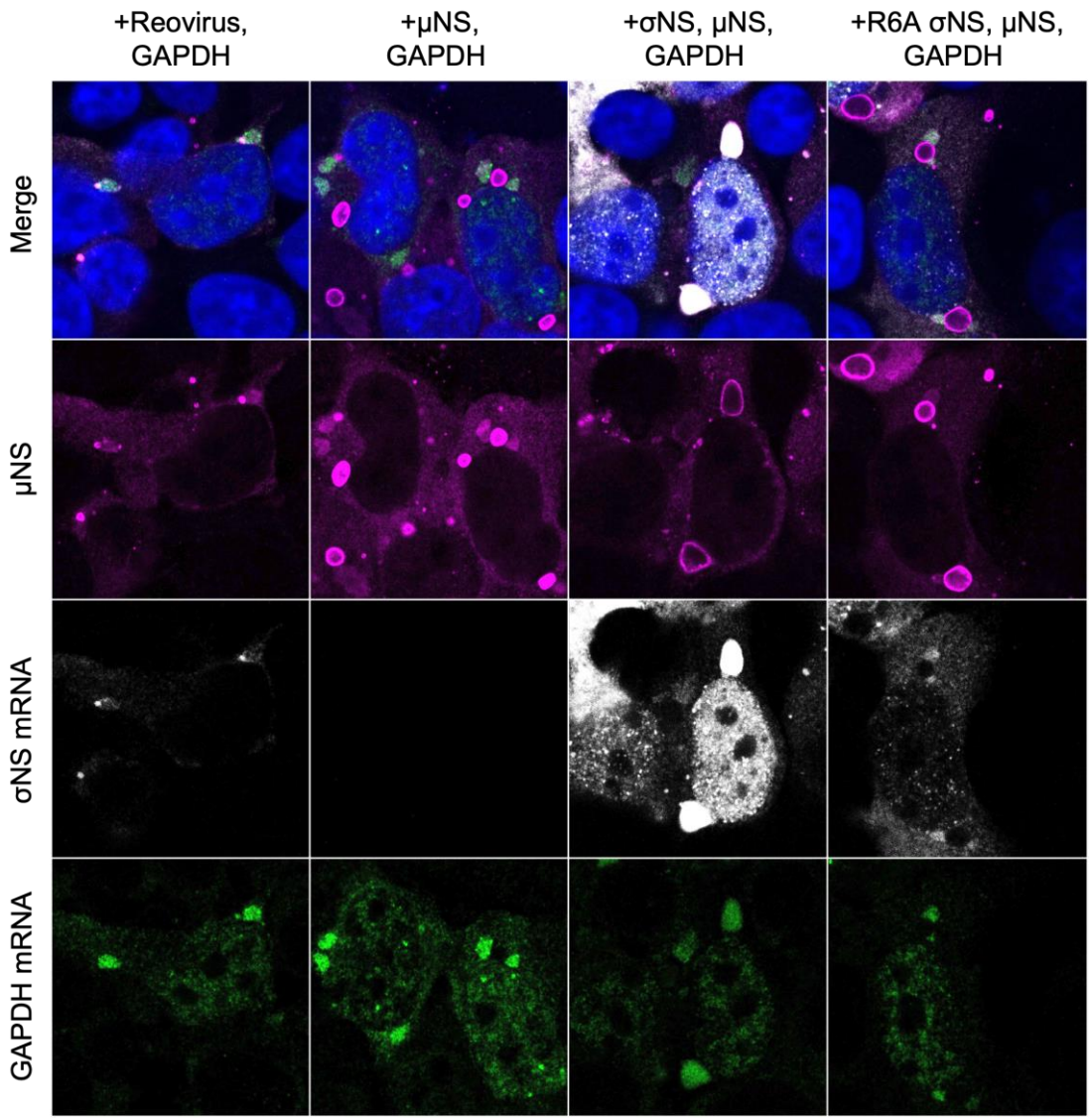

Figure 27. σNS only recurits overexpressed GAPDH mRNAs to factory-like strctures

HEK293T cells were transfected with expression plasmids encoding GAPDH, μNS, and σNS. At 24 h post-transfection, cells were either adsorbed with reovirus strain T3D at an MOI of 10 PFU/cell (+Reovirus) or left untreated. At 24 h post-adsorption or 48 h post-transfection, cells were fixed, stained using RNA FISH probes specific for σNS mRNA (white) or GAPDH mRNA (green), μNS-specific antiserum (magenta), and DAPI (blue), and imaged using confocal microscopy.

4.2.3 Early-stage factories are embedded with parental cores

Early-stage factories are formed by μNS, which can recruit reovirus core proteins and σNS (29). To determine whether actively-transcribing reovirus cores embed within early-stage factories, I imaged parental cores following transfection of cells with fluorescently-labeled cores. This approach is preferable to immunofluorescence imaging of cores, which also would detect newly synthesized core proteins. Since unlabeled reovirus cores are infectious when transfected into cells (148), I first confirmed that fluorescently-labeled cores retain infectivity. Purified reovirus virions were treated with chymotrypsin to remove the outer capsid, and the resultant cores were purified using cesium-chloride gradient ultracentrifugation (Fig. 28A & B). Cores were fluorescently labeled using amine-dependent conjugation and re-purified (Fig. 28C). To determine whether fluorescence labeling alters synthesis and release of reovirus transcripts, I conducted *in vitro* transcription assays (Fig. 28D). Levels of mRNA produced by unlabeled cores were approximately two-fold greater than those produced by fluorescently-labeled cores. Diminished recovery of viral transcripts from fluorescently-labeled cores relative to unlabeled cores suggests that some mRNA release channels are blocked by fluorescence labeling. While labeled cores transcribed less mRNA than unlabeled cores, I proceeded with experiments to transfect labeled cores into cells, as RNA accumulation was substantially greater than in mock conditions.

To visualize the intracellular distribution of cores relative to early-stage factories, I transfected BHK cells with fluorescently-labeled cores and, at 12 h post-transfection, I processed the cells for confocal immunofluorescence microscopy to visualize σNS and μNS (Fig. 29). Viral factories and fluorescently-labeled cores were detected only in

transfected cells and absent when cores were adsorbed onto cells (data not shown). By 12 h post-transfection, early-stage viral factories were readily detectable in the cytoplasm and displayed a characteristically small, spherical morphology (100). The fluorescent punctae corresponding to cores also varied in size. The presence of large puncta suggest that some cores were clumped or trapped within transfection complexes. Cores were predominately detected within early-stage factories marked by σNS and μNS. However, cores also were observed outside of factories, and some μNS condensates were not embedded with reovirus cores (Fig. 29). These observations suggest that parental cores can embed within early-stage viral factories, but factories are not seeded by cores as previously thought (29).

To visualize the intracellular distribution of cores relative to early-stage factories and viral transcripts, BHK cells were transfected with fluorescently-labeled cores. At 12 h post-transfection cells were fixed, stained using RNA FISH probes specific for σNS mRNA and μNS-specific antiserum, and imaged using confocal microscopy. Unfortunately, fluorescent cores were not visible with this protocol since the cells were permeabilized using ethanol, which significantly diminishes fluorescence signals (149). Our futures studies will focus on alternative methods to permeabilize cells that avoid quenching fluorescence with ethanol (150). These studies should clarify the displacement of viral transcripts from cores during infection and yield insights that suggest how viral transcripts are selectively concentrated in early-stage factories.

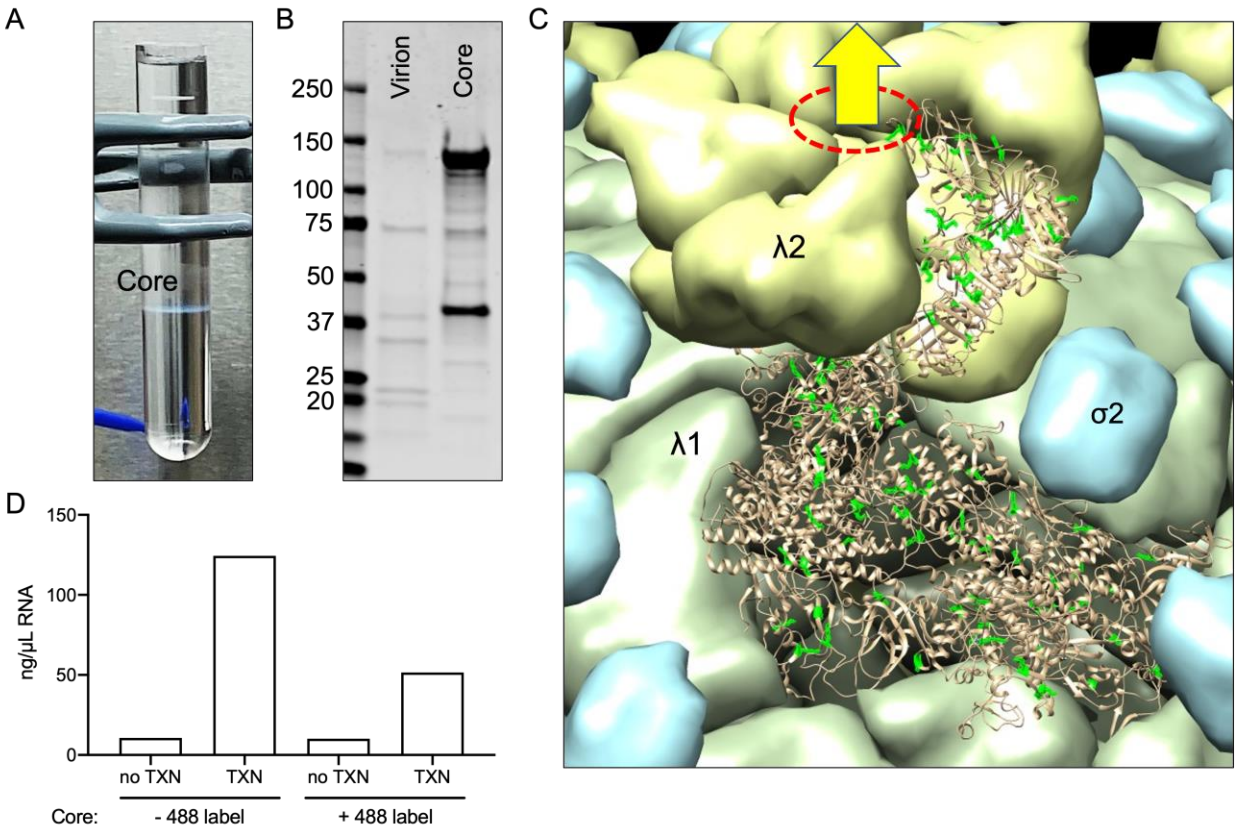

Figure 28. Fluorescently-labeled reovirus cores retain infectivity

(A) Purified reovirus virions were treated with chymotrypsin *in vitro*, and cores were purified using cesium-chloride gradient ultracentrifugation. (B) Immunoblot analysis of proteins present in purified reovirus virions or cores. Viral protein content was evaluated using rabbit antiserum specific for reovirus structural proteins. (C) Potential sites for amine-dependent conjugation of Alexa-488 (green) on the core surface. Viral transcripts can exit cores through pores at the icosahedral five-fold axes (dotted-red circle) (D) Non-fluorescently labeled (-488) and fluorescently labeled (+488) reovirus cores were incubated with only three classes of NTPs (no TXN) or all classes of NTPs (TXN) and $MgCl_2$ and incubated for 2 h. Following incubation, total RNAs were purified and quantified using UV spectroscopy.

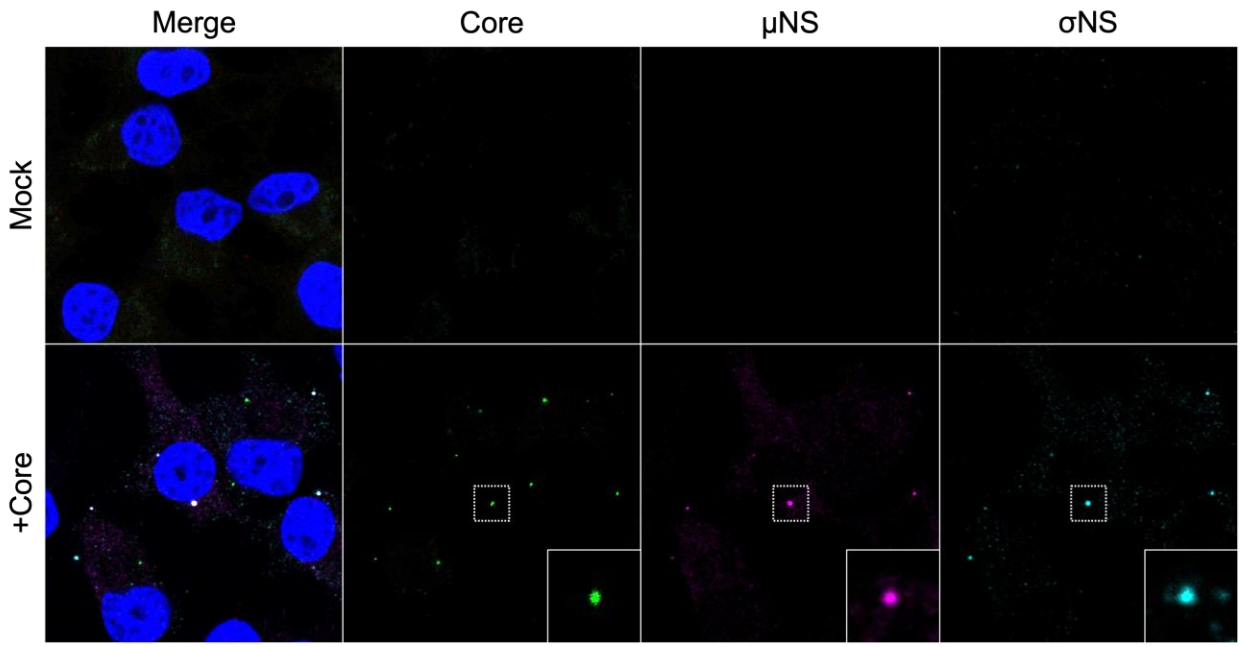

Figure 29. Reovirus cores embed within early-stage reovirus factories

BHK-T7 cells were transfected with fluorescently labeled reovirus cores (green). At 12 h post-transfection, cells were fixed, stained using μNS-specific antiserum (magenta), σNS-specific monoclonal antibody 3E10 (cyan), and DAPI (blue), and imaged using confocal microscopy.

4.3 Discussion

In this chapter, I report the discovery that reovirus factories do not concentrate GAPDH mRNA, which was used as a surrogate host mRNA. In fact, reovirus factories exclude either endogenous or overexpressed GAPDH mRNA. However, factory-like structures formed by σNS and μNS concentrate overexpressed GAPDH mRNA but not endogenous GAPDH mRNA. I also observed that early-stage factories are embedded with parental reovirus cores. These data suggest that early-stage reovirus factories preferentially concentrate viral mRNAs by collecting transcripts produced from parental

reovirus cores embedded within rather than recruiting RNAs into factories following synthesis elsewhere in the cytoplasm.

Endogenous GAPDH mRNAs are not enriched in cytoplasmic punctate structures, such as P-bodies or SGs (151). However, I found that overexpressed GAPDH mRNA concentrates within distinct punctate structures of unknown origin. µNS proteins concentrated within these unknown structures slightly more than in the cytoplasm. However, µNS was most concentrated within viral factory scaffolds or factory-like structures. Interestingly, the unknown GAPDH mRNA-containing structures were absent when GAPDH was co-expressed WT σNS and µNS. I hypothesize that overexpressing GAPDH mRNA drives excess GAPDH transcripts into SGs to regulate the expression of a gene that is normally tightly regulated (152). If these structures are indeed SGs, my results are consistent with previous observations suggesting that σNS recruits SG proteins to factory-like structures (92). The disappearance of the unknown structures when WT σNS and µNS are transfected along with GAPDH and the concentration of GAPDH mRNA in factory-like structures suggests that σNS non-specifically binds and recruits RNAs that are in high quantities in the cytoplasm. However, if early-stage factories are saturated with viral RNAs the factory surface could coarsen and impede fusion with other cytosolic condensates like SGs (153).

To assess whether transcripts from embedded reovirus cores drive viral mRNA accumulation in factories, methods should be used to permeabilize cells that avoid alcohols. While alcohol fixation and permeabilization improve RNA-FISH signals, alcohols significantly quench fluorescence (149). Alternative cell permeabilization methods (150) could preserve fluorescence from labeled cores, while still allowing

detection of viral transcripts. With improvement to this experimental protocol, it may be possible to determine whether viral transcripts concentrate within μNS scaffolds embedded with viral cores when σNS expression is diminished using siRNAs. Results from these experiments will help define whether viral transcripts are usually broadly diffuse in the cytoplasm before concentrating in factories or whether factories grow by retaining transcripts derived from embedded cores (29).

The ability to recover infectious reovirus following transfection of plasmid copies of the viral gene segments (reverse genetics) appears to question the validity of the hypothesis that factories specifically concentrate viral mRNAs by retaining transcripts from embedded, actively-transcribing cores. Cores are not present immediately following transfection of cDNA copies of the reovirus gene segments, yet these cDNAs can launch viral replication and lead to assembly of infectious virions. It is possible that reovirus reverse genetics plasmids remain closely associated within the cytoplasm following release from lipid transfection complexes (154). As such, cytoplasmic T7 polymerase transcribes viral mRNAs within a small cytoplasmic region, and early-stage condensates likely form nearby. Additionally, since viral mRNAs are more efficiently expressed than cellular RNAs in transfected cells, σNS could preferentially bind and recruit viral mRNAs. We conclude that these hypotheses are not mutually exclusive, and reovirus may use multiple strategies to concentrate viral mRNAs within factories.

5.0 Summary and future directions

5.1 Thesis summary

Viral factories house the majority of replication functions to produce progeny virions in host cells. Factories simultaneously concentrate essential viral and host components and exclude nonessential and antiviral elements. While all factories achieve similar results, mechanisms used to form factories differ depending on the virus type. Understanding how factories are constructed can help elucidate mechanisms that govern the specificity and efficiency of these structures.

Reoviridae viruses package genomes of 9-12 segments of dsRNA. These viruses induce the formation of distinct cytoplasmic factories that are not enclosed by membranes. As infection proceeds, *Reoviridae* virus factories enlarge and become filled with viral RNA and protein that assemble into virions. Viral nonstructural proteins are required to construct factories, but how these proteins form factories is not well understood. Insights into *Reoviridae* factory formation could enlighten an understanding of mechanisms of genome assortment and viral packaging that occur within factories, which have been puzzling features of *Reoviridae* virus replication.

Mammalian reovirus is a member of the *Reoviridae* family. It infects a broad range of mammalian hosts and, in infected cells, induces the formation of factories using two nonstructural proteins, μNS and σNS. Ectopically-expressed μNS protein coalesces into cytoplasmic structures that morphologically resemble reovirus factories (77). μNS also recruits viral structural proteins to the factory scaffolds (73). However,

following infection in which σNS expression is impeded by siRNA, viral factories are small, and progeny infectious virions are not produced (89). While σNS was known to be essential for viral replication, its role in viral factory formation was not well-defined. The goal of my dissertation studies was to define a function of σNS that enhanced reovirus replication. Since σNS binds to ssRNAs and interacts with μNS (88, 93), I hypothesized that σNS recruits viral RNAs to factory scaffolds to promote efficient packaging of viral RNAs into progeny particles.

My first approach to define a function of σNS was to disrupt its RNA-binding property. In chapter 2, I engineered σNS mutants deficient in the capacity to bind RNA. I found that replacement of positively charged residues with alanine in a predicted RNA-binding domain decreases RNA-dependent oligomerization. To define a step in reovirus replication facilitated by the RNA-binding property of σNS, I established a complementation system in which WT or mutant forms of σNS could be tested for the capacity to overcome siRNA-mediated inhibition of σNS expression. Using this system, I discovered that mutations in σNS that disrupt RNA binding also diminish viral replication and σNS distribution to viral factories. Moreover, viral mRNAs only incorporate into viral factories or factory-like structures when σNS is present and capable of binding RNA. Collectively, these findings indicate that σNS requires positively charged residues in a putative RNA-binding domain to recruit viral mRNAs to sites of viral replication and establish a function for σNS in reovirus replication.

To better understand the function of σNS, we aimed to determine its structure using X-ray crystallography. Previous attempts to determine the structure of WT σNS were unsuccessful, as the protein non-specifically binds bacterial RNA, yielding crystals

that diffract to low resolution. My discovery of σNS mutants deficient in RNA-binding allowed our collaborators to obtain σNS crystals that diffracted to 2.8 Å. In chapter 3, I describe the crystal structure of R6A σNS. We characterized that R6A σNS similarly folded like WT σNS (Fig. 7), and computational reversion of the mutation to the WT sequence did not change its overall structure (data not shown). The structure indicates that σNS forms curved dimers that can oligomerize into helical fibers when stabilized by SetMet substitution or binding to RNA. Surprisingly, residues in the N-terminus of σNS, which were thought previously to form an RNA-binding domain, likely do not directly interact with RNA. Instead, this region contains a flexible domain that interacts with other σNS dimers, thus stabilizing helical fiber formation. Analysis of surface electrostatic potential of σNS suggests that RNA interacts with an electropositive concave face of the dimer. This region also lines the interior channel when σNS forms a helix. The structure of σNS thus suggests a unique oligomerization structure and allows additional hypotheses to be tested with mutagenesis studies.

In chapter 4, I sought to determine whether σNS is directly responsible for viral RNA enrichment within factories. I first confirmed that viral factories are deficient in cellular mRNAs relative to the levels of these mRNAs in the cytoplasm. Since I could not evaluate all cellular mRNAs, I used a surrogate host transcript, GAPDH. I observed that early-stage viral factories or factory-like structures are not enriched with endogenous GAPDH mRNA. However, ectopically expressed GAPDH mRNA is enriched in factory-like structures, suggesting that σNS is not solely responsible for enriching for viral RNAs within factories. Based on these results, I hypothesized that reovirus cores embed within sponge-like factory scaffolds and transcribe RNAs that are preferentially retained

within viral factories. Future studies will determine whether embedded viral cores or preferential σNS-RNA interactions enrich for reovirus mRNA in factory structures.

Collectively, I discovered that σNS recruits RNAs to factories, forms curved dimers and helical oligomers, and is not solely responsible for regulating RNAs recruited to factories. My findings define a function for σNS in factory formation and provide the foundation for additional studies that will lead to enhanced understanding of reovirus factory formation and replication.

5.2 Future directions

5.2.1 Nucleotide resolution of σNS-RNA binding specificity

In chapter 2, I discovered that σNS is required to enrich viral mRNAs in reovirus factories. Based on this finding, I hypothesized that σNS recruits reovirus mRNAs to factory scaffolds formed by µNS. In chapter 4, I discovered that σNS also recruits host GAPDH mRNA when this RNA is over-expressed. Despite apparently lacking stringent specificity for viral mRNA over host mRNA (94)., σNS could still preferentially bind RNA structures unique to viral transcripts. Determining the sequences bound by RBPs in cells has been technically challenging, but the advent of high-throughput sequencing technologies has provided innovative strategies to identify RNA sequences bound by RBPs at single-nucleotide resolution (155).

While our data suggest that σNS directly binds RNA and recruits bound RNAs to viral factories, it is possible that σNS binds other RNA-binding proteins and indirectly

binds viral RNAs. As such, σNS could recruit RNAs through other protein intermediaries. In support of this idea, co-IP studies indicate that σNS binds host RNA-binding proteins (68). To define direct interactions of σNS with ssRNA in infected cells, I suggest using HITS-CLIP (155). Cells should be either infected with reovirus or transfected with plasmids encoding for σNS. In infected cells, RNA sequences bound by σNS should be defined at three intervals that comprise the early, middle, and late phases of reovirus genome replication (Fig. 31). In transfected cells, RNA sequences bound by σNS should be defined at 24 h post transfection. At each time point, cells will be irradiated with 254-nm UV light, crosslinking RNA-protein interactions. Crosslinking RNA to proteins allows for stringent washes to disrupt any artifactual RNA-protein interactions. The cells will then be lysed, treated with RNase specific for ssRNA (RNase A), and immunoprecipitated for σNS using σNS-specific monoclonal antibodies (100). The immunoprecipitated σNS-RNA complexes will be stringently washed, size-selected to ensure selective purification of RNA bands that match the footprint of σNS (156) and treated with proteinase K to remove covalently bound σNS. RNAs will be purified, reverse transcribed, and prepared for paired-end deep sequencing using Illumina NextSeq technology. These results will define the types or sequences of RNA to which σNS binds in cells.

Once sequences of RNA bound by σNS are identified, RNA-structure prediction algorithms should be used to identify RNA structural motifs that favorable bind within the concave surface of σNS dimers. Based on these computational predictions, experiments could be conducted to assess whether purified σNS preferentially binds synthesized fragments of RNA with predicted RNA structures using biolayer

interferometry (141). These experiments will determine whether σNS preferentially binds specific RNA structures, which should improve an understanding of how the binding preferences of σNS mediate specific enrichment of viral RNAs within reovirus factories.

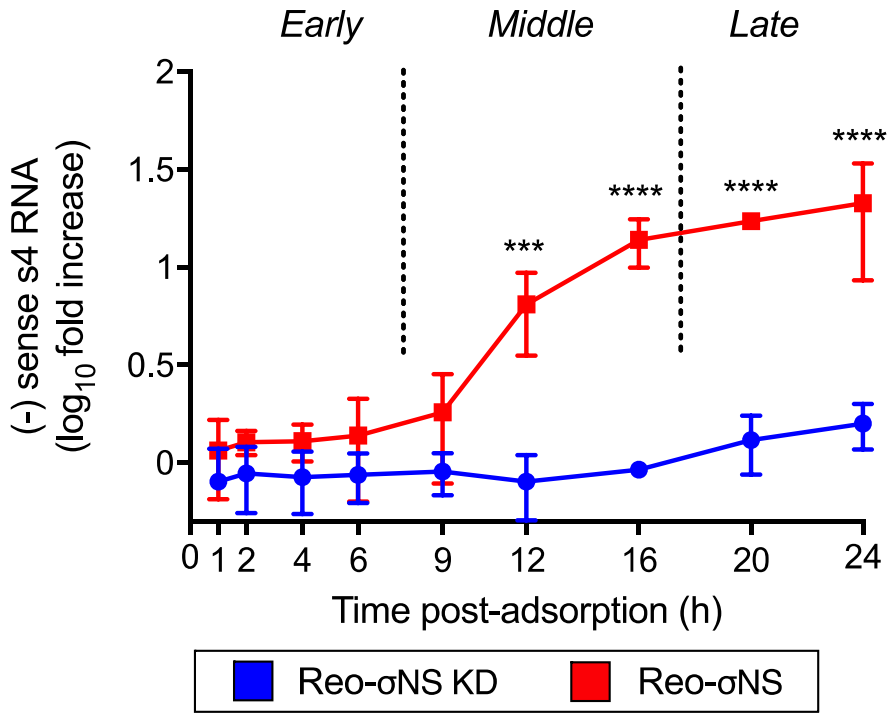

Figure 30. Time course for reovirus genome replication

σNS-siRNA cells were adsorbed with reovirus susceptible or resistant to σNS-targeted siRNAs at an MOI of 1 PFU/cell. At the time points shown, infected cells were lysed, and the negative-sense S4 RNA was quantified by RT-qPCR. The results shown are mean RNA levels ± SD (n=3). Two-way ANOVA followed by Sidak's multiple comparisons test was performed to identify values that significantly differed from the value at 0 h (***, $P < 0.001$; ****, $P < 0.0001$). Figure adapted with permission from (89)

5.2.2 The role of σNS phosphorylation in σNS oligomerization

In chapter 3, I report the structure of σNS determined by the Prasad laboratory in collaboration with our group. With a crystal structure in hand, we are now capable of defining how specific σNS residues mediate its functions. A previous member of our lab, Dr. Paula Zamora, conducted a preliminary mass spectrometric analysis of σNS purified from transfected mammalian cells to identify post-translational modifications. She found that tyrosine 240 was phosphorylated in 12% of identified σNS peptide fragments. When we mapped this residue onto the structure of σNS, we found that it resides within a binding pocket for the N-terminal σNS arm that promotes oligomerization (Fig. 32). Thus, this residue may regulate σNS oligomer formation. This regulation may have inhibitory effects on oligomerization as observed with influenza NP (157). Similarly, phosphorylation of σNS could act as a regulatory mechanism that induces σNS to release bound RNA. I hypothesize that phosphorylation of Y240 destabilizes σNS oligomers and releases bound RNAs for subsequent packaging into viral capsids.

To define the importance of this phosphorylation site, this residue should be exchanged with alanine using site-directed mutagenesis. Based on alpha-fold predictions, the monomer is not disrupted by the mutation (data not shown). The mutant should be expressed *in vitro* using RRLs and assessed for RNA-dependent oligomerization using native PAGE. The mutant then should be tested for native function using our complementation system. These studies will define the importance of phosphorylation in σNS oligomerization and its functions in reovirus replication.

5.2.3 Identification of a site to tag σNS

A tagged version of a protein is a useful tool for studies of intracellular protein distribution and function. Before the structure of σNS was known, we attempted to tag σNS by adding GFP onto its N- or C-terminus. Unfortunately, these modified proteins did not complement σNS function. Using structural analyses, we realized that these sites are not amendable for tagging, as the N-terminus is required for oligomer formation and the C-terminus is buried within the σNS core. Therefore, we inspected the structure for protein regions that contained flexible residues on the convex surface of the σNS dimer. We identified a site between residues 130 and 131 that fit these criteria (Fig. 32). Preliminary structural predictions suggest that σNS containing a His tag and GGGGS linkers between residues 130 and 131 folds like WT σNS and contains a properly folded tag. To confirm that this construct functions similarly to WT σNS, the tagged version should be tested for function using our complementation system. If this site is amenable to inserting a His tag, it is possible that larger fluorescent tags will be tolerated. These experiments will identity a site on σNS that can be tagged, which will enhance future studies of σNS function and factory formation. While the helical oligomerization of σNS was observed *in vitro*, the formation of similar structures within cells should be confirmed. I suggest using fluorescently tagged constructs of σNS for correlative light and electron microscopy and cryo-electron tomography studies (158). These correlative studies would allow improved tracking and 3D imaging of σNS in infected cells.

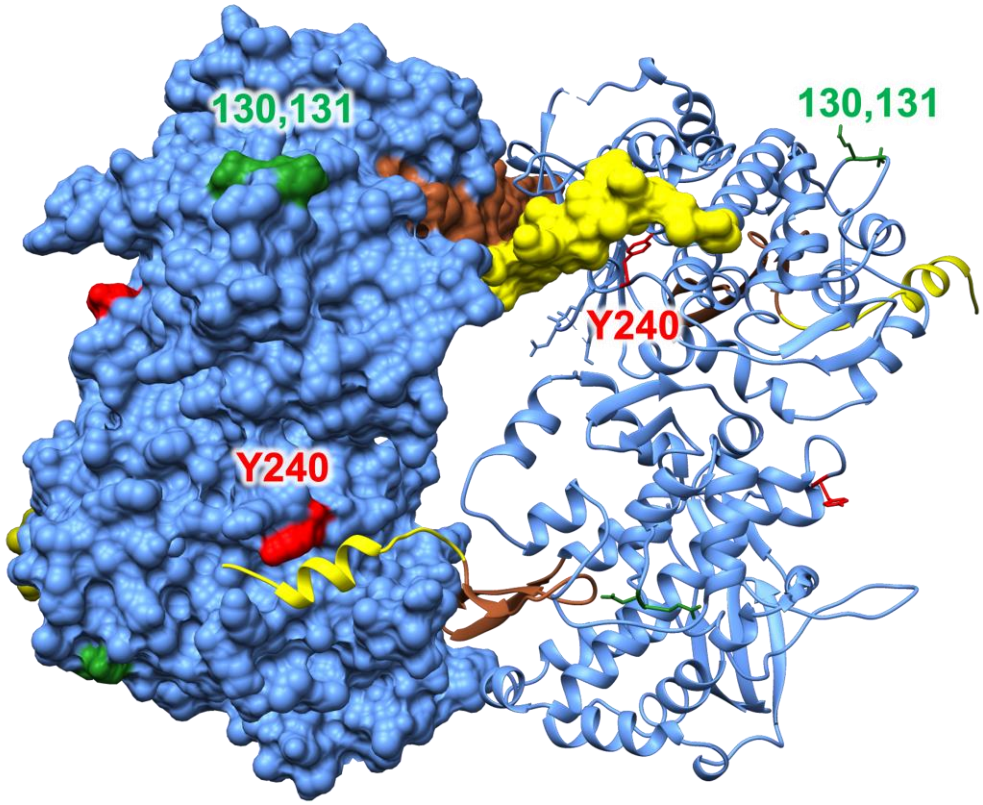

Figure 31. Potential sites to mutate on the convex surface of σNS dimers

The interaction of two σNS dimers (surface model and ribbon model) is mediated by residues in the N-terminus. Residues 1-17 residues are shown in yellow, and residues 18-47 shown in brown. Y240 (red) can be phosphorylated, which could regulate σNS oligomerization. Residues 130 and 131 might allow insertion of a protein tag.

5.2.4 Studies of σNS-λ3 interactions

While my findings enhance an understanding of σNS function during reovirus factory formation, important questions remain about other potential functions of this protein. It is possible that σNS enhances interactions between the viral polymerase and mRNAs, as observed for other viral RNA-binding proteins (109-113). Many members of

the *Reoviridae* family express predicted functional homologs of σNS, including the rotavirus NSP2 and bluetongue virus NS2 proteins, which interact with their respective polymerases in an RNA-independent manner (140, 141). In preliminary studies, I found that the reovirus polymerase, λ3, concentrates in reovirus factories (Fig. 33A) and binds σNS in an RNA-independent manner (Fig. 33B). The biological significance of these conserved interactions of σNS and its homologs with their respective polymerases suggests that these interactions are required for efficient viral replication. Based on the functions of other viral RNA-binding proteins that interact with viral polymerases, interactions of σNS and λ3 could be required for polymerase recruitment to the template mRNA or polymerase processivity (135, 159, 160). As a first step to investigate the function of σNS-λ3 engagement, biochemical interactions between the proteins should be more carefully characterized. Purified σNS and λ3 proteins should be incubated with or without reovirus mRNA and imaged using cryo-EM. Since the structures of both proteins have been determined using X-ray crystallography, the X-ray coordinates can be placed within the class-averaged cryo-EM density maps. If a binding interface is observed between σNS and λ3, residues in σNS at the binding surface should be exchanged with alanine (or charge clusters to alanine) to destabilize interactions with the polymerase, which could be tested biochemically using co-IP analyses. If *in vitro* interactions are disrupted, studies of the effect of these mutations on viral replication could be conducted to determine the functional significance of the interactions.

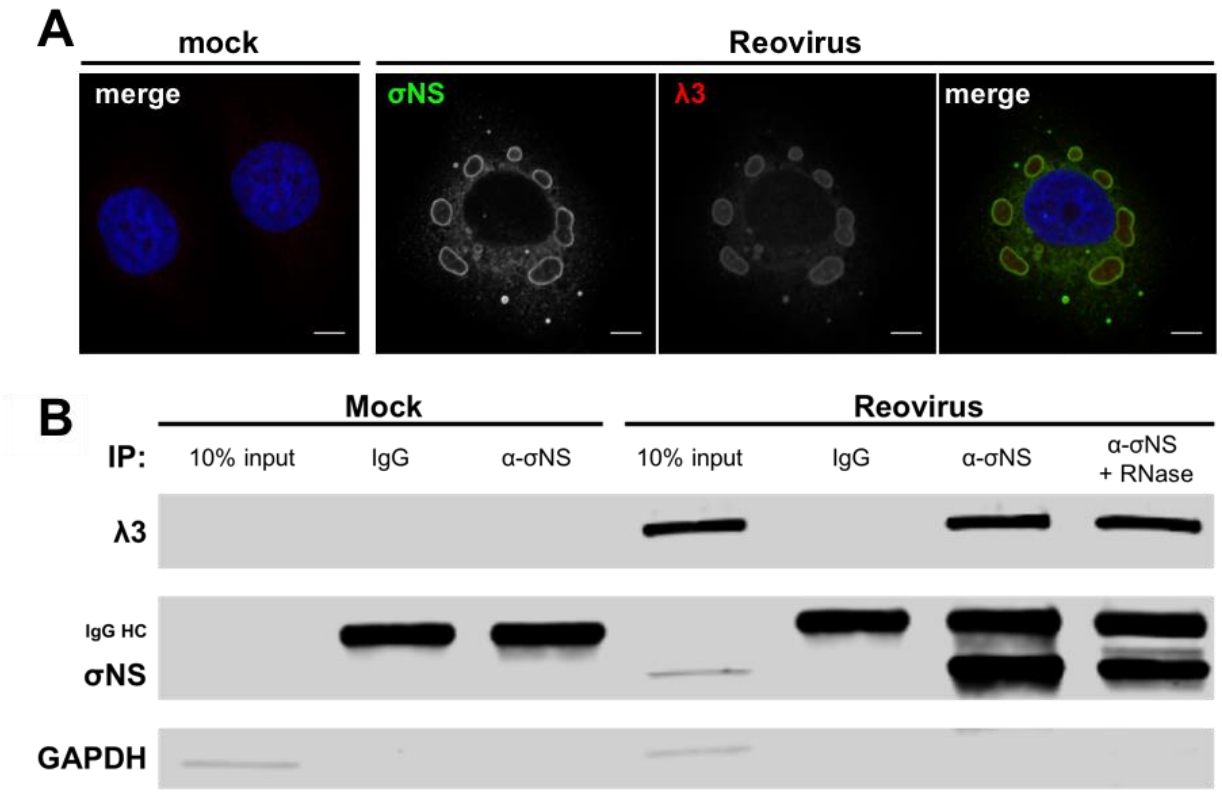

Figure 32. Reovirus polymerase, λ3, interacts with σNS

(A) σNS and λ3 co-localize. HBMECs were adsorbed with reovirus T3D at an MOI of 100 PFU/cell. Cell were fixed 24 hours post-adsorption and imaged using indirect immunofluorescence with antibodies specific for σNS and λ3. (B) σNS and λ3 co-immunoprecipitate. Human brain microvascular endothelial cells (HBMECs) were adsorbed with reovirus at an MOI of 100 PFU/cell. Cell lysates were collected 24 hours post-adsorption and analyzed for co-immunoprecipitation of λ3 with σNS. Lysates were treated with RNase A at 37ºC for 30 minutes prior to IP.

5.2.5 Delineate displacement of reovirus transcripts following transcription from transfected cores

In chapter 4, I attempted to visualize newly synthesized viral transcripts in relation to reovirus cores. Unfortunately, our current FISH protocol significantly

diminished the fluorescence of Alexa-488 labeled cores, as I used ethanol to permeabilize cells. Permeabilization of cells with ethanol improves RNA-FISH signals (161) but significantly diminishes other fluorescence signals (149). Thus, other FISH protocols that avoid alcohol permeabilization should be used for these experiments (150). Cells should be permeabilized following fixation using a low percentage of triton-X in lieu of 70% ethanol (150). If sufficient RNA-FISH signal is not observed using alternative permeabilization conditions, nascent viral transcripts can be visualized using 5-bromouridine (BrU) labeling (70). Cells should be transfected with fluorescently labeled cores and incubated at 37º C. At 4 h post-transfection, cells will be treated with actinomycin D to inhibit host transcription (162). BrU will be added to cells for up to 6 hours. Nascent viral transcripts can be visualized by immunofluorescence microscopy using monoclonal antibodies specific for BrU. These experiments will determine the displacement of viral transcripts from actively transcribing cores and define whether RNAs diffuse in the cytoplasm before early-factory formation.

5.2.6 Investigate whether viral transcripts from cores embedded within factories are sequestered by σNS

In chapter 4, I discovered that σNS does not specifically recruit viral mRNAs to factory-like structures. Additionally, I observed that viral cores embed within early-stage viral factories, suggesting that factory scaffolds preferentially retain viral transcripts produced within these structures rather than recruiting RNAs from the cytoplasm. RNA recruitment to other host condensates, like SGs and P-bodies, is an inefficient process (163). Interestingly, *in vitro* transcribed rotavirus mRNAs are not recruited to rotavirus

factories when transfected into infected cells (164). However, non-rotavirus RNAs appended with rotavirus-specific 3' UTRs expressed in rotavirus-infected cells are preferentially recruited to rotavirus factories (165). To determine whether actively transcribing reovirus cores, embedded within factories, saturate factory structures with viral mRNA, cores should be transfected into cells that constitutively express siRNAs directed against σNS or μNS transcripts produced by cores. σNS-siRNA cells should express plasmids that yield scaffolds that do not contain σNS (+ WT μNS plasmid only), contain σNS (+ WT σNS and WT μNS plasmids), or contain σNS that cannot bind RNA (+ R6A σNS and WT μNS plasmids). Factory-like structures with different σNS properties will allow us to determine if σNS sequesters transcripts originating from cores embedded in the structures. μNS-siRNA cells (139) should express plasmids that yield scaffolds that can recruit cores (+ WT μNS plasmid) or cannot recruit cores (+ Δ173-221 μNS plasmids) (Miller et. al., 2009). Cells expressing factory-like structures that cannot recruit cores will allow us to determine if σNS efficiently recruits transcripts originating from cores in the cytoplasm to factory-like structures. At 12 hours post-transfection of cores in cells expressing factory-like structures, cells should be processed to visualize fluorescent cores and nascent viral transcripts using protocols optimized in the previous section. These results will clarify whether viral transcripts are enriched within factories by actively transcribing cores and sequestered by σNS that is capable of binding RNAs.

5.3 Conclusions

The results of my dissertation research define a role for σNS in RNA recruitment to reovirus factories. More broadly, this work provides future avenues of research for studying early-stages of cytoplasmic, non-membrane-enclosed factory formation by a dsRNA virus. Understanding mechanisms of viral factory formation could help identify new targets for antiviral therapeutics that disrupt assembly of these structures and inform the use of nonpathogenic viruses for biotechnological applications.

6.0 Materials and methods

6.1 Cells

BHK cells expressing T7 polymerase (BHK-T7 cells) (166) were maintained in Dulbecco's modified Eagle's minimal essential medium (DMEM) supplemented to contain 5% fetal calf serum (FBS), 2 mM L-glutamine (Life Technologies), 2% MEM nonessential amino acids (Sigma-Aldrich), and 1 mg/ml geneticin. HEK 293T cells and HEK 293T cells expressing a GFP-specific siRNA (GFP-siRNA cells) (89) or an S3-specific siRNA (σNS-siRNA cells) (89) were maintained in DMEM supplemented to contain 5% FBS and 2 mM L-glutamine. Culture medium for the siRNA-expressing cells was additionally supplemented to contain 5 µg/mL of puromycin (Invivogen). L929 (L) cells adapted for growth in spinner cultures were maintained in Joklik's minimal essential medium (JMEM) supplemented to contain 5% FBS, 1% L-glutamine, 50 U/mL of penicillin, 50 µg/mL of streptomycin (Life Technologies), and 0.25 µg/ml amphotericin B (Sigma). Hela CCL2 cells were grown in DMEM supplemented to contain 10% FBS, 1% sodium pyruvate (Gibco), 1% MEM nonessential amino acids (Sigma-Aldrich), 1% L-glutamine, 50 U/mL of penicillin, 50 µg/mL of streptomycin, and 0.25 µg/ml amphotericin B.

6.2 Preparation of virions and cores

WT reovirus strain T3D was recovered using reverse genetics (166). Site-directed mutagenesis of the reverse genetics plasmid encoding σNS was used to engineer σNS with R6A, K11A, and R29A mutations. Viruses encoding these mutations could not be recovered using reverse genetics. Primers used for mutagenesis are listed in Supplemental Table 1. Reovirus strain T1L M1-P208S (167) was recovered using reverse genetics (166). Reovirus T1L M1-P208S contains a point mutation in the M1 gene that causes viral factories to have a globular morphology similar to the morphology of factories formed by reovirus T3D (167). Viruses were amplified in L cells and purified by cesium chloride gradient centrifugation as described (168). Viral titers were determined by plaque assay using L cells (169).

Reovirus cores were prepared with virions pelleted by ultracentrifugation from reovirus-infected L cells (22). Resuspended virions were digested with chymotrypsin (0.25 mg/ml) for 2 h at 37°C. Digestion was terminated with addition of phenylmethylsulfonyl fluoride (PMSF) to 2 mM. Cores were purified by banding on two successive preformed CsCl gradients (1.3 to 1.5 g/cm^3) and dialyzed extensively against virion buffer. Core generation was assessed by analyzing protein content with SDS-PAGE and colloidal staining.

6.3 Plasmids

Reovirus T3D σ3 (170), WT σNS (89), ∆38 σNS (89), and GFP (170) expression plasmids have been described elsewhere. T3D μNS expression plasmid was engineered by amplification of the T3D M3 open reading frame to contain 5′ KpnI and 3′ NotI restriction sites using reverse-genetics plasmid pT7-M3T3D (171) and T3D M3 5'-KpnI-NotI-3' primers listed in Supplemental Table 1. The amplified DNA was digested with NotI-HF and KpnI-HF (New England BioLabs [NEB]) and purified from agarose gel fragments following electrophoresis. The purified PCR product was ligated into pcDNA3.1+ vectors between the NotI-HF and KpnI-HF restriction sites. Site-directed mutagenesis was used to engineer σNS expression plasmids encoding R6A, K11A, R14A, TriA, Y25A, R29A, K35A, R38A with primers listed in Table 2. Fidelity of cloning and mutagenesis was confirmed using Sanger sequencing (Genewiz) and Genewiz primers. Human GAPDH expression plasmid was acquired from DNASU (HsCD00075499).

	Sequence (5′→3′)	
	Forward (F)	**Reverse (R)**
T3D M3 5'-KpnI-NotI-3'	CGACGGTACCATGGCTTCATTCAAGGGATTCTCCG	ATCACAGGCGGCCGCTTACAACTCATCAGTTGGAACAGAGAAATC
T3D S3 R6A	CTTGGAGATCGCAGCTGCGAGTGAGGAAGCCATG	CATGGCTTCCTCACTCGCAGCTGCGATCTCCAAG
T3D S3 K11A	CGTCATCCCTCTTGATCGCGGAGATCGCAGCTCTGA	TCAGAGCTGCGATCTCCGCGATCAAGAGGGATGACG
T3D S3 R14A	GCTGACCGACGTCATCCGCCTTGATCTTGGAGATCG	CGATCTCCAAGATCAAGGCGGATGACGTCGGTCAGC
T3D S3 TriA	CACTCAGAGCTGCGATCTCCGCGATCGCGGCGGATGACGTCGGTCAGCAAG	CTTGCTGACCGACGTCATCCGCCGCGATCGCGGAGATCGCAGCTCTGAGTG
T3D S3 Y25A	CGTCGGTCAGCAAGTTTGTCCTAATGCTGTCATGCTGCGG	CCGCAGCATGACAGCATTAGGACAAACTTGCTGACCGACG
T3D S3 R29A	CTTTGTTGTGACAGAGGACGCCAGCATGACATAATTAGGA	TCCTAATTATGTCATGCTGGCGTCCTCTGTCACAACAAAG
T3D S3 K35A	ACATTTCGTACCACCGCTGTTGTGACAGAGGACCGCAG	CTGCGGTCCTCTGTCACAACAGCGGTGGTACGAAATGT
T3D S3 R38A	AATTTGATACTCAACCACATTTGCTACCACCTTTGTTGTGACAGAG	CTCTGTCACAACAAAGGTGGTAGCAAATGTGGTTGAGTATCAAATT

Table 2. Primers used for mutagenesis

6.4 Expression, proteolysis, and RNA-dependent oligomerization assays

Reovirus σNS proteins were expressed from plasmids *in vitro* using the TNT T7 polymerase coupled, rabbit-reticulocyte lysate system (Promega, L4610) (89). Reactions were supplemented with [^{35}S]-methionine (Perkin Elmer, NEG709A500UC), incubated at 30°C for 1.5 h, and terminated with a fourfold dilution in stop buffer (20 mM

HEPES-KOH pH 7.4, 100 mM potassium acetate, 5 mM magnesium acetate, 5 mM EDTA, 2 mM methionine, and freshly supplemented to contain 1 mM dithiothreitol (DTT) and 2 mM puromycin). Terminated reactions were used for proteolysis and RNA-dependent oligomerization assays.

Proteolysis assays were conducted by incubating translation reactions with 1 µg/mL proteinase K (Sigma) at 37°C for 0, 5, 10, or 15 min. Samples were prepared for sodium dodecyl sulfate polyacrylamide gel electrophoresis (SDS-PAGE).

RNA-dependent oligomerization assays were conducted by incubating translation reactions with 10 µg of RNase A (Thermo Fisher) or 125 mM of NaCl at 37°C for 1 h. Samples were prepared for native- and SDS-PAGE.

6.5 Native PAGE, SDS-PAGE, phosphorimaging, and immunoblotting

Samples for native PAGE were diluted in 4x native PAGE sample buffer (Thermo Fisher) and electrophoresed in 4-16% native PAGE Bis-Tris acrylamide gels (Thermo Fisher) using the Blue Native PAGE Novex Bis-Tris gel system (Thermo Fisher) at 4ºC as described (89). Samples for denaturing SDS-PAGE were boiled in SDS-PAGE sample buffer (Bio-Rad) containing β-mercaptoethanol and electrophoresed in 4-20% Mini-Protean TGX gels (Bio-Rad).

Polyacrylamide gels containing ^{35}S-labeled proteins were fixed with 40% methanol and 10% acetic acid at room temperature (RT) for 30 min, washed with ddH_2O, and dried onto filter paper using a gel dryer (Bio-Rad). Dried gels were exposed

on a phosphorimaging screen and imaged using a phosphor system scanner (Perkin Elmer, B431200). Band intensities were quantified using ImageJ software.

Polyacrylamide gels containing unlabeled proteins were transferred to nitrocellulose membranes (Bio-Rad) and immunoblotted using the following antibodies: guinea pig σNS-specific polyclonal antiserum (89), chicken μNS-specific polyclonal antiserum (89), and mouse α-tubulin-specific monoclonal antibody (Cell Signaling Technology). IRDye800CW donkey anti-guinea pig, IRDye680RD donkey anti-chicken, and IRDye680LT goat anti-mouse (Li-Cor) were used as detection reagents. Antibodies were diluted at the following dilutions: 1:1,000 for guinea pig σNS-specific antiserum, 1:5,000 for chicken μNS-specific antiserum, 1:1000 for mouse α-tubulin-specific antibody, and 1:7500 for secondary antibodies Immunoblot images were captured using an Odyssey CLx imaging system (Li-Cor).

6.6 Immunoprecipitation and co-immunoprecipitation assays

HEK 293T cells were transfected with σNS expression plasmids alone or in combination with μNS expression plasmid using FuGene 6 transfection reagent (Promega) at a reagent:DNA ratio of 3:1 in Opti-MEM (Life Technologies). At 24 h post-transfection, cells were lysed with IP lysis buffer (25 mM Tris pH 7.4, 150 mM NaCl, 1% NP-40 substitute [VWR], 0.5% DOC, 0.1% SDS) on ice for 30 min or co-IP buffer (20 mM Tris pH 7.5, 137 mM NaCl, 2 mM EDTA, 0.1% NP-40 substitute) at 4 °C for 30 min with rotation. Lysis buffers were supplemented with protease inhibitors (Roche, 11873580001) before use. Following lysis, cellular debris was collected by

centrifugation at 20,000 x *g* at 4 °C for 20 min. Supernatants were incubated with protein G Dynabeads (Thermo Fisher, 10004D) saturated with σNS-specific monoclonal antibodies 2A9 (IP, (100)) or 3E10 (co-IP, (100)) at 4 °C for 4 h with rotation. Antibodies were saturated on Dynabeads using the manufacturer's protocol. Dynabeads were washed with cold lysis buffer, and bound proteins were eluted by boiling in SDS-PAGE sample buffer (Bio-Rad) with β-mercaptoethanol for 10 min. Proteins were analyzed by immunoblotting.

6.7 σNS complementation assays

GFP or σNS siRNA-expressing cells were cultivated in 6-well plates for virus quantification or 8-well cell-culture slides for immunofluorescence (Ibidi, 80826; fluorescence in situ hybridization: Matek, CCS-8). Cells were transfected with GFP or σNS expression plasmids using FuGene 6 transfection reagent. At 24 h post-transfection, cells were adsorbed with reovirus at a multiplicity of infection (MOI) of 5 PFU/cell. Following incubation at 37 ºC for 48 h, the supernatant was collected, and viral titers were determined by plaque assay. Cells cultivated on slides were processed for fluorescence microscopy

6.8 Immunogold labeling of Tokuyasu cryosections

HeLa cells were adsorbed with reovirus T1L M1 P208S at an MOI of 1 PFU/cell. Following incubation at 37ºC for 14 h, cells were fixed with 4% PFA in 0.2 M HEPES buffer (pH 7.4) at RT for 2 h. Free aldehyde groups were quenched with 50 mM NH_4Cl. Cells were removed from the plates with a rubber policeman and pelleted by centrifugation in a 1.5 mL Eppendorf tube. The cell pellet was embedded in 12% gelatin (TAAB Laboratories) in PBS, and after solidification, cubes of 1 mm^3 were cut and infiltrated with 2.3 M sucrose in PBS at 4°C overnight. Cubes were mounted on metal pins and frozen in liquid nitrogen. Thin cryosections were obtained at -120°C using an FC6 cryo-ultramicrotome (Leica Microsystems), collected from the diamond knife into a 1:1 mixture of 2% methylcellulose in H_2O and 2.3 M sucrose in PBS, and placed after thawing on 200 mesh grids with a carbon-coated Formvar film. Grids were incubated with σNS-specific monoclonal antibody 2F5 (100) diluted 1:200 in saturation buffer (1% BSA in PBS) at RT for 1 h. Secondary antibody conjugated with 10 nm colloidal gold particles (British Biocell Int.) was diluted 1:50 in saturation buffer, and grids were incubated at RT for 30 min. After labeling, images were captured using a JEOL JEM-1011 transmission electron microscope operating at 100 kV. At least two independent labeling assays were conducted for each experimental condition.

6.9 Factory-like structure assays

HEK 293T σNS siRNA-expressing cells or HEK 293T cells were cultivated in 8-well cell-culture slides (Immunofluorescence: Ibidi, fluorescence in situ hybridization: Matek). Cells were transfected with various combinations of σ3, σNS, and μNS expression plasmids using FuGene 6 transfection reagent. For combinations of less than three plasmids, empty pcDNA 3.1 + plasmid was added to the transfection mixtures to maintain identical DNA concentration for all conditions. At 24 to 48 h post-transfection, cells were processed for fluorescence microscopy.

6.10 Transfection of Alexa-488 labeled cores

Reovirus cores were labeled with Alexa Fluor 488 TFP ester (Invitrogen) to generate fluorescent cores (62). For labeling, reovirus cores were diluted to 6×10^9 particles/μL in freshly prepared 5 mM sodium bicarbonate buffer and incubated with 20 μM dye at RT for 1.5 h, protected from light. Labeled virions were dialyzed at 4°C overnight against PBS, exchanging the buffer 2 times to remove unreacted dye.

For assessing 488-labeling did not prevent transcription from cores, Alexa-488 labeled cores were incubated with transcription buffer (100 mM Tris pH 7.5 and 10 mM $MgCl_2$) that contained 2 mM of ATP, UTP, CTP, and GTP at 45°C for 2 h. Total RNAs were purified with PureLink RNA Mini Kit (Thermo Fisher) and quantified with a Synergy H1 BioTek plate reader, using the Take3 plate.

BHK-T7 cells were transfected with reovirus cores using Lipofectamine 3000 transfection reagent (Thermo Fisher) (148). Single wells in a 24-well plate were transfected with a mixture of 1uL transfection reagent, 1uL p300 reagent, and 1.8×10^3 cores diluted in up to 48 µL of Opti-MEM (Life Technologies). At 12 h post transfection cells were processed for immunofluorescence or fluorescence in situ hybridization microscopy.

6.11 Immunofluorescence assays

Cells were fixed with 4% paraformaldehyde (PFA) diluted in PBS at RT for 30 min, permeabilized in 1% triton-X 100 in PBS at RT for 10 min, and blocked with PBS-BGT (0.5% bovine serum albumin, 0.1% glycine, 0.05% Tween 20) at 37°C for 10 min. Cells were incubated with σNS-specific monoclonal antibody 3E10 and chicken µNS-specific polyclonal antiserum diluted in PBS-BGT at RT for 1 h, washed with PBS-BGT, probed with species-specific secondary antibodies conjugated with Alexa Fluors 488 or 647 (Thermo Fisher), and counterstained with 4′,6-diamidino-2-phenylindole (DAPI, Invitrogen) to label nuclei. Cells were washed with PBS-BGT and stored in PBS. Antibodies were diluted 1:1,000 for antibody 3E10, 1:1,000 for µNS-specific antiserum, and 1:1000 for secondary antibodies.

Cell images were captured using a Leica SP8 laser scanning confocal microscope equipped with a 63x oil objective. Images were processed and analyzed using ImageJ software with the Fiji processing package. Brightness of each channel was adjusted to the appropriate mock signals and normalized for all experimental

conditions. The percentage of σNS immunofluorescence signal intensities in factories and factory-like structures was calculated by marking high-intensity μNS immunofluorescence as regions of interest (ROIs). Total σNS immunofluorescence signal intensities within all ROIs of a single cell were determined and then divided by the total σNS immunofluorescence signal intensities detected within the cytoplasm.

6.12 Fluorescence in situ hybridization microscopy

Cells were fixed with 3% PFA diluted in PBS for 30 min and permeabilized in 70% EtOH at 4°C overnight. Cells were rehydrated with wash buffer (10% formamide and 2x saline sodium citrate [SSC] in diethyl pyrocarbonate (DEPC)-treated water) and incubated with hybridization buffer (10% dextran sulfate, 2 mM vanadyl-ribonucleoside complex [NEB], 0.02% UltraPure BSA [Thermo Fisher], 1 mg/mL E.coli tRNA [Sigma], 2x SSC, and 10% formamide in DEPC-treated water) containing a 1:1000 dilution of chicken μNS-specific antiserum and 100 nM of σNS (quasar670) or σ3 (quasar570) mRNA FISH probes (BioSearch Technologies) at 28°C overnight. The mRNA FISH probe sets consisted of at least 20 probes of ~ 20 base-pairs in length, and individual probes were designed to bind target sequences at a minimum spacing of two nucleotides between probes (BioSearch Technologies). Following hybridization, cells were washed with wash buffer and incubated with anti-chicken Alexa Fluor 488-conjugated antibody (Thermo Fisher) diluted to 1:1000 in secondary buffer (2 mM vanadyl-ribonucleoside complex, 0.02% RNA-free BSA, 1 mg/mL E.coli tRNA, 2X SSC, and 10% formamide in DEPC-treated water) at RT for 1 h. Cells were washed with

wash buffer and counterstained with DAPI. Glass coverslips were mounted on labeled cells using Prolong Diamond anti-fade mounting media (Thermo Fisher).

Cell images were captured using a Leica SP8 laser scanning confocal microscope equipped with a 63x oil objective. Images were processed and analyzed using ImageJ software with the Fiji processing package. Brightness of each channel was adjusted to the appropriate mock signals and normalized for all experimental conditions. The percentage of FISH signal intensities in factories and factory-like structures was calculated by marking high-intensity µNS immunofluorescence as ROIs. Total FISH signal intensities within all the ROIs of a cell were determined and then divided by the total FISH signal intensities detected within the cytoplasm.

6.13 σNS structural analysis

Native and SeMet-substituted R6A σNS were expressed and purified from *E. coli* in the same manner as previously described (89, 172). Purified proteins were crystalized and exposed to X-ray beams (173). X-ray diffraction data of SeMet-substituted R6A protein were solved with single-wavelength anomalous diffraction (SAD) phasing (174). All protein figures were generated with UCSF chimera.

6.14 Statistical analysis

All experiments were conducted with two-to-three biological replicates. Data are presented as the mean ± standard error of the mean unless otherwise indicated. Ordinary one-way ANOVA analyses were conducted with Dunnett's multiple comparisons test. All data and statistical analyses were conducted using GraphPad Prism 8 data analysis software.

Appendix A Abbreviations glossary

BrU	5-bromouridine
A3E	Alkaloid cyclopamine analog
BSDV	Black rice-streaked dwarf virus
EM	Electron microscopy
EMSA	Electrophoretic mobility shift assay
ER	Endoplasmic reticulum
eIF3A	Eukaryotic translation initiation factor 3 subunit A
FRAP	Fluorescence recovery after photobleaching
GAPDH	Glyceraldehyde 3-phosphate dehydrogenase
hsp70	Heat shock protein 70
ISVP	Infectious subvirion particle
IRF3	Interferon regulatory factor 3
IDR	Intrinsically disordered regions
JAM-A	Junctional adhesion molecule A
LLPS	Liquid-liquid phase separation
MeV	Measles virus
MDA5	Melanoma differentiation-associated protein 5
NgR1	Nogo receptor 1
PAMP	Pathogen-associated molecular patterns
pRPS6	Phosphorylated ribosomal protein S6

PAGE	Polyacrylamide gel electrophoresis
PLA	Proximity-ligation assay
G3BP1	Ras-GAP SH3 domain binding protein 1
RSV	Respiratory syncytial virus
RIG-I	Retinoic acid-inducible gene 1
RdRp	RNA-dependent-RNA polymerase
SeMet	Seleno-methionine
SAD	Single-wavelength anomalous diffraction
SG	Stress granule
TDP-43	Transactive response DNA-binding protein-43
T1L	Type 1 Lang
T2J	Type 2 Jones
T3D	Type 3 Dearing
UTR	Untranslated region
XFFL	X-ray free-electron lasers

Bibliography

1. Lee CH, Raghunathan K, Taylor GM, French AJ, Tenorio R, Fernández de Castro I, Risco C, Parker JSL, Dermody TS. 2021. Reovirus Nonstructural Protein σNS Recruits Viral RNA to Replication Organelles. mBio 12:e0140821.

2. Knipe DM, Howley PM. 2013. Fields virology, 6th ed. Wolters Kluwer/Lippincott Williams & Wilkins Health, Philadelphia, PA.

3. Sabin AB. 1959. Reoviruses: a new group of respiratory and enteric viruses formerly classified as ECHO type 10 is described. Science 130:1387-1389.

4. Ramos-Alvarez M, Sabin AB. 1954. Characteristics of poliomyelitis and other enteric viruses recovered in tissue culture from healthy American children. Proc Soc Exp Biol Med 87:655-61.

5. Bouziat R, Hinterleitner R, Brown JJ, Stencel-Baerenwald JE, Ikizler M, Mayassi T, Meisel M, Kim SM, Discepolo V, Pruijssers AJ, Ernest JD, Iskarpatyoti JA, Costes LM, Lawrence I, Palanski BA, Varma M, Zurenski MA, Khomandiak S, McAllister N, Aravamudhan P, Boehme KW, Hu F, Samsom JN, Reinecker HC, Kupfer SS, Guandalini S, Semrad CE, Abadie V, Khosla C, Barreiro LB, Xavier RJ, Ng A, Dermody TS, Jabri B. 2017. Reovirus infection triggers inflammatory responses to dietary antigens and development of celiac disease. Science 356:44-50.

6. Mata CP, Luque D, Gómez-Blanco J, Rodríguez JM, González JM, Suzuki N, Ghabrial SA, Carrascosa JL, Trus BL, Castón JR. 2017. Acquisition of functions on the outer capsid surface during evolution of double-stranded RNA fungal viruses. PLOS Pathogens 13:e1006755.

7. Fiore L, Greenberg HB, Mackow ER. 1991. The Vp8 Fragment of Vp4 Is the Rhesus Rotavirus Hemagglutinin. Virology 181:553-563.

8. Chandran K, Zhang X, Olson NH, Walker SB, Chappell JD, Dermody TS, Baker TS, Nibert ML. 2001. Complete in vitro assembly of the reovirus outer capsid produces highly infectious particles suitable for genetic studies of the receptor-binding protein. J Virol 75:5335-42.

9. Attoui H, Mohd Jaafar F, Belhouchet M, Biagini P, Cantaloube JF, de Micco P, de Lamballerie X. 2005. Expansion of family Reoviridae to include nine-segmented dsRNA viruses: isolation and characterization of a new virus designated Aedes pseudoscutellaris reovirus assigned to a proposed genus (Dinovernavirus). Virology 343:212-23.

10. Bellamy AR, Shapiro L, August JT, Joklik WK. 1967. Studies on reovirus RNA. Journal of Molecular Biology 29:1-17.

11. Attoui H, Fang Q, Mohd Jaafar F, Cantaloube JF, Biagini P, de Micco P, de Lamballerie X. 2002. Common evolutionary origin of aquareoviruses and orthoreoviruses revealed by genome characterization of Golden shiner reovirus, Grass carp reovirus, Striped bass reovirus and golden ide reovirus (genus Aquareovirus, family Reoviridae). J Gen Virol 83:1941-51.

12. Attoui H, Charrel RN, Billoir F, Cantaloube JF, de Micco P, de Lamballerie X. 1998. Comparative sequence analysis of American, European and Asian isolates of viruses in the genus Coltivirus. J Gen Virol 79 (Pt 10):2481-9.

13. Attoui H, Mertens PPC, Becnel J, Belaganahalli S, Bergoin M, Brussaard CP, Chappell JD, Ciarlet M, del Vas M, Dermody TS, Dormitzer PR, Duncan R, Fang Q, Graham R, Guglielmi KM, Harding RM, Hillman B, Makkay A, Marzachì C, Matthijnssens J, Milne RG, Mohd Jaafar F, Mori H, Noordeloos AA, Omura T, Patton JT, Rao S, Maan M, Stoltz D, Suzuki N, Upadhyaya NM, Wei C, Zhou H. 2012. Reoviridae, p 541-637. *In* King AMQ, Adams MJ, Carstens EB, Lefkowitz EJ (ed), Virus Taxonomy: Classification and Nomenclature of Viruses Ninth Report of the International Committee on Taxonomy of Viruses. Elsevier/Academic Press, London.

14. Joklik WK, Roner MR. 1995. What Reassorts When Reovirus Genome Segments Reassort. Journal of Biological Chemistry 270:4181-4184.

15. Borodavka A, Ault J, Stockley PG, Tuma R. 2015. Evidence that avian reovirus sigmaNS is an RNA chaperone: Implications for genome segment assortment. Nucleic Acids Res 43:7044-57.

16. Diprose JM, Grimes JM, Sutton GC, Burroughs JN, Meyer A, Maan S, Mertens PP, Stuart DI. 2002. The core of bluetongue virus binds double-stranded RNA. J Virol 76:9533-6.

17. Rodriguez KR, Bruns AM, Horvath CM. 2014. MDA5 and LGP2: accomplices and antagonists of antiviral signal transduction. J Virol 88:8194-200.

18. Starnes MC, Joklik WK. 1993. Reovirus protein l3 is a poly(C)-dependent poly(G) polymerase. Virology 193:356-366.

19. Cohen J. 1977. Ribonucleic acid polymerase activity associated with purified calf rotavirus. J Gen Virol 36:395-402.

20. Tao Y, Farsetta DL, Nibert ML, Harrison SC. 2002. RNA synthesis in a cage--structural studies of reovirus polymerase lambda3. Cell 111:733-45.

21. Dryden KA, Wang G, Yeager M, Nibert ML, Coombs KM, Furlong DB, Fields BN, Baker TS. 1993. Early steps in reovirus infection are associated with dramatic changes in supramolecular structure and protein conformation: analysis of virions and subviral particles by cryoelectron microscopy and image reconstruction. J Cell Biol 122:1023-41.

22. Chandran K, Walker SB, Chen Y, Contreras CM, Schiff LA, Baker TS, Nibert ML. 1999. In vitro recoating of reovirus cores with baculovirus-expressed outer-capsid proteins m1 and s3. Journal of Virology 73:3941-3950.

23. Shatkin AJ, LaFiandra AJ. 1972. Transcription by infectious subviral particles of reovirus. J Virol 10:698-706.

24. Moore MJ, Proudfoot NJ. 2009. Pre-mRNA processing reaches back to transcription and ahead to translation. Cell 136:688-700.

25. Decroly E, Ferron F, Lescar J, Canard B. 2011. Conventional and unconventional mechanisms for capping viral mRNA. Nat Rev Microbiol 10:51-65.

26. McDonald SM, Patton JT. 2011. Assortment and packaging of the segmented rotavirus genome. Trends Microbiol 19:136-44.

27. Neeleman L, Olsthoorn RC, Linthorst HJ, Bol JF. 2001. Translation of a nonpolyadenylated viral RNA is enhanced by binding of viral coat protein or polyadenylation of the RNA. Proc Natl Acad Sci U S A 98:14286-91.

28. Fernández de Castro I, Tenorio R, Risco C. 2020. Virus factories, Reference Module in Life Sciences doi:https://doi.org/10.1016/B978-0-12-814515-9.00001-1. Elsevier.

29. Broering TJ, Kim J, Miller CL, Piggott CD, Dinoso JB, Nibert ML, Parker JS. 2004. Reovirus nonstructural protein mNS recruits viral core surface proteins and entering core particles to factory-like inclusions. Journal of Virology 78:1882-1892.

30. Fabbretti E, Afrikanova I, Vascotto F, Burrone OR. 1999. Two non-structural rotavirus proteins, NSP2 and NSP5, form viroplasm-like structures in vivo. J Gen Virol 80 (Pt 2):333-9.

31. Netherton CL, Wileman T. 2011. Virus factories, double membrane vesicles and viroplasm generated in animal cells. Curr Opin Virol 1:381-7.

32. Zhang Z, He G, Filipowicz NA, Randall G, Belov GA, Kopek BG, Wang X. 2019. Host Lipids in Positive-Strand RNA Virus Genome Replication. Front Microbiol 10:286.

33. Schwartz M, Chen J, Janda M, Sullivan M, den Boon J, Ahlquist P. 2002. A positive-strand RNA virus replication complex parallels form and function of retrovirus capsids. Mol Cell 9:505-14.

34. Nevers Q, Albertini AA, Lagaudrière-Gesbert C, Gaudin Y. 2020. Negri bodies and other virus membrane-less replication compartments. Biochim Biophys Acta Mol Cell Res 1867:118831.

35. Shah PNM, Stanifer ML, Hohn K, Engel U, Haselmann U, Bartenschlager R, Krausslich HG, Krijnse-Locker J, Boulant S. 2017. Genome packaging of reovirus is mediated by the scaffolding property of the microtubule network. Cell Microbiol 19.

36. Xu P, Miller SE, Joklik WK. 1993. Generation of reovirus core-like particles in cells infected with hybrid vaccinia viruses that express genome segments L1, L2, L3, and S2. Virology 197:726-731.

37. Shin Y, Brangwynne CP. 2017. Liquid phase condensation in cell physiology and disease. Science 357.

38. Feng Z, Chen X, Wu X, Zhang M. 2019. Formation of biological condensates via phase separation: Characteristics, analytical methods, and physiological implications. J Biol Chem 294:14823-14835.

39. Banani SF, Rice AM, Peeples WB, Lin Y, Jain S, Parker R, Rosen MK. 2016. Compositional Control of Phase-Separated Cellular Bodies. Cell 166:651-663.

40. van der Lee R, Buljan M, Lang B, Weatheritt RJ, Daughdrill GW, Dunker AK, Fuxreiter M, Gough J, Gsponer J, Jones DT, Kim PM, Kriwacki RW, Oldfield CJ, Pappu RV, Tompa P, Uversky VN, Wright PE, Babu MM. 2014. Classification of intrinsically disordered regions and proteins. Chem Rev 114:6589-631.

41. Ditlev JA, Case LB, Rosen MK. 2018. Who's In and Who's Out-Compositional Control of Biomolecular Condensates. J Mol Biol 430:4666-4684.

42. Alberti S. 2017. Phase separation in biology. Curr Biol 27:R1097-r1102.

43. Alberti S, Gladfelter A, Mittag T. 2019. Considerations and Challenges in Studying Liquid-Liquid Phase Separation and Biomolecular Condensates. Cell 176:419-434.

44. Wheeler JR, Matheny T, Jain S, Abrisch R, Parker R. 2016. Distinct stages in stress granule assembly and disassembly. Elife 5.

45. Babinchak WM, Haider R, Dumm BK, Sarkar P, Surewicz K, Choi JK, Surewicz WK. 2019. The role of liquid-liquid phase separation in aggregation of the TDP-43 low-complexity domain. J Biol Chem 294:6306-6317.

46. Lafontaine DLJ, Riback JA, Bascetin R, Brangwynne CP. 2021. The nucleolus as a multiphase liquid condensate. Nat Rev Mol Cell Biol 22:165-182.

47. Hnisz D, Shrinivas K, Young RA, Chakraborty AK, Sharp PA. 2017. A Phase Separation Model for Transcriptional Control. Cell 169:13-23.

48. Galloux M, Risso-Ballester J, Richard CA, Fix J, Rameix-Welti MA, Eléouët JF. 2020. Minimal elements required for the formation of respiratory syncytial virus cytoplasmic inclusion bodies in vivo and in vitro. mBio 11.

49. Zhou Y, Su JM, Samuel CE, Ma D. 2019. Measles Virus Forms Inclusion Bodies with Properties of Liquid Organelles. J Virol 93.

50. Guseva S, Milles S, Jensen MR, Salvi N, Kleman JP, Maurin D, Ruigrok RWH, Blackledge M. 2020. Measles virus nucleo- and phosphoproteins form liquid-like phase-separated compartments that promote nucleocapsid assembly. Sci Adv 6:eaaz7095.

51. Jobe F, Simpson J, Hawes P, Guzman E, Bailey D. 2020. Respiratory Syncytial Virus Sequesters NF-κB Subunit p65 to Cytoplasmic Inclusion Bodies To Inhibit Innate Immune Signaling. J Virol 94.

52. Risso-Ballester J, Galloux M, Cao J, Le Goffic R, Hontonnou F, Jobart-Malfait A, Desquesnes A, Sake SM, Haid S, Du M, Zhang X, Zhang H, Wang Z, Rincheval V, Zhang Y, Pietschmann T, Eléouët JF, Rameix-Welti MA, Altmeyer R. 2021. A condensate-hardening drug blocks RSV replication in vivo. Nature 595:596-599.

53. Dolgin E. 2021. Drug startups coalesce around condensates. Nature Biotechnology 39:123-125.

54. Eichwald C, Ackermann M, Nibert ML. 2018. The dynamics of both filamentous and globular mammalian reovirus viral factories rely on the microtubule network. Virology 518:77-86.

55. Geiger F, Papa G, Arter WE, Acker J, Saar KL, Erkamp N, Qi R, Bravo J, Strauss S, Krainer G, Burrone OR, Jungmann R, Knowles TPJ, Engelke H, Borodavka A.

2020. Rotavirus Replication Factories Are Complex Ribonucleoprotein Condensates. bioRxiv doi:10.1101/2020.12.18.423429:2020.12.18.423429.

56. Superti F, Amici C, Tinari A, Donelli G, Santoro MG. 1998. Inhibition of rotavirus replication by prostaglandin A: evidence for a block of virus maturation. J Infect Dis 178:564-8.

57. Phillips MB, Stuart JD, Rodríguez Stewart RM, Berry JT, Mainou BA, Boehme KW. 2018. Current understanding of reovirus oncolysis mechanisms. Oncolytic Virother 7:53-63.

58. Rosen L. 1960. Serologic grouping of reovirus by hemagglutination-inhibition. American Journal of Hygiene 71:242-249.

59. Komoto S, Kawagishi T, Kobayashi T, Ikizler M, Iskarpatyoti J, Dermody TS, Taniguchi K. 2014. A plasmid-based reverse genetics system for mammalian orthoreoviruses driven by a plasmid-encoded T7 RNA polymerase. J Virol Methods 196:36-9.

60. Dermody TS, Parker JS, Sherry B. 2013. Orthoreoviruses, p 1304-1346. *In* Knipe DM, Howley PM (ed), Fields Virology, 6th ed, vol 2. Lippincott Williams & Wilkins, Philadelphia.

61. Roth AN, Aravamudhan P, Fernández de Castro I, Tenorio R, Risco C, Dermody TS. 2021. Ins and Outs of Reovirus: Vesicular Trafficking in Viral Entry and Egress. Trends Microbiol 29:363-375.

62. Aravamudhan P, Raghunathan K, Konopka-Anstadt J, Pathak A, Sutherland DM, Carter BD, Dermody TS. 2020. Reovirus uses macropinocytosis-mediated entry and fast axonal transport to infect neurons. PLoS Pathog 16:e1008380.

63. Ivanovic T, Agosto MA, Zhang L, Chandran K, Harrison SC, Nibert ML. 2008. Peptides released from reovirus outer capsid form membrane pores that recruit virus particles. EMBO J 27:1289-98.

64. Danthi P, Guglielmi KM, Kirchner E, Mainou B, Stehle T, Dermody TS. 2010. From touchdown to transcription: the reovirus cell entry pathway. Curr Top Microbiol Immunol 343:91-119.

65. Lemay G. 1988. Transcriptional and translational events during reovirus infection. Biochem Cell Biol 66:803-12.

66. Bussiere LD, Choudhury P, Bellaire B, Miller CL. 2017. Characterization of a replicating mammalian orthoreovirus with tetracysteine-tagged muNS for live-cell visualization of viral factories. J Virol 91.

67. Becker MM, Peters TR, Dermody TS. 2003. Reovirus sigma NS and mu NS proteins form cytoplasmic inclusion structures in the absence of viral infection. J Virol 77:5948-63.

68. Desmet EA, Anguish LJ, Parker JS. 2014. Virus-mediated compartmentalization of the host translational machinery. MBio 5:e01463-14.

69. Fernandez de Castro I, Zamora PF, Ooms L, Fernandez JJ, Lai CM, Mainou BA, Dermody TS, Risco C. 2014. Reovirus forms neo-organelles for progeny particle assembly within reorganized cell membranes. MBio 5:e00931-13.

70. Tenorio R, Fernández de Castro I, Knowlton JJ, Zamora PF, Lee CH, Mainou BA, Dermody TS, Risco C. 2018. Reovirus σNS and μNS proteins remodel the endoplasmic reticulum to build replication neoorganelles. MBio 9:e01253-18.

71. Acs G, Klett H, Schonberg M, Christman J, Levin DH, Silverstein JC. 1971. Mechanism of reovirus double-stranded RNA synthesis in vivo and in vitro. Journal of Virology 8:684-689.

72. Murray KE, Nibert ML. 2007. Guanidine hydrochloride inhibits mammalian orthoreovirus growth by reversibly blocking the synthesis of double-stranded RNA. J Virol 81:4572-84.

73. Broering TJ, Parker JS, Joyce PL, Kim J, Nibert ML. 2002. Mammalian reovirus nonstructural protein μNS forms large inclusions and colocalizes with reovirus microtubule-associated protein μ2 in transfected cells. J Virol 76:8285-97.

74. Mudogo CN, Falke S, Brognaro H, Duszenko M, Betzel C. 2020. Protein phase separation and determinants of in cell crystallization. Traffic 21:220-230.

75. Munder MC, Midtvedt D, Franzmann T, Nüske E, Otto O, Herbig M, Ulbricht E, Müller P, Taubenberger A, Maharana S, Malinovska L, Richter D, Guck J, Zaburdaev V, Alberti S. 2016. A pH-driven transition of the cytoplasm from a fluid- to a solid-like state promotes entry into dormancy. Elife 5.

76. Parry BR, Surovtsev IV, Cabeen MT, O'Hern CS, Dufresne ER, Jacobs-Wagner C. 2014. The bacterial cytoplasm has glass-like properties and is fluidized by metabolic activity. Cell 156:183-94.

77. Miller CL, Arnold MM, Broering TJ, Hastings CE, Nibert ML. 2010. Localization of mammalian orthoreovirus proteins to cytoplasmic factory-like structures via nonoverlapping regions of μNS. J Virol 84:867-82.

78. Nagaratnam N, Tang Y, Botha S, Saul J, Li C, Hu H, Zaare S, Hunter M, Lowry D, Weierstall U, Zatsepin N, Spence JCH, Qiu J, LaBaer J, Fromme P, Martin-Garcia JM. 2020. Enhanced X-ray diffraction of in vivo-grown μNS crystals by viscous jets at XFELs. Acta Crystallogr F Struct Biol Commun 76:278-289.

79. McCutcheon AM, Broering TJ, Nibert ML. 1999. Mammalian reovirus M3 gene sequences and conservation of coiled-coil motifs near the carboxyle terminus of the mNS protein. Virology 264:16-24.

80. Arnold MM, Murray KE, Nibert ML. 2008. Formation of the factory matrix is an important, though not a sufficient function of nonstructural protein mu NS during reovirus infection. Virology 375:412-23.

81. Newton JC, Naik MT, Li GY, Murphy EL, Fawzi NL, Sedivy JM, Jogl G. 2021. Phase separation of the LINE-1 ORF1 protein is mediated by the N-terminus and coiled-coil domain. Biophys J 120:2181-2191.

82. Utterström J, Naeimipour S, Selegård R, Aili D. 2021. Coiled coil-based therapeutics and drug delivery systems. Adv Drug Deliv Rev 170:26-43.

83. Carl PL, Fried HM, Cohen PL. 2020. Proteins in assemblages formed by phase separation possess properties that promote their transformation to autoantigens: Implications for autoimmunity. J Autoimmun 111:102471.

84. Antczak JB, Joklik WK. 1992. Reovirus genome segment assortment into progeny genomes studied by the use of monoclonal-antibodies directed against reovirus proteins. Virology 187:760-776.

85. Stanifer ML, Kischnick C, Rippert A, Albrecht D, Boulant S. 2017. Reovirus inhibits interferon production by sequestering IRF3 into viral factories. Sci Rep 7:10873.

86. Kaufer S, Coffey CM, Parker JS. 2012. The cellular chaperone hsc70 is specifically recruited to reovirus viral factories independently of its chaperone function. J Virol 86:1079-89.

87. McCrae MA, Joklik WK. 1978. The nature of the polypeptide encoded by each of the ten double-stranded RNA segments of reovirus type 3. Virology 89:578-593.

88. Miller CL, Broering TJ, Parker JS, Arnold MM, Nibert ML. 2003. Reovirus sigma NS protein localizes to inclusions through an association requiring the mu NS amino terminus. J Virol 77:4566-76.

89. Zamora PF, Hu L, Knowlton JJ, Lahr RM, Moreno RA, Berman AJ, Prasad BVV, Dermody TS. 2018. Reovirus nonstructural protein SigmaNS acts as an RNA-stability factor promoting viral genome replication. J Virol 92:e00563-18.

90. Gomatos PJ, Stamatos NM, Sarkar NH. 1980. Small reovirus-specific particle with polycytidylate-dependent RNA polymerase activity. J Virol 36:556-65.

91. Matsuki H, Takahashi M, Higuchi M, Makokha GN, Oie M, Fujii M. 2013. Both G3BP1 and G3BP2 contribute to stress granule formation. Genes Cells 18:135-46.

92. Choudhury P, Bussiere L, Miller CL. 2017. Mammalian orthoreovirus factories modulate stress granule protein localization by interaction with G3BP1. J Virol doi:10.1128/JVI.01298-17.

93. Huismans H, Joklik WK. 1976. Reovirus-coded polypeptides in infected cells: isolation of two native monomeric polypeptides with high affinity for single-stranded and double-stranded RNA, respectively. Virology 70:411-424.

94. Gillian AL, Schmechel SC, Livny J, Schiff LA, Nibert ML. 2000. Reovirus protein sigmaNS binds in multiple copies to single-stranded RNA and shares properties with single-stranded DNA binding proteins. J Virol 74:5939-48.

95. Stamatos NM, Gomatos PJ. 1982. Binding to selected regions of reovirus mRNAs by a nonstructural reovirus protein. Proc Natl Acad Sci U S A 79:3457-61.

96. Gillian AL, Nibert ML. 1998. Amino terminus of reovirus nonstructural protein sNS is important for ssRNA binding and nucleoprotein complex formation. Virology 240:1-11.

97. Richardson MA, Furuichi Y. 1985. Synthesis in Escherichia coli of the reovirus nonstructural protein sigma NS. J Virol 56:527-33.

98. Goral MI, MochowGrundy M, Dermody TS. 1996. Sequence diversity within the reovirus S3 gene: Reoviruses evolve independently of host species, geographic locale, and date of isolation. Virology 216:265-271.

99. Corley M, Burns MC, Yeo GW. 2020. How RNA-binding proteins interact with RNA: molecules and mechanisms. Mol Cell 78:9-29.

100. Becker MM, Goral MI, Hazelton PR, Baer GS, Rodgers SE, Brown EG, Coombs KM, Dermody TS. 2001. Reovirus sigmaNS protein is required for nucleation of viral assembly complexes and formation of viral inclusions. J Virol 75:1459-75.

101. Parker JS, Broering TJ, Kim J, Higgins DE, Nibert ML. 2002. Reovirus core protein mu2 determines the filamentous morphology of viral inclusion bodies by interacting with and stabilizing microtubules. J Virol 76:4483-96.

102. Touris-Otero F, Martinez-Costas J, Vakharia VN, Benavente J. 2005. Characterization of the nucleic acid-binding activity of the avian reovirus non-structural protein sigma NS. J Gen Virol 86:1159-69.

103. Borodavka A, Desselberger U, Patton JT. 2018. Genome packaging in multi-segmented dsRNA viruses: distinct mechanisms with similar outcomes. Curr Opin Virol 33:106-112.

104. Bravo JPK, Bartnik K, Venditti L, Gail EH, Davidovich C, Lamb DC, Tuma R, Calabrese AN, Borodavka A. 2020. Structural basis of rotavirus RNA chaperone displacement and RNA annealing. bioRxiv doi:10.1101/2020.10.26.354233:2020.10.26.354233.

105. Lovci MT, Bengtson MH, Massirer KB. 2016. Post-translational modifications and RNA-binding proteins. Adv Exp Med Biol 907:297-317.

106. Jankowsky E, Harris ME. 2015. Specificity and nonspecificity in RNA-protein interactions. Nat Rev Mol Cell Biol 16:533-44.

107. Garcia-Jove Navarro M, Kashida S, Chouaib R, Souquere S, Pierron G, Weil D, Gueroui Z. 2019. RNA is a critical element for the sizing and the composition of phase-separated RNA-protein condensates. Nat Commun 10:3230.

108. Tenorio R, Fernández de Castro I, Knowlton JJ, Zamora PF, Sutherland DM, Risco C, Dermody TS. 2019. Function, Architecture, and Biogenesis of Reovirus Replication Neoorganelles. Viruses 11.

109. Stork J, Kovalev N, Sasvari Z, Nagy PD. 2011. RNA chaperone activity of the tombusviral p33 replication protein facilitates initiation of RNA synthesis by the viral RdRp in vitro. Virology 409:338-47.

110. Arnoldi F, Campagna M, Eichwald C, Desselberger U, Burrone OR. 2007. Interaction of rotavirus polymerase VP1 with nonstructural protein NSP5 is stronger than that with NSP2. J Virol 81:2128-37.

111. Mir MA, Panganiban AT. 2006. The bunyavirus nucleocapsid protein is an RNA chaperone: possible roles in viral RNA panhandle formation and genome replication. Rna 12:272-82.

112. Mir MA, Panganiban AT. 2006. Characterization of the RNA chaperone activity of hantavirus nucleocapsid protein. J Virol 80:6276-85.

113. Ruigrok RW, Crépin T. 2010. Nucleoproteins of negative strand RNA viruses; RNA binding, oligomerisation and binding to polymerase co-factor. Viruses 2:27-32.

114. Smith RE, Zweerink HJ, Joklik WK. 1969. Polypeptide components of virions, top component and cores of reovirus type 3. Virology 39:791-810.

115. Fernández de Castro I, Tenorio R, Risco C. 2016. Virus assembly factories in a lipid world. Curr Opin Virol 18:20-6.

116. Qin Q, Hastings C, Miller CL. 2009. Mammalian orthoreovirus particles induce and are recruited into stress granules at early times postinfection. J Virol 83:11090-101.

117. Smith JA, Schmechel SC, Raghavan A, Abelson M, Reilly C, Katze MG, Kaufman RJ, Bohjanen PR, Schiff LA. 2006. Reovirus induces and benefits from an integrated cellular stress response. J Virol 80:2019-33.

118. Lutz MMt, Worth MP, Hinchman MM, Parker JSL, Ledgerwood ED. 2019. Mammalian orthoreovirus infection is enhanced in cells pre-treated with sodium arsenite. Viruses 11.

119. Boeynaems S, Alberti S, Fawzi NL, Mittag T, Polymenidou M, Rousseau F, Schymkowitz J, Shorter J, Wolozin B, Van Den Bosch L, Tompa P, Fuxreiter M. 2018. Protein phase separation: a new phase in cell biology. Trends Cell Biol 28:420-435.

120. Nakashima KK, Vibhute MA, Spruijt E. 2019. Biomolecular chemistry in liquid phase separated compartments. Front Mol Biosci 6:21.

121. Nikolic J, Le Bars R, Lama Z, Scrima N, Lagaudrière-Gesbert C, Gaudin Y, Blondel D. 2017. Negri bodies are viral factories with properties of liquid organelles. Nat Commun 8:58.

122. Heinrich BS, Maliga Z, Stein DA, Hyman AA, Whelan SPJ. 2018. Phase transitions drive the formation of vesicular stomatitis virus replication compartments. mBio 9.

123. Fay MM, Anderson PJ. 2018. The role of RNA in biological phase separations. J Mol Biol 430:4685-4701.

124. Bracha D, Walls MT, Wei MT, Zhu L, Kurian M, Avalos JL, Toettcher JE, Brangwynne CP. 2018. Mapping local and global liquid phase behavior in living cells using photo-oligomerizable seeds. Cell 175:1467-1480.e13.

125. Li P, Banjade S, Cheng HC, Kim S, Chen B, Guo L, Llaguno M, Hollingsworth JV, King DS, Banani SF, Russo PS, Jiang QX, Nixon BT, Rosen MK. 2012. Phase transitions in the assembly of multivalent signalling proteins. Nature 483:336-40.

126. Hu L, Chow DC, Patton JT, Palzkill T, Estes MK, Prasad BV. 2012. Crystallographic Analysis of Rotavirus NSP2-RNA Complex Reveals Specific Recognition of 5' GG Sequence for RTPase Activity. J Virol 86:10547-57.

127. Rodrigues CHM, Myung Y, Pires DEV, Ascher DB. 2019. mCSM-PPI2: predicting the effects of mutations on protein-protein interactions. Nucleic Acids Res 47:W338-w344.

128. Moras D, Dock AC, Dumas P, Westhof E, Romby P, Ebel JP, Giegé R. 1986. Anticodon-anticodon interaction induces conformational changes in tRNA: yeast tRNAAsp, a model for tRNA-mRNA recognition. Proc Natl Acad Sci U S A 83:932-6.

129. Pace CN, Scholtz JM. 1998. A helix propensity scale based on experimental studies of peptides and proteins. Biophys J 75:422-7.

130. Wu J, Li J, Mao X, Wang W, Cheng Z, Zhou Y, Zhou X, Tao X. 2013. Viroplasm protein P9-1 of Rice black-streaked dwarf virus preferentially binds to single-stranded RNA in its octamer form, and the central interior structure formed by this octamer constitutes the major RNA binding site. J Virol 87:12885-99.

131. Akita F, Higashiura A, Shimizu T, Pu Y, Suzuki M, Uehara-Ichiki T, Sasaya T, Kanamaru S, Arisaka F, Tsukihara T, Nakagawa A, Omura T. 2012. Crystallographic analysis reveals octamerization of viroplasm matrix protein P9-1 of Rice black streaked dwarf virus. J Virol 86:746-56.

132. Wang Q, Tao T, Zhang Y, Wu W, Li D, Yu J, Han C. 2011. Rice black-streaked dwarf virus P6 self-interacts to form punctate, viroplasm-like structures in the cytoplasm and recruits viroplasm-associated protein P9-1. Virology Journal 8:24.

133. Arranz R, Coloma R, Chichón FJ, Conesa JJ, Carrascosa JL, Valpuesta JM, Ortín J, Martín-Benito J. 2012. The Structure of Native Influenza Virion Ribonucleoproteins. Science 338:1634-1637.

134. Arragain B, Reguera J, Desfosses A, Gutsche I, Schoehn G, Malet H. 2019. High resolution cryo-EM structure of the helical RNA-bound Hantaan virus nucleocapsid reveals its assembly mechanisms. eLife 8:e43075.

135. Turrell L, Lyall JW, Tiley LS, Fodor E, Vreede FT. 2013. The role and assembly mechanism of nucleoprotein in influenza A virus ribonucleoprotein complexes. Nat Commun 4:1591.

136. Lee N, Le Sage V, Nanni AV, Snyder DJ, Cooper VS, Lakdawala SS. 2017. Genome-wide analysis of influenza viral RNA and nucleoprotein association. Nucleic Acids Research 45:8968-8977.

137. Peisley A, Jo MH, Lin C, Wu B, Orme-Johnson M, Walz T, Hohng S, Hur S. 2012. Kinetic mechanism for viral dsRNA length discrimination by MDA5 filaments. Proceedings of the National Academy of Sciences of the United States of America 109:E3340-E3349.

138. Peisley A, Lin C, Wu B, Orme-Johnson M, Liu M, Walz T, Hur S. 2011. Cooperative assembly and dynamic disassembly of MDA5 filaments for viral dsRNA recognition. Proceedings of the National Academy of Sciences 108:21010-21015.

139. Kobayashi T, Chappell JD, Danthi P, Dermody TS. 2006. Gene-specific inhibition of reovirus replication by RNA interference. J Virol 80:9053-63.

140. Modrof J, Lymperopoulos K, Roy P. 2005. Phosphorylation of bluetongue virus nonstructural protein 2 is essential for formation of viral inclusion bodies. J Virol 79:10023-31.

141. Viskovska M, Anish R, Hu L, Chow DC, Hurwitz AM, Brown NG, Palzkill T, Estes MK, Prasad BV. 2014. Probing the sites of interactions of rotaviral proteins involved in replication. J Virol 88:12866-81.

142. Samacoits A, Chouaib R, Safieddine A, Traboulsi AM, Ouyang W, Zimmer C, Peter M, Bertrand E, Walter T, Mueller F. 2018. A computational framework to study sub-cellular RNA localization. Nat Commun 9:4584.

143. Chin A, Lécuyer E. 2017. RNA localization: Making its way to the center stage. Biochim Biophys Acta Gen Subj 1861:2956-2970.

144. Luby-Phelps K, Castle PE, Taylor DL, Lanni F. 1987. Hindered diffusion of inert tracer particles in the cytoplasm of mouse 3T3 cells. Proc Natl Acad Sci U S A 84:4910-3.

145. Bertrand E, Chartrand P, Schaefer M, Shenoy SM, Singer RH, Long RM. 1998. Localization of ASH1 mRNA particles in living yeast. Mol Cell 2:437-45.

146. Fusco D, Accornero N, Lavoie B, Shenoy SM, Blanchard JM, Singer RH, Bertrand E. 2003. Single mRNA molecules demonstrate probabilistic movement in living mammalian cells. Curr Biol 13:161-167.

147. Stewart MJ, Smoak K, Blum MA, Sherry B. 2005. Basal and reovirus-induced beta interferon (IFN-b) and IFN-b-stimulated gene expression are cell type specific in the cardiac protective response. Journal of Virology 79:2979-2987.

148. Jiang J, Coombs KM. 2005. Infectious entry of reovirus cores into mammalian cells enhanced by transfection. J Virol Methods 128:88-92.

149. Schwarz MK, Scherbarth A, Sprengel R, Engelhardt J, Theer P, Giese G. 2015. Fluorescent-protein stabilization and high-resolution imaging of cleared, intact mouse brains. PLoS One 10:e0124650.

150. Xie F, Timme KA, Wood JR. 2018. Using Single Molecule mRNA Fluorescent in Situ Hybridization (RNA-FISH) to Quantify mRNAs in Individual Murine Oocytes and Embryos. Sci Rep 8:7930.

151. Matheny T, Rao BS, Parker R. 2019. Transcriptome-Wide Comparison of Stress Granules and P-Bodies Reveals that Translation Plays a Major Role in RNA Partitioning. Mol Cell Biol 39.

152. Colell A, Green DR, Ricci JE. 2009. Novel roles for GAPDH in cell death and carcinogenesis. Cell Death Differ 16:1573-81.

153. Cochard A, Navarro MG-J, Kashida S, Kress M, Weil D, Gueroui Z. 2021. RNA at the surface of phase-separated condensates impacts their size and number. bioRxiv doi:10.1101/2021.06.22.449254:2021.06.22.449254.

154. Wang X, Le N, Denoth-Lippuner A, Barral Y, Kroschewski R. 2016. Asymmetric partitioning of transfected DNA during mammalian cell division. Proc Natl Acad Sci U S A 113:7177-82.

155. Moore MJ, Zhang C, Gantman EC, Mele A, Darnell JC, Darnell RB. 2014. Mapping Argonaute and conventional RNA-binding protein interactions with RNA at single-nucleotide resolution using HITS-CLIP and CIMS analysis. Nat Protoc 9:263-93.

156. Bravo JPK, Borodavka A, Barth A, Calabrese AN, Mojzes P, Cockburn JJB, Lamb DC, Tuma R. 2018. Stability of local secondary structure determines selectivity of viral RNA chaperones. Nucleic Acids Res 46:7924-7937.

157. Mondal A, Potts GK, Dawson AR, Coon JJ, Mehle A. 2015. Phosphorylation at the Homotypic Interface Regulates Nucleoprotein Oligomerization and Assembly of the Influenza Virus Replication Machinery. PLOS Pathogens 11:e1004826.

158. Fu X, Ning J, Zhong Z, Ambrose Z, Charles Watkins S, Zhang P. 2019. AutoCLEM: An Automated Workflow for Correlative Live-Cell Fluorescence Microscopy and Cryo-Electron Tomography. Scientific Reports 9:19207.

159. Cheng E, Wang Z, Mir MA. 2014. Interaction between hantavirus nucleocapsid protein (N) and RNA-dependent RNA polymerase (RdRp) mutants reveals the requirement of an N-RdRp interaction for viral RNA synthesis. J Virol 88:8706-12.

160. Rajendran KS, Nagy PD. 2006. Kinetics and functional studies on interaction between the replicase proteins of Tomato Bushy Stunt Virus: requirement of p33:p92 interaction for replicase assembly. Virology 345:270-9.

161. Shaffer SM, Wu MT, Levesque MJ, Raj A. 2013. Turbo FISH: a method for rapid single molecule RNA FISH. PLoS One 8:e75120.

162. Guo L, Smith JA, Abelson M, Vlasova-St Louis I, Schiff LA, Bohjanen PR. 2018. Reovirus infection induces stabilization and up-regulation of cellular transcripts that encode regulators of TGF-β signaling. PLoS One 13:e0204622.

163. Khong A, Matheny T, Jain S, Mitchell SF, Wheeler JR, Parker R. 2017. The Stress Granule Transcriptome Reveals Principles of mRNA Accumulation in Stress Granules. Mol Cell 68:808-820.e5.

164. Silvestri LS, Taraporewala ZF, Patton JT. 2004. Rotavirus replication: plus-sense templates for double-stranded RNA synthesis are made in viroplasms. J Virol 78:7763-74.

165. Strauss S, Borodavka A, Papa G, Desiró D, Schueder F, Jungmann R. 2021. Principles of RNA recruitment to viral ribonucleoprotein condensates in a segmented dsRNA virus. bioRxiv doi:10.1101/2021.03.22.435476:2021.03.22.435476.

166. Kobayashi T, Ooms LS, Ikizler M, Chappell JD, Dermody TS. 2010. An improved reverse genetics system for mammalian orthoreoviruses. Virology 398:194-200.

167. Fernández de Castro I, Tenorio R, Ortega-González P, Knowlton JJ, Zamora PF, Lee CH, Fernández JJ, Dermody TS, Risco C. 2020. A modified lysosomal organelle mediates nonlytic egress of reovirus. J Cell Biol 219.

168. Furlong DB, Nibert ML, Fields BN. 1988. Sigma 1 protein of mammalian reoviruses extends from the surfaces of viral particles. J Virol 62:246-56.

169. Virgin HW, Bassel-Duby R, Fields BN, Tyler KL. 1988. Antibody protects against lethal infection with the neurally spreading reovirus type 3 (Dearing). J Virol 62:4594-604.

170. Knowlton JJ, Fernandez de Castro I, Ashbrook AW, Gestaut DR, Zamora PF, Bauer JA, Forrest JC, Frydman J, Risco C, Dermody TS. 2018. The TRiC chaperonin controls reovirus replication through outer-capsid folding. Nat Microbiol 3:481-493.

171. Kobayashi T, Antar AA, Boehme KW, Danthi P, Eby EA, Guglielmi KM, Holm GH, Johnson EM, Maginnis MS, Naik S, Skelton WB, Wetzel JD, Wilson GJ, Chappell JD, Dermody TS. 2007. A plasmid-based reverse genetics system for animal double-stranded RNA viruses. Cell Host Microbe 1:147-57.

172. Ogden KM, Hu L, Jha BK, Sankaran B, Weiss SR, Silverman RH, Patton JT, Prasad BV. 2015. Structural basis for 2'-5'-oligoadenylate binding and enzyme activity of a viral RNase L antagonist. J Virol 89:6633-45.

173. Smyth MS, Martin JH. 2000. x ray crystallography. Mol Pathol 53:8-14.

174. Kumar D, Yu X, Crawford SE, Moreno R, Jakana J, Sankaran B, Anish R, Kaundal S, Hu L, Estes MK, Wang Z, Prasad BVV. 2020. 2.7 Å cryo-EM structure of rotavirus core protein VP3, a unique capping machine with a helicase activity. Science Advances 6:eaay6410.